10.1081-0-8247-0633-1-120000874

ULTRASOUND-BASED TECHNIQUES FOR CHARACTERIZING CONCENTRATED DISPERSIONS

Andrei S. Dukhin
Philip J. Goetz
Dispersion Technology Inc., Mt Kisco, New York

ABSTRACT

Ultrasound has a certain advantage over light for characterizing various dispersions, because it can propagate through the intact concentrated dispersions that are not transparent for light. There are two different techniques (acoustics and electroacoustics), both based on ultrasound. We give a short overview of the theory, available hardware, experiments, and applications.

There are several versions of the theory. We chose the version that is based on the ''coupled phase model'' and ''cell model.'' This version of the theory exists for both acoustics and electroacoustics. It is valid for concentrates, which justifies our choice.

We present only the new electroacoustic theory that has been developed so far for colloid vibration current only assuming a thin double layer but for any value of the Dukhin number. This theory has been experimentally tested with equilibrium dilution of the concentrated rutile (45% vl) and silica (35% vl) dispersions.

Acoustic theory has been expanded as well due to incorporation of the ''structural losses'' in addition to the existing mechanisms of the particles interaction with the sound field. There is a version now that is supposed to work in the structured dispersions. We give here the first example of this new application for acoustics.

Another important new application for acoustics is a ''mixed dispersions,'' which is a dispersed system with several dispersed phases. A specially developed ''effective media'' approach allows us to tackle successfully these very complicated systems.

Hardware has been improved during past two years as well. We mention here just one new device: ζ-potential probe. It makes electrokinetic measurement very simple, fast (down to 15 seconds), precise (0.1 mV), and accurate. It can work on-line. We give here some examples of the results obtained with this probe.

New hardware is much more sensitive and is suitable for characterizing dispersions where previous instruments failed. First of all, they are latex dispersions with low-density contrast. We give several examples of the successful characterization of these dispersions. One of the problems in the acoustic characterization of these dispersions is related to the often unknown value of the thermal expansion coefficient. We show that it is possible to extract the value of this parameter straight from the acoustic attenuation spectra.

We also present some general applications, including CMP slurries; rigid solid particles like alumina, barium titanate, zinc sulfate, kaolin, calcium carbonate, zirconia; and water-in-oil and oil-in-water emulsions and microemulsions.

INTRODUCTION

The past two years have been a time of the intensive growth of the new ultrasound-based techniques for characterizing heterogeneous colloidal systems. New theories have been developed, and new instruments became available. We are going to describe these new developments in this article.

The first technique described here is referred to as ''acoustics.'' It is somewhat simpler than the second, which is referred to as ''electroacoustics''. Acoustics deals only with the acoustics properties of the dispersion, such as the ''attenuation'' and ''sound speed.'' Electroacoustics is more complicated because it is related to the coupling between the acoustic and electric properties of the dispersion.

The history of the acoustics can be traced back to the creation of the first hardware for measuring the acoustic properties of liquids more than 50 years ago at MIT (1) by Pellam and Galt. The first attempt to develop an acoustic theory for heterogeneous systems was by Sewell 90 years ago (2), whereas the general acoustic principles for dilute systems were successfully formulated 45 years ago by Epstein and Carhart (3). A long list of applications and ex-

periments using acoustic spectroscopy appears in several reviews (4, 5). Despite all these developments, acoustic spectroscopy is rarely mentioned in modern handbooks of colloid science (6, 7).

Acoustics can provide reliable particle size information for concentrated dispersions without any dilution. There are examples for which acoustics yields size information at volume fractions above 40%. Such in situ characterization of concentrated systems makes the acoustic method very useful and quite unique compared to alternative methods including light scattering where extreme dilution is usually required. Acoustics is also able to deal with low dispersed phase volume fractions, and some systems can be characterized at less than 0.1% vl. This flexibility in concentration range provides an important overlap with classical methods.

Acoustics does not require calibration with a known colloid. It is calibrated on first principles and provides an absolute particle size distribution (within the constraints of the model). It is a big advantage over modern back-light scattering technique, which is also supposed to work in moderate concentrated dispersions (8). In addition, acoustics theory takes into account particle interaction (9), whereas back-light scattering technique is lacking such a theory.

Acoustics is more suitable than light scattering methods for characterizing polydisperse systems. Acoustics yields particle size on a weight basis, which makes it similar to sedimentation techniques. Light scattering methods are much more sensitive to the presence of larger particles because this phenomenon exhibits a stronger dependence on the particle size, such as fifth or sixth power. As a result, light scattering methods tend to overestimate the number of larger particles and are often not able to resolve the presence of small particles in very polydisperse systems.

In addition to particle size, acoustics can also provide information about the microstructure of dispersed systems. The acoustic spectrometer can be considered as a micro-rheometer. Unlike traditional rheometers, an acoustic spectrometer applies stresses over a very short distance, on the scale of microns, thus sensing the microstructure of the dispersed system. This feature of acoustics is only beginning to be exploited.

The operating principles of the acoustic spectrometer are quite simple. The acoustic spectrometer generates sound pulses that, after passing through a sample, are measured by a receiver. The passage through the sample system causes the sound energy to change in intensity and phase. The acoustic instrument measures the sound energy losses (attenuation) and the sound speed. The sound attenuates due to the interaction with the particles and liquid in the sample system. Acoustic spectrometers work generally in the frequency range of 1 to 100 MHz. This is a much higher sound frequency than the upper limit of our hearing, which is approximately 0.02 MHz. Acoustic spectrometer is nondestructive; energy of the ultrasound is very low in contrast with traditional sonicators built for eliminating aggregation.

While the operating principles are relatively simple, the analysis of the attenuation data to obtain particle size distributions does involve a degree of complexity, because the experimental results must be fitted to rather complex theoretical models based on various acoustic loss mechanisms. The advent of high-speed computers and the refinement of these theoretical models have made the inherent complexity of this analysis of little consequence. In comparison, many other particle sizing techniques such as photon correlation spectroscopy also rely on similar levels of complexity in analyzing the experimental results.

Acoustic methods are very robust and precise (10). They are much less sensitive to contamination compared to the traditional light-based techniques, because the high concentration of particles in the fresh sample dominates any small residue from the previous sample. It is a relatively fast technique as well. Normally, one particle size measurement can be done in a few minutes. These features make acoustic very attractive for on-line particle size monitoring.

Electroacoustics is a relatively new technique compared to acoustics. The first reference to an electroacoustic effect was made by Debye (11), and there are several short historical reviews (12, 13). Electroacoustics is more complex than acoustics because an additional electric field is involved. Electroacoustics, in principle, can provide particle size information as well as zeta potential. There are two different implementations of electroacoustics, depending on which field is used as the driving force. Electrokinetic sonic amplitude (ESA) involves the generation of sound energy caused by the driving force of an applied electric field. Colloid vibration current (CVI) is the phenomenon where sound energy is applied to a system, and a resultant electric field or current is created by the vibration of the colloid electric double layers.

There are two different opinions about the application of ultrasound-based techniques to characterizing colloidal dispersions discussed in the article (14). We believe that acoustics is much more powerful than electroacoustics for particle size characterization. At the same time, electroacoustics is the wonderful tool for ζ-potential characterization. We gave several positive arguments supporting our viewpoint years ago in the article (14). Here, we repeat them with some additions resulting from our long experience.

Table 1 Advantages of the acoustics over the electroacoustics for particle sizing

1.	No calibration using colloid with the known particle size
2.	Much wider particle size range from 10 nm to 100 microns, compared to the typical electroacoustic range from 100 nm to 10 microns
3.	Particle size is independent of any assumptions and any influence of the particle's double layers
4.	Particle sizing of uncharged particles
5.	Particle size at high conductivity
6.	Much less sensitive to the temperature variation
7.	Much less sensitive to contamination

Taking into account these arguments, we suggested the combination of acoustics and electroacoustics. According to this scheme, acoustics provides the particle size distribution, whereas electroacoustics is used only for ζ-potential characterization. We would like to stress here that electroacoustics has many advantages over traditional microelectrophoretic method of the ζ-potential measurement. These advantages are summarized in Table 2.

Interaction of ultrasound with a heterogeneous dispersed system involves various thermodynamic, hydrodynamic, and electrodynamic effects. The general theoretical picture is rather complex; however, there is always an opportunity to apply some simplification in the case of the particular real dispersion. This fortunate feature of acoustics historically has been implemented in terms of various mechanisms of the ultrasound interactions with a dispersed system. All together, six mechanisms are known: 1) viscous; 2) thermal; 3) scattering; 4) intrinsic; 5) structural; and 6) electrokinetic.

1. The ''viscous'' mechanism is hydrodynamic in nature. It is related to the shear waves generated by the particle oscillating in the acoustic pressure field. These shear waves appear because of the difference in the densities of the particles and medium. The density contrast causes the particle motion with respect to the medium. As a result, the liquid layers in the particle vicinity slide relative to each other. The sliding non-stationary motion of the liquid near the particle is referred to as the ''shear wave.'' This mechanism is important for acoustics. It causes loss of acoustic energy due to the shear friction. Viscous dissipative losses are dominant for small rigid particles with sizes below 3 microns, such as oxides, pigments, paints, ceramics, cement, and graphite.

   The viscous mechanism is closely related to the electrokinetic mechanism, which is also associated with the shear waves.

2. The ''thermal'' mechanism is thermodynamic in nature, and it is related to the temperature gradients generated near the particle surface. Temperature gradients are due to the thermodynamic coupling between pressure and temperature. This mechanism is also important for acoustics. Dissipation of the acoustic energy caused by thermal losses is the dominant attenuation effect for soft particles, including emulsion droplets and latex beads.

   For yet unknown reasons, this thermodynamic effect does not show up in electroacoustics. There is a hypothesis (13) that it might be explained by different symmetry of thermodynamic and electrodynamic fields that eliminates their coupling.
3. The ''scattering'' mechanism is essentially the same as in the case of the light scattering. Acoustic scattering does not produce dissipation of acoustic energy. Particles simply redirect a part of the acoustic energy flow, and, as a result, this portion of the sound does not reach the sound transducer. Scattering mechanism contributes to the overall attenuation and is important for acoustics. This contribution is significant for larger particles (> 3 microns) and high frequency (> 10 MHz).
4. The ''intrinsic'' mechanism is the part of acoustics. It causes loss of acoustic energy due to the interaction of the sound wave with the materials of the particles and medium as homogeneous phases on a molecular level. It must be taken into account when overall attenuation is low, which might happen for the small particles or low volume fractions.
5. The ''structural'' mechanism bridges acoustics with reology. Actually, one can consider acoustic spectrometer as microreometer. In both cases, we apply stress and measure response. The difference is a scale of the applied stress. In the case of acoustics, we apply stress over a half wavelength, which is only about tenths of a micron on the me-

Table 2 Advantages of the electroacoustics over microelectrophoresis for ζ-potential characterization

1.	No dilution, volume fraction up to 50%
2.	Less sensitive to contamination
3.	Higher precision (± 0.1 mV)
4.	Low surface charges (down to 0.1 mV)
5.	Electroosmotic flow is not important
6.	Convection is not important
7.	Accurate for nonaqueous dispersions

gahertz scale. Structural mechanism might contribute to the acoustic attenuation. Unfortunately, this mechanism is still well described.

6. The ''electrokinetic'' mechanism describes interaction of the ultrasound with the double layer of particles. Oscillation of charged particles in the acoustic field leads to the generation of an alternating electrical field, and consequently to alternating electric current. This mechanism is a basis for elerctroacoustics. It turned out that its contribution to the acoustic attenuation is negligible. It is a very important feature of acoustics because it makes it independent of the electric properties of the dispersion, including properties of the double layers.

There is no theory that would take into account all six mechanisms. Derivation of such a theory is complicated by possible coupling between various mechanisms. Particle-particle interaction brings an additional factor that must be considered in the concentrated systems. Fortunately, there is an opportunity to simplify this theory dramatically, applying so called ''long wave requirement'' (15), which requires the wave length of the sound wave λ to be larger than particle radius a.

$$\lambda >> a \tag{1}$$

The ''long wave requirement'' (Eq. 1) restricts particle size for a given set of frequencies. Our experience shows that particle size must be below several tenths of a micron for the frequency range from 1 to 100 MHz. This restriction is helpful for characterizing small particles.

Long wave requirement allows us to consider all mechanisms separately. For instance, we can express the total attenuation measured with the acoustic spectrometer α as a the sum of these five partial attenuations:

$$\alpha = \alpha_{\text{vis}} + \alpha_{\text{th}} + \alpha_{\text{sc}} + \alpha_{\text{int}} + \alpha_{\text{str}} \tag{2}$$

where α_{vis} is the contribution of the viscous mechanism, α_{th} is the contribution of the thermal mechanism, α_{sc} is the contribution of the scattering mechanism, α_{int} is the attenuation in the pure liquid, and α_{str} is the attenuation caused by oscillation of the particles bounds in the structured dispersion.

There is another approach to acoustics that employs a ''short wave requirement.'' It was introduced by Riebel (16). This approach works only for large particles above 10 microns and requires limited input data about the sample.

Adopting long wave requirement allows us to use a ''coupled phase model'' (9, 17, 18) for describing relative motion of the particles and liquid and ''cell model concept'' (19, 20, 25, 26) for incorporating hydrodynamic and electrodynamic particle interaction. These two useful theoretical methods are described below.

This review describes the present state of both acoustics and electroacoustics. We give here a short overview of the modern theory using the same basic notions and principles for both acoustics and electroacoustics. Then, we describe experimental tests that have been performed in order to verify this theory. At the end, we give some examples that illustrate the usefulness of these ultrasound-based techniques for characterizing real dispersions.

THEORY

Theories of various ultrasound-based techniques have a lot in common. Here, we present the general basis of the theory and particular implementations for acoustics and electroacoustics, which are valid for concentrated dispersions.

Coupled Phase Model

Let us consider the infinitesimal volume element in the dispersed system There is a differential force acting on this element proportional to the pressure gradient of the sound wave ∇P. This external force is applied to both the particles and liquid and is distributed between particles and liquid according to the volume fraction φ.

Both particles and liquid move with an acceleration created by the sound wave pressure gradient. In addition, because of inertia effects, the particles move relative to the liquid, which causes viscous friction forces acting between the particles and liquid.

The balance of these forces can be presented using the following system of equations written separately for particles and liquid:

$$-\varphi \nabla P = \varphi\rho_p \frac{\partial u_p}{\partial t} + \gamma(u_p - u_m) \tag{3}$$

$$-(1-\varphi) \nabla P = (1-\varphi)\rho_m \frac{\partial u_m}{\partial t} - \gamma(u_p - u_m) \tag{4}$$

where u_m and u_p are velocities of the medium and particles in the laboratory frame of references, t is time, and γ is a friction coefficient that is proportional to the volume fraction and particle hydrodynamic drag coefficient Ω

$$\gamma = \frac{9\eta\varphi\Omega}{2a^2}$$
$$F_f = 6\pi\eta a\Omega(u_p - u_m)$$

where η is dynamic viscosity and a is the particle's radius.

In addition, we can use the mass conservation law, which might be presented as follows:

$$-\frac{\partial P}{\partial t} = M^*(1-\varphi)\nabla u_m + M^*\varphi\nabla u_p \tag{5}$$

where M^* is a stress modulus (the reciprocal of compressibility) of the dispersed system and t is a time.

The system of Eqs. 3–5 is well known in the field of acoustics. It has been used in several papers (9, 17, 18) for calculating sound speed and acoustic attenuation. It is valid without any restriction on volume fraction. Importantly, it is known that this system of equations yields a correct transition to the dilute case.

This system of equations is normally referred to as the ''coupled phase model.'' The word ''model'' usually suggests the existence of some alternative formulation, but it is hard to imagine what one can change in this set of force balance equations, which essentially express Newton's second law. Perhaps, the word ''model'' is too pessimistic in this case.

The ''coupled phase model'' opens an opportunity to describe a polydisperse system without using superposition assumption. In order to do this, we have to reformulate equations of the force balance for the polydisperse system.

Let us assume now that we have a polydisperse system with conventional N fractions. Each fraction of particles has certain particle diameter d_i , volume fraction φ_i , drag coefficient γ_i , particle velocity u_i in laboratory frame of reference. We assume density of the particles to be the same for all fractions ρ_p. Total volume fraction of the dispersed phase is φ. Liquid is characterized by dynamic viscosity η, density ρ_m, and velocity in the laboratory frame of reference u_m.

Coupled phase model suggests to apply force balance to each fraction of the dispersed system including dispersion medium. We did it before for one fraction. Now, we apply the same principle to the N fractions. In addition, we consider time and space dependent on the unknown field variables P, u_m, and u_p as a monochromatic wave $Ae^{j(\omega t-x)}$; where j is a complex unit, l is a complex wavenumber, and ω is a frequency of the ultrasound. As a result, we obtain the following system of N + 1 equations:

$$\left.\begin{aligned} -\varphi_1\nabla P &= \varphi_1\rho_p j\omega u_1 \\ &\quad + \gamma_1(u_1-u_m) \\ &\cdots\cdots\cdots\cdots\cdots\cdots \\ -\varphi_i\nabla P &= \varphi_i\rho_p j\omega u_i \\ &\quad + \gamma_i(u_i-u_m) \end{aligned}\right| \text{ N equations for particles} \tag{6}$$

$$-(1-\varphi)\nabla P = (1-\varphi)\rho_m j\omega u_m - \sum_i \gamma_i(u_i-u_m)$$

equation for the liquid (7)

where

$$\gamma_i = \frac{18\eta\varphi_i\Omega}{d_i^2}$$

$$F^i_{stockers} = 3\pi\eta d\Omega(u_i-u_m)$$

Coupled phase model (13) allows us to calculate the particle velocity relative to the liquid (u_i-u_m) for each fraction without using superposition assumption. We can solve system of N + 1 equations following our previous paper (13). In order to do this, we reformulate all equations, introducing desirable quantities $x_i = u_i-u_m$, and eliminate parameter u_m using the last equation, which specifies the liquid velocity in a form:

$$u_m = -\frac{\nabla P}{j\omega\rho_m} + \frac{\sum_i \gamma_i x_i}{(1-\varphi)j\omega\rho_m} \tag{8}$$

The new system of N equations is:

$$\left(\frac{\rho_p}{\rho_m}-1\right)\nabla P = \left(j\omega\rho_p + \frac{\gamma_i}{\varphi_i}\right)x_i + \frac{\rho_p}{(1-\varphi)\rho_m}\times\sum_i \gamma_i x_i \tag{9}$$

This system can be solved using the principle of mathematical induction. We guess solution for N fractions and then prove that the same solution works for N + 1 fraction. As a result, we obtain the following expression for velocity of the i-th fraction particle relative to the liquid:

$$u_i-u_m = \frac{\left(\frac{\rho_p}{\rho_m}-1\right)\nabla P}{\left(j\omega\rho_p+\frac{\gamma_i}{\varphi_i}\right)\left(1+\frac{\rho_p}{(1-\varphi)\rho_m}\sum_{i=1}^{N}\frac{\gamma_i}{j\omega\rho_p+\frac{\gamma_1}{\varphi_i}}\right)} \tag{10}$$

This particle velocity is important for further calculation in the electroacoustic theory. At the same time the ''coupled phase model'' yields an important result for the acoustic theory. System of Eqs. 6–7 combined with the mass conservation law allows us to calculate the complex

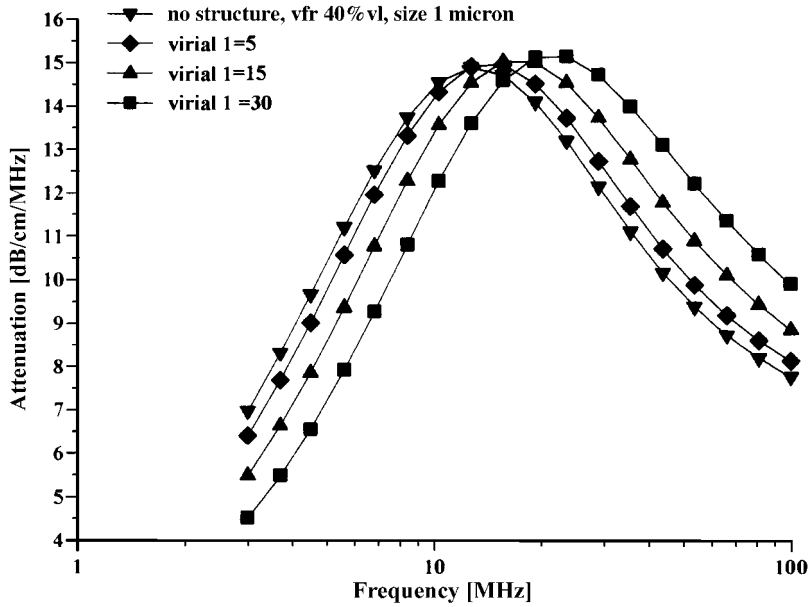

Fig. 1 Theoretical attenuation of the 40%vl alumina slurry with 1 micron particles at different values of the first virial coefficient assuming the second virial coefficient to be a zero.

wavenumber without using superposition assumption. This was done in another paper (9). We reproduce the result below (see Eq. 11) where

$$Den_i = -\omega^2\varphi_i\rho_p + j\omega\gamma_i + j\omega\delta_i + \beta_i$$

Parameters β_i and δ_i are two first virial coefficients that characterize oscillation of the structure in the case when particles are bound. These parameters link this theory to the reology. We show in this article, following another paper (52), how to use these parameters on the example of the real structured concentrated dispersions of alumina.

F1/F2 Figs. 1 and 2 illustrate the effect of the structure on the attenuation spectra of 40%vl alumina dispersion with median size of 1 micron. It is seen that the first virial coefficient just shifts the critical frequency, keeping the shape of the curve more or less intact and the peak attenuation constant. Because the particle size is reciprocally proportional to the square root of this critical frequency, the influence of the structure must be very substantial in order to create large errors in the particle size.

Influence of the first virial coefficient could not affect quality of fitting. For instance, it cannot explain possible excess attenuation. Elastic structure does not change the amplitude of attenuation.

In principle, this second virial coefficient can be extracted from the attenuation spectra as an adjustable parameter as it is shown below.

Eq. 11 specifies the complex wavenumber neglecting thermodynamic effects. There is a version of the coupled phase model that takes into account thermodynamic effects as well (21). It is important in the case of the flexible particles when the ''thermal'' mechanism becomes significant.

Coupled phase model does not assume the absence of the particle-particle interaction. Parameters β_i and δ_i reflect the specific particles, interaction like polymer bonds,AQ3 whereas the hydrodynamic particle-particle interaction is incorporated into the drag coefficient γ. We can take into account this hydrodynamic effect calculating γ using ''cell model concept,'' which is described in the following section.

$$\frac{l^2M^*}{\omega^2} = \frac{(1-\varphi)\rho_m + \sum_{i=1}^{N}\frac{\gamma_i(Den_i - j\omega\gamma_i)}{j\omega Den_i}}{\left(1-\varphi+\sum_{i=1}^{N}\frac{j\omega\varphi_i\gamma_i}{Den_i}\right)^2 - \sum_{i=1}^{N}\frac{\omega^2\varphi_i^2}{Den_i}\left(\rho_m - \varphi\rho_m + \sum_{i=1}^{N}\frac{\gamma_i(Den_i - j\omega\gamma_i)}{j\omega Den_i}\right)} \tag{11}$$

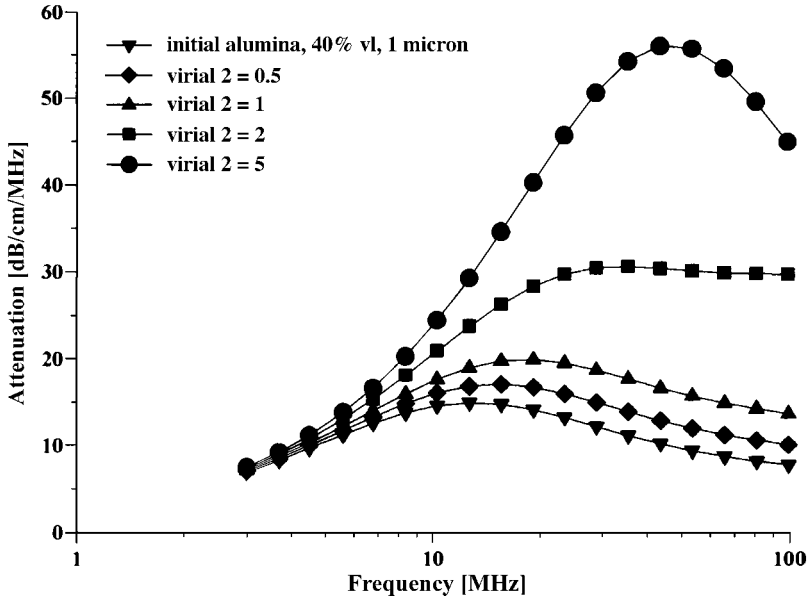

Fig. 2 Theoretical attenuation of the 40%vl alumina slurry with 1 micron particles at different values of the second virial coefficient assuming the first virial coefficient to be a zero.

Cell Model Concept

The main idea of the ''cell model'' is that each particle in the concentrated system is considered separately inside of a spherical cell of liquid associated only with a given individual particle. The cell boundary conditions formulated on the outer boundary of the cell reflect the particle-particle interaction.

In the past, the cell model has been applied only to monodisperse systems. This restriction allows one to define the radius of the cell. Equating the solid volume fraction of each cell to the volume fraction of the entire system yields the following expression for the cell radius b

$$b = \frac{a}{\sqrt[3]{\varphi}} \tag{12}$$

In the case of a polydisperse system, the introduction of the cell is more complicated because the liquid can be distributed between fractions in an infinite number of ways. However, the condition of mass conservation is still necessary.

Each fraction can be characterized by particles radii a_i, cell radii b_i, thickness of the liquid shell in the spherical cell $l_i = b_i - a_i$ and volume fraction φ_i. The mass conservation law relates these parameters together as follows:

$$\sum_{i=1}^{N} \left(1 + \frac{l_i}{a_l}\right)^3 \varphi_i = 1 \tag{13}$$

This expression might be considered as an equation with N unknown parameters l_i. An additional assumption is still necessary to determine the cell properties for the polydisperse system. This additional assumption should define the relationship between particle radii and shell thickness for each fraction. We suggest the following simple relationship:

$$l_i = l a_i^n \tag{14}$$

This assumption reduces the number of unknown parameters to only two, which are related by the following expression:

$$\sum_{i=1}^{N} (1 + l a_i^{n-1})^3 \varphi_i = 1 \tag{15}$$

The parameter n is referred to as a ''shell factor''. Two specific values of the shell factor correspond to easily understood cases. A shell factor of 0 depicts the case in which the thickness of the liquid layer is independent of the particle size. A shell factor of 1 corresponds to the normal ''superposition assumption,'' which gives the same relationship between particles and cell radii in the monodisperse case, i.e., each particle is surrounded by a liquid shell that provides each particle the same volume concentration as the volume concentration of the overall system.

In general, the ''shell factor'' might be considered an adjustable parameter because it adjusts the dissipation of

energy within the cells. However, our experience using this cell model with acoustics for particle sizing (22) indicates that a shell factor equal to 1 is almost always suitable. We take this value of n for the further derivations.

Cell model concept can be applied for describing the hydrodynamic effects as well as electrokinetc effects. The following sections present the short review of both types of the cell models.

Hydrodynamic Cell Model

Two of the most widely used hydrodynamic cell models are named according to the names of their authors: Happel cell model (23) and Kuwabara cell model (24). Both are formulated for incompressible liquid. The long wavelength requirement (Eq. 1) allows us to use these traditional hydrodynamics in the nonstationary case of the ultrasound field. The system of equations for liquid velocity u and hydrodynamic pressure P is as follows:

$$\rho_m \frac{du}{dt} = \eta \; rot \; rot \; u + gradP \tag{16}$$

$$div \; u = 0 \tag{17}$$

Both models apply the same boundary conditions at the surface of the particle:

$$u_r(r = a) = u_p - u_m \tag{18}$$

$$u_\theta(r = a) = -(u_p - u_m) \tag{19}$$

The boundary conditions at the surface of the cell are different. For the Kuwabara cell model, it is given by the following equations:

$$rot \; u_{r=b} = 0 \tag{20}$$

$$u_r(r = b) = 0 \tag{21}$$

In the case of the Happel cell model, they are

$$\prod_{r\theta}(r = b) = \frac{1}{r}\frac{\partial u_r}{\partial \theta} + r\frac{\partial \frac{u_\theta}{r}}{\partial r} = 0 \tag{22}$$

$$u_r(r = b) = 0 \tag{23}$$

The general solution for the velocity field contains three unknown constants: C, C_1, and C_2.

$$u_r(r) = C\left(1 - \frac{b^3}{r^3}\right) + 1.5\int_r^b \left(1 - \frac{x^3}{r^3}\right)h(x)dx \tag{24}$$

$$u_\theta(r) = -C\left(1 + \frac{b^3}{2r^3}\right) - 1.5\int_r^b \left(1 + \frac{x^3}{2r^3}\right)h(x)dx \tag{25}$$

$$h(x) = C_1 h_1(x) + C_2 h_2(x) \tag{26}$$

The drag coefficient can be expressed in the following general form for both Kuwabara and Happel cell models:

$$\Omega = -\frac{\alpha^2}{3}\left(\frac{d(C_1h_1 + C_2h_2)}{dx} + \frac{C_1h_1 + C_2h_2}{\alpha}\right)_{x=\alpha} - \frac{4j\alpha^2}{9} \tag{27}$$

where x is normalized same way as α, coefficients C_1 and C_2 are different for two cell models:

	Kuwabara	Happel
C_1	$\frac{h_2(b)}{I}$	$\frac{bh_2(b) - 2I_{23}}{bI + 2(I_2I_{13} - I_1I_{23})}$
C_2	$-\frac{h_1(b)}{I}$	$-\frac{bh_1(b) - 2I_{13}}{bI + 2(I_2I_{13} - I_1I_{23})}$

The Happel cell model is more suitable more for acoustics because it describes more adequately energy dissipation, whereas the Kuwabara cell model is better for electroacoustics because it automatically yields the Onsager relationship (25, 20).

Electrokinetic Cell Model

Electrokinetic cell models are the results of some generalization of the hydrodynamic cell model. There are many ways to perform this generalization and, correspondingly, many ways to create a different electrokinetic cell model. The difference between electrokinetic cell models is related to the description of the electric characteristics. The relationship between macroscopic, experimentally measured electric properties and local electric properties calculated using cell concept varies for different cell models. For instance, the Levine-Neale cell model (27) specifies this relationship using one of the many possible analogies between local and macroscopic properties. Macroscopic properties are current density $< I >$ and electric field strength $< E >$. They are related with local electric current density I and electric field $\nabla\phi$ according to the Levine-Neale cell model with the following expressions:

$$< I > = \frac{I_r}{b \; cos\theta_{r=b}} \tag{28}$$

$$<E> = -\frac{1}{cos\theta}\frac{\partial\phi}{\partial r}_{r=b} \tag{29}$$

Eq. 28–29 are not unique. There are many other ways to relate macroscopic and local fields. It means that we need a set of criteria to select a proper cell model. These criteria have been suggested in the electrokinetic cell model created by Shilov and Zharkikh (25, 26). Their two criteria determine a proper choice of the macroscopic ''fields'' and ''flows.''

The first criterion is a well-known Onsager relationship (6) that constrains values of the macroscopic particles velocity relative to the liquid $< V >$, macroscopic pressure $< P >$, electric current $< I >$, and field $< E >$:

$$\frac{<V>}{<I>}_{<\nabla P>=0} = \frac{<E>}{<\nabla P>}_{<I>=0} \tag{30}$$

This relationship requires a certain expression for entropy production Σ:

$$\sum = \frac{1}{T}(<I><E> + <V><\nabla P>) \tag{31}$$

Shilov and Zharkikh used this relationship between ''fields,'' ''flows,'' and entropy production in order to derive the cell model condition for macroscopic properties. It turned out that the expression for the macroscopic field strength is different compared with Levine-Neale:

$$<E> = \frac{\phi}{b\ cos\theta_{r=b}} \tag{32}$$

whereas expression for the macroscopic current is the same in both models.

This cell model yields the correct transition to the Smoluchowski law. Smoluchowski law is a very important test for any electrokinetic theory because it is valid for any geometry and volume fraction. Failure to satisfy the Smoluchowski law test is a clear indication that the theory is not correct. Shilov and Zharkikh wrote in their paper that their theory met the Smoluchowski law requirement. They even made a stronger conclusion that it was the Levine-Neale cell model that did not reduce to the Smoluchowski law. These opinions are discussed in their paper (20). It was shown again that this difference comes from the misunderstanding of the Smoluchowski law in the case of concentrated systems. The version of the Smoluchowski law that is valid in concentrated systems confirms the Shilov-Zharkikh cell model.

Theory of Acoustics

The most well-known acoustic theory for heterogeneous systems was developed by Epstein, Carhart (3), Allegra, and Hawley (28). The theory takes into account the four most important mechanisms (viscous, thermal, scattering, and intrinsic) and is termed the ''ECAH theory.'' It describes the acoustic attenuation for a monodisperse system of spherical particles and is valid only for dilute systems. Extensions of the ECAH theory to include polydispersity have typically assumed a simple linear superposition of the attenuation for each size fraction. The term ''spherical'' is used to denote that all calculations are performed assuming that each particle can be adequately represented as a sphere.

Most importantly, the term ''dilute'' is used to indicate the assumption that there are no particle-particle interactions. This fundamental limitation normally restricts the application of the resultant theory to dispersions with a volume fraction of less than a few volume percent. However, there is some evidence that the ECAH theory, in some very specific situations, does nevertheless provide a correct interpretation of experimental data, even for volume fractions surprisingly as large as 30%.

An early demonstration of this ability of the ECAH theory was provided by Allegra and Hawley. They observed almost perfect correlation between experiment and ECAH theory for the following dispersions: a 20% by volume toluene emulsion; a 10% by volume hexadecane emulsion; and a 10% by volume polystyrene latex. Experiments with emulsions by McClements (29, 30) have provided similar results. The recent work by Holmes, Challis, and Wedlock (31, 32) also shows good agreement between ECAH theory and experiments, even for 30% by volume polystyrene latex. An absence of particle-particle interaction was also observed with neoprene latex (33).

It is important to note that the unexpected validity of the dilute ECAH theory for moderately concentrated systems has only been demonstrated in systems where the ''thermal losses'' were dominant, such as emulsions and latex systems.

The difference between the ''viscous depth'' and the ''thermal depth'' provides an answer to the observed differences between emulsions and solid particle dispersions. These parameters characterize the penetration of the shear wave and thermal wave correspondingly into the liquid. Particles oscillating in the sound wave generate these waves, which damp in the particle vicinity. The characteristic distance for the shear wave amplitude to decay is the ''viscous depth'' δ_v. The corresponding distance for the thermal wave is the ''thermal depth'' δ_t. The following expressions give values for the parameters in dilute systems:

$$\delta_v = \sqrt{\frac{2v}{\omega}} \tag{33}$$

$$\delta_t = \sqrt{\frac{2\tau_m}{\omega\rho_m C_p^m}} \tag{34}$$

where ν is the kinematic viscosity, ω is the sound frequency, ρ_m is the density, τ_m is heat conductance, C_p^m is a heat capacity at constant pressure of liquid.

The relationship between δ_v and δ_t has been considered before. For instance, McClements plots ''thermal depth'' and ''viscous depth'' versus frequency (29, 30). It is easy to show that the ''viscous depth'' is 2.6 times more than the ''thermal depth'' in aqueous dispersions. As a result, the particle viscous layers overlap at the lower volume fraction more than the particle thermal layers. Overlap of the boundary layers is the measure of the corresponding particle-particle interaction. There is no particle interaction when corresponding boundary layers are sufficiently separated.

Thus, an increase in the dispersed volume fraction for a given frequency first leads to the overlap of the viscous layers because they extend further into the liquid. Thermal layers overlap at higher volume fractions. Therefore, the particle hydrodynamic interaction becomes more important at the lower volume fractions than the particle thermodynamic interaction.

Overlap of the boundary layers affects a critical frequency at which attenuation expressed in dB/cm/MHz reaches maximum. For systems where the viscous acoustic losses dominate, the maximum is shifted to higher frequencies at high concentrations, which will result in a lower attenuation value for a given frequency. Therefore, if the attenuation is considered at a single frequency, the attenuation will at first increase with higher dispersed phase. Once the concentration is high enough, the attenuation curve and maximum shift to higher frequencies, and the attenuation at the considered single frequency decreases. This effect is illustrated with calculated attenuation spectra in Fig. 3, and later it is proved with equilibrium dilution test (13).

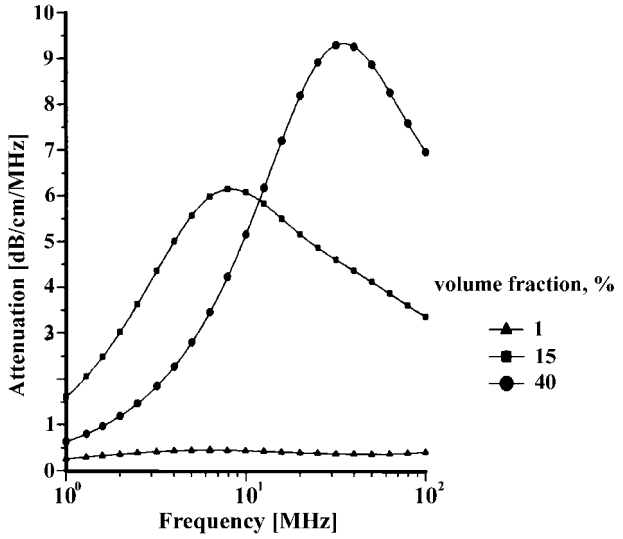

Fig. 3 Attenuation spectra calculated for various volume fractions of the dispersion of 1 micron particles.

The 2.6 times difference between δ_v and δ_t leads to a large difference in the volume fractions corresponding to the beginning of the boundary layer overlap. It is interesting that this important feature of the ''thermal losses'' works for almost all liquids (34, 21). Therefore, ''thermal losses'' are much less sensitive to the particle-particle interaction than ''viscous losses'' for almost all known liquids. It makes ECAH theory valid in a much wider range of emulsion volume fractions than one would expect.

There is one fact that follows from the values of the liquid's thermal properties that makes it convenient to use ECAH theory. In general, ECAH theory requires information about three thermodynamic properties: thermal conductivity τ, heat capacity C_p, and thermal expansion β. It turns out that τ and C_p are almost the same for all liquids except water (35). The number of required parameters is then reduced to one thermal expansion. The parameter of the thermal expansion then plays the same role in ''thermal losses'' as density in ''viscous losses.''

ECAH theory has a big disadvantage of being mathematically complex. It cannot be generalized for particle-particle interactions. Long wave requirement allows us to overcome this problem by simplifying the theory. We can express the total attenuation measured with the acoustic spectrometer as the sum of these five partial attenuations (see Eq. 2) if long wave requirement is valid. In addition, by restricting frequency and particle size with the long-wave requirement, we can use the simpler explicit expression for the thermal losses α_{th} obtained initially by Isakovich (36) and confirmed later by Epstein, Carhart (3), Allegra, and Hawley (28):

$$\alpha_{th} = \frac{3\varphi T c_m \rho_m \tau_m}{2a^2}\left(\frac{\beta_m}{\rho_m C_p^m} - \frac{\beta_P}{\rho_p C_p^p}\right)^2 \times \mathrm{Re}\left(\frac{1}{1 - jz_m} - \frac{\tau_m \tanh z_p}{\tau_p \tanh z_p - z_p}\right) \tag{35}$$

where

$$z = (1 + j)a\sqrt{\frac{\omega\rho C_p}{2\tau}}$$

At the same time, the long wave requirement provides a sufficient simplification of the theory for taking into account particle-particle hydrodynamic interaction into the theory of the viscous losses. It has been done (9) on the basis of the ''coupled phase model'' (17, 18). This new theory works up to 40%vol and yields the following expression for the complex wavenumber l assuming viscous losses as the only mechanism of the particles' interaction with the sound wave:

$$\frac{l^2 M^*}{\omega^2} = \frac{\rho_m(1-\varphi) + \rho_p \sum_{i=1}^{N} \frac{\varphi_i \gamma_i}{j\omega\rho_p\varphi_i + \gamma_i}}{(1-\varphi)^2 + \sum_{i=1}^{N} \frac{\varphi_i(\varphi-2)\gamma_i - \varphi_i^2(1-\varphi)\rho_m}{j\omega\rho_p\varphi_i - \gamma_i}} \tag{36}$$

where Ω is a drag coefficient specified above, M^* is stress modulus, which can be expressed in terms of densities and sound speeds as follows:

$$M^* = \frac{\rho_p \rho_m c_p^2 c_m^2}{\varphi\rho_m c_m^2 + (1-\varphi)\rho_p c_p^2}$$

Eq. 36 specifies the value of viscous losses:

$$\alpha_{vis} = -\mathrm{Im}\, l \tag{37}$$

This theory can be used also for calculating sound speed of the dispersions where viscous losses are dominant.

$$c_s = \frac{\omega}{\mathrm{Re}\, l} \tag{38}$$

Eq. 36 neglects contribution from the specific forces or particle bonds. It means that it is valid only in non-structured dispersions. In the case of the structured dispersions, the more general Eq. 11 must be used. That equation presents the contribution of both the viscous and structural losses. It is interesting to consider an extreme case when viscous losses are negligible, but structural ones are dominant. It is a case of the gels made either by very small nano-particles or by polymers. Eq. 11 yields the following expression for the structural losses of gels:

$$\frac{l^2 K^*}{\omega^2} = \frac{\rho_0(\beta - \omega^2\rho_p\varphi) + j\omega\delta\rho_0}{[(1-\varphi)(\beta - \omega^2\rho_p\varphi) - \omega^2\varphi^2\rho_0] + j(1-\varphi)\omega\delta} \tag{39}$$

Expressions for calculating intrinsic α_{int} and scattering losses α_{sc} for long wave limit are given in the papers of McClements (4, 29, 30). He uses the term ''lossless scatters'' for describing sound propagation through the system when dissipative mechanisms of viscous and thermal losses are negligible. Intrinsic attenuation in such a system can be expressed as follows (33):

$$\alpha_{int} = \frac{(1-\varphi)\frac{\alpha_m}{c_m} + \varphi\frac{\rho_m\alpha_p}{\rho_p\alpha_m}}{\sqrt{\frac{1-\varphi}{c_m^2} + \frac{\varphi\rho_m}{\rho_p c_p^2}}} \sqrt{\frac{\rho_s}{\rho_m}} \tag{40}$$

where α_m and α_p are attenuations of the medium and particle materials.

Scattering attenuation can be calculated following the Waterman-Truell theory (37), which yields the following expression for the complex wavenumber l_s associated with scattering:

$$\frac{l_s^2}{l_m^2} = \left(1 - \frac{3j\varphi}{(l_m a)^3} A_0\right)\left(1 - \frac{9j\varphi}{(l_m a)^3} A_1\right)$$

where A_0 and A_1 are monopole and dipole scattering coefficients calculated for a single particle,

$$l_s = \frac{\omega}{c_s} + j\alpha_{sc}$$

$$l_m = \frac{\omega}{c_m} + j\alpha_m$$

The simplest formula expressing the scattering losses in terms of densities and sound speeds can be derived from Ref. 10 for a single scattering:

$$\alpha_{sc} = \frac{\varphi\omega^4 a^3}{2c_m^4}\left[\frac{1}{3}\left(1 - \frac{\rho_m c_m^2}{\rho_p c_p^2}\right)^2 + \left(\frac{\rho_p - \rho_m}{2\rho_p + \rho_m}\right)^2\right] \tag{41}$$

It is seen that scattering losses depend on frequency very strongly. According to our experience, scattering is important only for large particles (> 3 microns) and at high frequencies (> 10 MHz).

There are two recent developments in the theory of acoustics that deserve to be mentioned here. The first one is a theory of acoustics for flocculated emulsions (38). It is based on ECAH theory, but it also uses an ''effective medium'' approach for calculating thermal properties of the flocs. The success of this idea is related to the feature of the thermal losses that allows for insignificant particle-particle interactions even at high-volume fractions. This mechanism of acoustic energy dissipation does not require relative motion of the particle and liquid. Spherical symmetrical oscillation is the major term in these kinds of losses. This provides the opportunity to replace the floc

with an imaginary particle assuming a proper choice for the thermal expansion.

Another significant recent development is due to Samuel Temkin. He offers in his recent papers (39–40) a new approach to the acoustic theory. Instead of assuming a model dispersion consisting of spherical particles in a Newtonian liquid, he suggests that the thermodynamic approach is explored as far as possible. This new theory is based on particle velocities and temperature fluctuations. Temkin's theory yields some unusual results, but has not yet been used in commercially available instruments.

Theory of Electroacoustics

Whereas acoustic spectroscopy describes the combined effect of all loss mechanisms, electroacoustic spectroscopy, as it is presently formulated, emphasizes only electrokinetic mechanisms.

In acoustic spectroscopy, sound is utilized as both the excitation and the measured variable, and therefore there is but one basic implementation. In contrast, electroacoustic spectroscopy deals with the interaction of electric and acoustic fields, and therefore there are two possible implementations. One can apply a sound field and measure the resultant electric current, which is referred to as the colloid vibration current (CVI), or conversely one can apply an electric field and measure the resultant acoustic field, which is referred to as the electronic sonic amplitude (ESA).

CVP occurs when the density of the particles ρ_p differs from that of the medium ρ_m, and the particles move relative to the medium under the influence of an acoustic wave. This motion causes a displacement of the internal and external parts of the double layer (DL) and is usually referred to as a polarization of the DL (44). The displacement of opposite charges gives rise to a dipole moment and the superposition of the electric fields of these induced dipole moments over the collection of particles gives rise to a macroscopic electric current defined as the CVI. Thus, the fourth mechanism of particles interaction with sound leads to the transformation of part of the acoustic energy to electric energy. This electric energy may then be dissipated if the opportunity for electric current flow exists.

ESA occurs when an alternating electric field is applied to the disperse system (12). If the zeta potential of the particle is greater than zero, then the oscillating electrophoretic motion of the charged dispersed particles generates a sound wave. Both electroacoustic parameters CVI and ESA can be experimentally measured. The CVI or ESA spectrum is the experimental output from electroacoustic spectroscopy. Both of these spectra contain information about ζ-potential and PSD; however, only one of the electroacoustic spectra is required because both of them contain essentially the same information about the dispersed system.

The conversion of electroacoustic spectra into particle size distribution (PSD) requires a theoretical model of the electroacoustic phenomena. This conversion procedure is much more complicated for electroacoustics compared to acoustics because of the additional complications arising from the added electric field.

There are two quite different approaches to derive an electroacoustic theory. Historically, the first began with works by Enderby and Booth (41, 42). They simply tried to solve a system of classical electrokinetic equations without using any thermodynamic relationships. It was very complex because they took into account surface conductivity effects. Although this initial theory was valid only for dilute systems, this approach was later expanded by Malrow, Fairhurst, and Pendse (43), who tried to generalize it for concentrated systems using a Levine cell model. Unfortunately, this first attempt to create electroacoustic theory for concentrates was not successful because the Levine cell model is not suitable for this purpose (13).

An alternative approach to electroacoustic theory was suggested later by O'Brien (45, 46). He introduced the concept of a dynamic electrophoretic mobility μ_{d} and suggested a relationship between this parameter and the measured electroacoustic parameters such as CVI or ESA:

$$\mathrm{ESA(CVI)} = C_{\mathrm{cal}} \frac{\rho_p - \rho_m}{\rho_m} \varphi \mu_d E(\nabla P) \tag{42}$$

where C_{cal} is a cell constant, P is the hydrodynamic pressure, and E is the external electric field strength.

According to O'Brien's theory, a complete functional dependence of ESA(CVI) on the key parameters like ζ-potential, particle size, and frequency is incorporated into dynamic electrophoretic mobility. Coefficient of proportionality between ESA(CVI) and μd is frequency independent as well as independent of particle size and ζ-potential. This peculiarity of Eq. 42 made dynamic electrophoretic mobility a central parameter of the electroacoustic theory.

The first theory of the dynamic electrophoretic mobility, which relates this parameter with other properties of the dispersed system, was created initially by O'Brien for dilute cases only, neglecting particle-particle interaction. We call this version the ''dilute O'Brien's theory.''

Later, he applied the Levine cell model, trying to expand dynamic electrophoretic theory to concentrated sys-

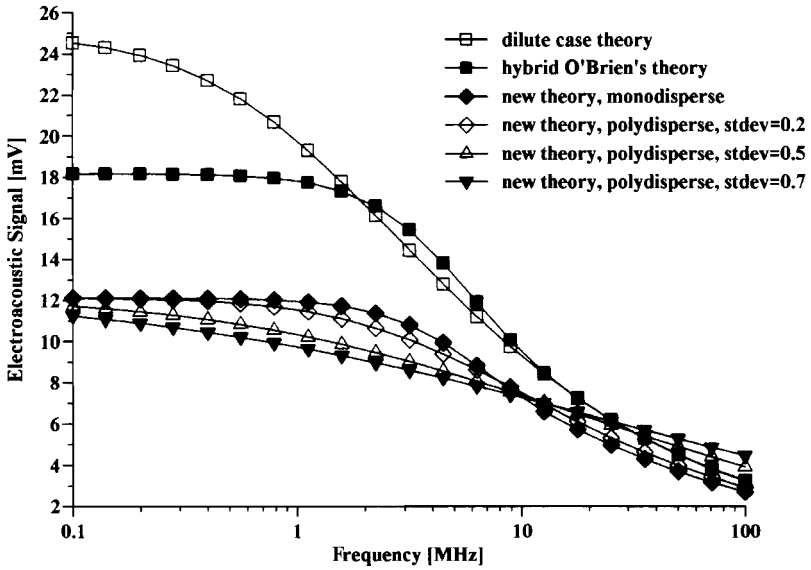

Fig. 4 Theoretically calculated normalized CVI Eq. 47 vs. frequency for dispersion with 20%vl of 1 micron particles. Density of the liquid is 1 g/cm^3, of the particles -2 g/cm^3.

tems (46). This work was generalized recently by Ohshima (47). We call this version the ''O'Brien-Levine'' theory. Fig. 4 shows the relationship between different theories.

Comparison of the O'Brien-Levine cell model with experiments did not provide agreement. For some time, this was considered as a total failure of the ''cell model approach.'' The next attempt made by Ohshima, Shilov, and A. Dukhin (20, 48, 49) using the Shilov-Zharkikh cell model for dynamic electrophoretic mobility was not successful either.

The reason for the ''cell model'' failure was not clear. It is known that it works fine in stationary hydrodynamics (19).

One of the possible reasons is related to the uncertainty with the frames of reference in the definition of the dynamic electrophoretic mobility in Eq. 42 left by O'Brien. We have tried two different frames of references (48), but neither was satisfactory. However, it became clear that this issue must be resolved.

The problem of the frames of reference can be easily resolved in the case of CVI. Liquid outside of the sound beam is immobile and can serve as a natural inertial frame of reference. We do not know the answer to this question for the ESA version of electroacoustics. There is no immobile liquid in this case because electric field is applied to the whole dispersion in the chamber, which makes this issue much more complex and even hardware dependent.

Successful resolution of the frames of references allowed us to build a completely new theory of electroacoustics for the CVI.

We have started with developing a low-frequency limit theory, which is supposed to be similar to the Smoluchowski theory for microelectrophoresis. It is known that the Smoluchowski theory works for any volume fraction when it is valid (6, 7). And yet, it is not ''cell model'' based. This unique feature of the Smoluchwski equation has much deeper roots, in particular in the space similarity of the hydrodynamic and electrodynamic fields. We decided to exploit the same similarity for the electroacoustic theory.

It is known that the space similarity of these fields exists only for thin double layer

$$\kappa a << 1 \tag{43}$$

where κ is reciprocal Debye length. The first attempt to eliminate this restriction in electroacoustic theory has been described elsewhere (58, 59).

The second condition is a negligible surface conductivity, which is expressed in the terms of the small Dukhin number (6):

$$\mathrm{Du} << 1 \tag{44}$$

In addition, we consider frequency only below Maxwell-Wagner dispersion (51):

$$\omega << \omega_e = \frac{K_m}{\varepsilon\varepsilon_0} \tag{45}$$

where ε and ε_0 are dielectric permittivities of the medium and vacuum, K_m is the conductivity of the medium.

The result of our efforts is the following equation:

$$CVI_{\omega \to 0} = \frac{\varepsilon\varepsilon_0\zeta(1-\varphi)\varphi}{\eta(1+0.5\varphi)}\frac{(\rho_p-\rho_s)}{\rho_s}\nabla P \tag{46}$$

This equation is the analog of the Smoluchowski equation for electroacoustics. It preserves all the wonderful features of the Smoluchowski law. It is valid for particles of any shape and any concentration when assumptions 43–45 are true. This equation is the natural low-frequency asymptotic test for all possible electroacoustic theories.

Resolution of the frame of reference and creation of the Smoluchowski electroacoustic limit allowed us to develop a new theory based on the first approach. This has been done by A. Dukhin, V. Shilov, H. Ohshima, and P. Goetz in papers (13, 50) for the simpler case of the CVI and/or CVP when the gradient of pressure is a driving force generating electroacoustic signal. We would like to be cautious concerning expanding this new theory to the ESA phenomenon. It turned out that problem of frame of reference has different implications for these different electroacoustic effects.

This new electroacoustic theory yields the following expression for CVI (see Eq. 47 below) where a is a particle size,$\alpha = a\sqrt{\omega}/2\nu, \beta = b\alpha/a$ special functions h, H, and I are given below, $H_i = H(\alpha_i)$, $I_i = I(\alpha_i)$ and

$$Du_i = \frac{\kappa^\sigma}{K_m a_i}$$

This theory takes into account surface conductivity effects and as a result is valid for any value of the Dukhin number. This dimensionless parameter was introduced by Lyklema (6).

It is interesting to mention that there might be a contradiction between O'Brien's relationship Eq. 42 and Smoluchowski low frequency (Eq. 46). Density contrast is different in these two equations. O'Brien's relationship contains density difference between particle and media, whereas the Smoluchowski limit has density difference between particle and dispersion. This contradiction does not mean that O'Brien's relationship is wrong. It is possible that this additional density contrast is incorporated into the dynamic mobility. Definition of the dynamic mobility allows for this because of the uncertainty with the frames of reference.

Recently published theory by Carnie and colleagues (66, 67) apparently confirms our guess because it employs O'Brien's relationship and yet succeeds in interpreting experimental data. It is also in good agreement with our new theory (see Eq. 47 below).

We would like to stress that, according to our knowledge, commercially available electroacoustic spectrometer based on the ESA principle Acoustosizer of Colloidal Dynamics applies empirical correction for calculating ζ-potential from the ESA signal. It follows directly from the recent review published by Prof. Hunter who is one of the Acoustosizer authors (12). This correction is necessary because, as Prof. Hunter admits, their theory is valid only up to 5%vl. This empirical correction works and dramatically reduces error of the Acoustosizer in some concentrated systems. Unfortunately, these empirical corrections mask results of theoretically justified calculations.

So far, the new electroacoustic theory has been tested with rigid heavy particles only. It is not clear yet how it will work for emulsions, as there were no experimental data with emulsions available. This concern is related to the fact that this new theory as well as O'Brien's theory neglect thermodynamic effects. It is rather surprising as the thermodynamic effect of ''thermal losses'' is dominant for acoustics of emulsions. It is not clear yet why electroacoustics is so different from acoustics for thermodynamic effects not to be important.

A simple hypothesis that might explain this difference is that electroacoustics is related to the displacement of the electric charges in the double layer (DL). This displacement is characterized by dipole symmetry ($E = f(r)\cos\theta$). At the same time, ''thermal losses'' measured by acoustics are associated mostly with spherical symmetry. They are caused by oscillation of the particle's volume in the sound wave. It is clear that such a spherical symmetrical oscillation does not necessarily cause displacement of electric charges with dipole structure.

This is a hypothesis and a fundamental theory that will take into account the thermodynamic effects in addition to

$$\mathrm{CVI} = \frac{9\varepsilon\varepsilon_0\zeta(\rho_p-\rho_m)\nabla P}{4\eta}\frac{\displaystyle\sum_{i=1}^{N}\frac{1}{(Du_i+1)-(Du_i-0.5)\varphi}\frac{\varphi_i h(\alpha_i)}{j\alpha_i I(\alpha_i)\left(\rho_p-\rho_m\left(\frac{3H_i}{2I_i}+1\right)\right)}}{1-\dfrac{\rho_p}{1-\varphi}\displaystyle\sum_{i=1}^{N}\frac{\varphi_i\left(\frac{3H_i}{2I_i}+1\right)}{\rho_p-\rho_m\left(\frac{3H_i}{2I_i}+1\right)}} \tag{47}$$

electrodynamic and hydrodynamic effects should resolve this question. The electroacoustic theory of emulsions will not be complete unless such a theory is developed.

Nevertheless, electroacoustics even at its present stage can yield very important information about electric surface properties of emulsions as will be shown below.

EXPERIMENTAL TESTS

There are two goals for experimental tests. The first one is to test the validity of the suggested theory in concentrated systems. Equilibrium dilution is the logical experimental protocol for achieving this goal because it provides a simply criterion of the theory. Equilibrium dilution maintains the same chemical composition of the dispersion medium for all volume fractions. As a result, parameters that are sensitive to the chemistry must be the same for all volume fractions. It means that ζ-potential calculated from CVI is supposed to remain the same for all volume fractions as well as particle size. Variation of either ζ-potential or particle size with volume fraction is the indication that particular theory does not reflect volume fraction dependence properly.

The second goal of the tests is determination of the precision, accuracy, and resolution of these new techniques.

We cover both of these goals in this section.

We show that existing theories take into account hydrodynamic particle interaction properly up to 45%vl.

Precision of the acoustic median particle size characterization is 1%, and standard deviation is about 5%. Accuracy of the median particle size characterization is about 1%. Acoustic predicts somewhat broader PSD compared to light-based methods. Resolution of the acoustics is about 1 micron particle per 100,000 particles of 100 nm size.

Precision of the electroacoustic ζ-potential characterization is about 0.1 mV.

It must be mentioned that these parameters are obtained for specially prepared stable dispersions. Aggregation and structure effects might affect these parameters.

Equilibrium Dilution

We used silica Ludox and rutile R-746 from Dupont for this experiment.

Selection of the silica Ludox is related to the small size of these particles. It allows us to eliminate any particle size dependence in the Eq. 47 and test Smoluchowski limit presented with Eq. 46. Using small particles gives one simple advantage: it eliminates contribution of attenuation because small particles do not attenuate sound at low frequency. It means that choice of the small particles allows us to test volume fraction dependence only. It is important because this dependence is the most pronounced difference between different theories.

Silica Ludox TM satisfies all specified conditions because its nominal particle size reported by DuPont is about 22 nm. We measured the size using acoustics. It is quite close to the nominal value as it will be shown below. At the same time, particle size should not be too small for the given ionic strength in order to satisfy the thin double layer restriction. Silica Ludox meets this requirement because of the relatively high ionic strength of about 0.1 mol/L. Otherwise, we would have to generalize the theory removing thin double layer restriction following Babchin et al. (58, 59).

Selection of rutile as the second dispersion gives us an opportunity to test particle size dependence and enhance the density contrast contribution. We used rutile R-746 produced by E. I. DuPont de Nemouirs. This product was a concentrated stable dispersion with weight fraction of solids 76.8% weight. We took 100 ml of this dispersion and weighed it. This weight was 234 g, which yields particles' material average density 3.9 g/cm^3. This density was somewhat lower than the density of the regular rutile, perhaps, because of the stabilizing additives.

Equilibrium dilution protocol requires a pure solvent that is identical to the medium of the given dispersed system. In principle, one can try to separate dispersed phase and dispersion medium using either sedimentation or centrifugation. This method does not work for silica Ludox because particle size is too small.

The other way to create an equilibrium solution for small silica Ludox is dialysis. We used this one. Dialysis

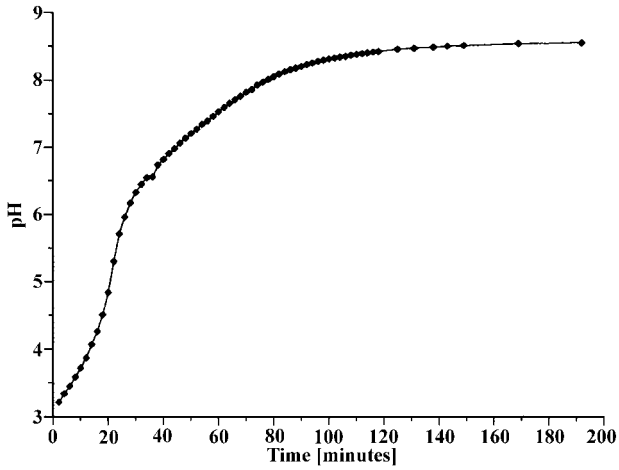

Fig. 5 Equilibration of 3%vl zirconia slurry prepared in the KCl 10^{-2} with pH adjusted initially to 4. It is seen that equilibration takes about 2 hours.

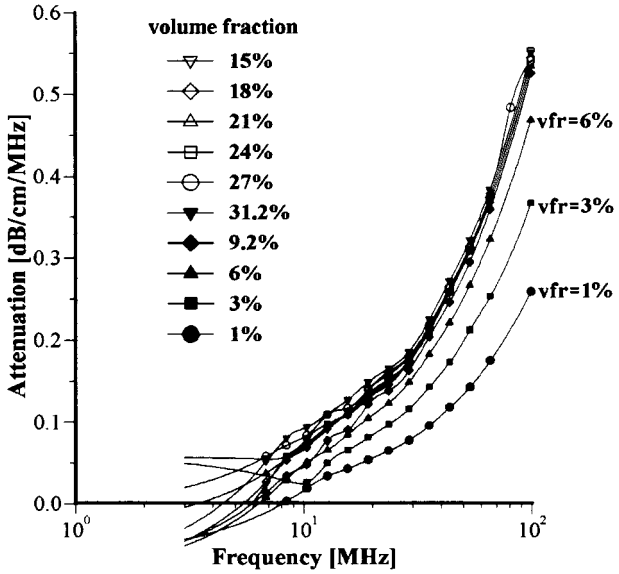

Fig. 6 Attenuation spectra measured for silica Ludox at different weight fractions. Equilibrium dilution.

allows us to equilibrate dispersion medium with external solution over some period of time. We used regenerated cellulose tubular membrane Cell*Sept4 with pore sizes of 12,000–14,000 Dalton. External solution was KCL 10^{-1} mol/L with pH adjusted to 9.5 using hydrochloric acid. Membrane filled with silica Ludox was placed inside of the KCl solution, which was continuously mixed with a magnetic stirrer. We made two samples in order to check reproducibility.

In addition, we prepared another setup using KCl solution with pH = 3. This setup allowed us to estimate the equilibration time. Initial pH of the silica Ludox is about 9 at 23°C. We monitor change of the pH in the external solution. Corresponding kinetic curve is shown in Fig. 5. It F5 is seen that pH becomes 8.6 after 3 hours of equilibration. It was close to the final pH value 8.7 after 12 days of the equilibration. We waited 12 days because equilibration time depends on the diffusion coefficient, which is the highest for H ions. The higher the diffusion coefficient, the lower the equilibration time.

Before starting dilution, we again checked the weight fraction of the silica Ludox using pyncnometer. We were concerned about losing silica particles through the membrane pores into the solution. Weight fraction remained unchanged, which means that pores were too small for silica particles.

We had two sets of 50% silica with corresponding equilibrium solution. It allowed us to check two methods of dilution. We used one set for diluting from the high weight fraction down. We did this by adding solution to the dispersed system. We used the opposite procedure with the other sample. We added dispersed system to the solution.

In the case of rutile, we used centrifugation of the initial 76.8%wt dispersion in order to create equilibrium super-

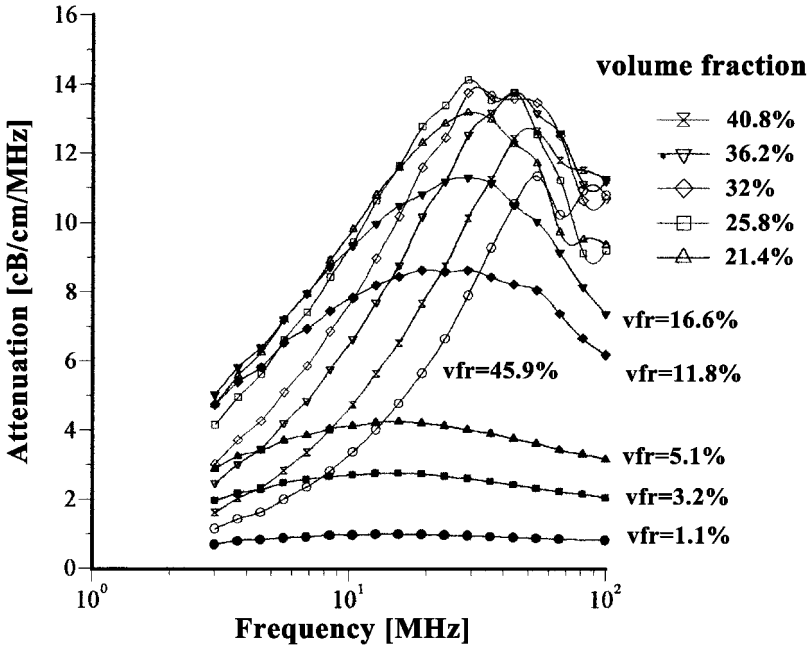

Fig. 7 Attenuation spectra measured for rutile R-746 by DuPont at different weight fractions. Equilibrium dilution.

nate. We used this supernate for preparing equilibrium 1.1% vl rutile dispersion diluting initial dispersion. After making measurement with this dilute system, we added more initial dispersion for preparing next volume fraction: 3.2% vl. We proceeded this way, making a more and more concentrated system. All together, 11 different volume fractions from 1.1%vl to 45.9%vl were tested (see Fig. 7).

For each volume fraction, we measured attenuation spectra, sound speed, pH, conductivity, temperature, magnitude, and phase of CVI.

Attenuation spectra were measured within the frequency range from 3 to 100 MHz, sound speed at 10 MHz, conductivity at 3 MHz, magnitude of CVI at 3 MHz, phase of CVI at 1.5 MHz. Some of the results are discussed below.

F6/F7 Measured attenuation spectra are shown in Figs. 6 and 7. It is seen that attenuation for silica Ludox is much lower than for rutile. This happens because of the smaller size and lower density contrast for silica. Attenuation spectra of silica become almost indistinguishable at volume fraction above 9%. This reflects a nonlinear dependence of the attenuation on the volume fraction. This nonlinearity appears because of the particle-particle interaction. This interaction shifts critical frequency to the higher values.

This peculiarity of the attenuation spectra was known before (9). It is even more pronounced for rutile (Fig. 7). Attenuation at low frequency decreases with increasing volume fraction above 16.6%vl. It is exactly the same effect, which makes attenuation constant for silica.

Existing theory takes into account this nonlinear effect. As a result, particle size calculated from this attenuation spectra is almost constant for all volume fractions for both silica and rutile (Fig. 8). Slight increase at high volume fraction can be caused by aggregation. It is important to mention here that dilute case theory would yield size decreasing dramatically with volume fraction. F8

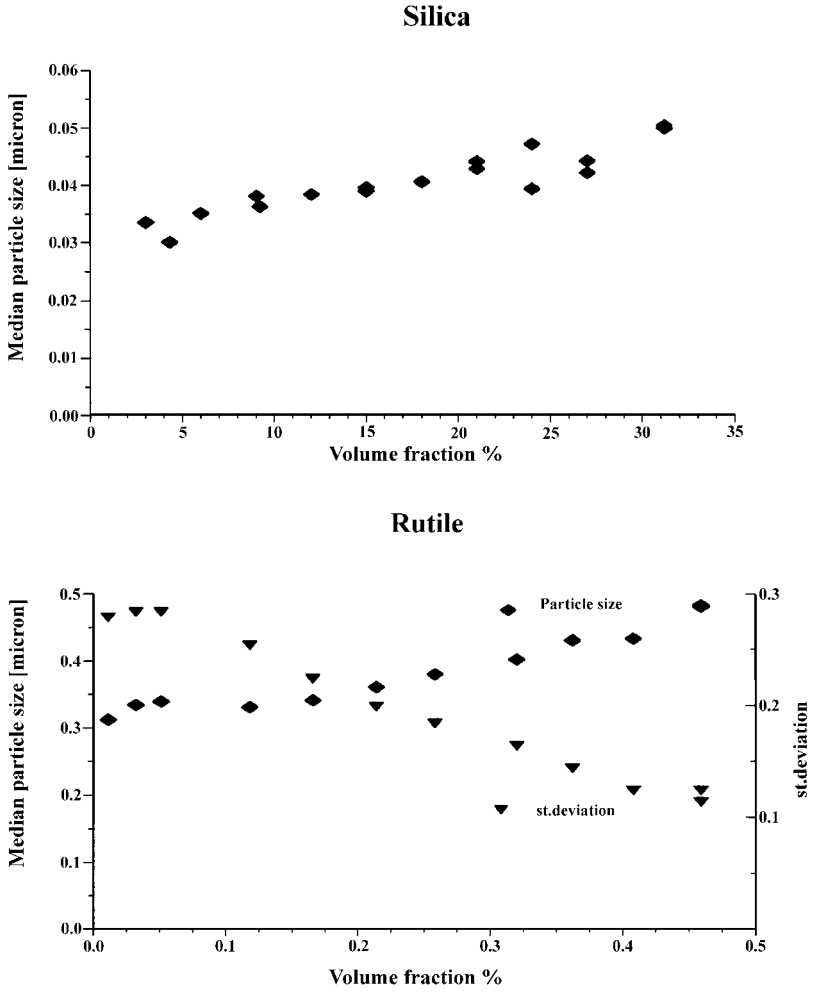

Fig. 8 Median particle size calculated for silica Ludox and rutile R-746 at different volume fraction prepared with equilibrium dilution.

It is seen that our size is somewhat larger than nominal. Perhaps, the difference with nominal value is caused by a different technique applied by DuPont for characterizing the size of these particles. It is also clear that nominal size corresponds to the dilute system, whereas we measured size for the concentrated one.

It is seen (Fig. 6) that attenuation for silica at 3 MHz is negligible indeed. It means that our expectations to eliminate this contribution to the CVI measurement using small particles were true.

At the same time, we have appreciable attenuation for rutile at 3 MHz. This gives us a chance to verify the way we correct CVI for sound attenuation.

Sound speed of the silica Ludox dispersion varies only within 2% for weight fraction changing from 1 to 50% (see F9 Fig. 9). It eliminates contribution from the changing of the acoustic impedance to the measured CVI for silica as well.

F10 Fig. 10 gives ζ-potential calculated from the measured CVI using various theoretical models. You can see that only our new theory yields ζ-potential that remains almost the same within the complete volume fraction range. Variations do not exceed 10%.

At the same time, ''hybrid O'Brien's theory'' produces a big drop in the ζ-potential at high volume fraction. This theory is the combination of O'Brien's relationship and our cell model theory for dynamic electrophoretic mobility. In the case of rutile, error reaches 300% at volume fraction 45.9%.

Similar results for silica allow us to conclude that the reason for this erroneous ζ-potential drop is O'Brien relationship, not our theory for the dynamic mobility. Our theory reduces in this case to the Smoluchowski law. It is O'Brien's relationship that brings about 100% error in ζ-potential for silica at 30%vl.

The situation becomes even worse for the original O'Brien's theory combined with the Levine cell model. In principle, we are able to apply the original O'Brien's theory as it is presented in the patent (46) with the Levine cell model. However, instead of recovering these complicated mathematical expressions, we decided just to show the effect of the missing volume fraction dependence. It is known (46) that the Levine cell model lacks multiplier K_s/K_m comparing to the Shilov-Zharkikh cell model (25). This difference is a major factor distinguishing the ''O'Brien-Levine theory'' and the ''hybrid O'Brien theory'' for this particular dispersion. These theories have different particle size dependence, but, in the case of the relatively small particles, this difference is not very important. Though, we neglect difference in particle size dependence and take into account only different volume fraction effect. The last curves marked as ''O'Brien-Levine theory'' illustrates the result produced by this theory fwithin the scope of the above mentioned assumption of the same particle size dependence for two theories.

Precision and Accuracy

Precision is a measure of the reproducibility. This section presents results concerning precision of the both acoustic and electroacoustic sensors.

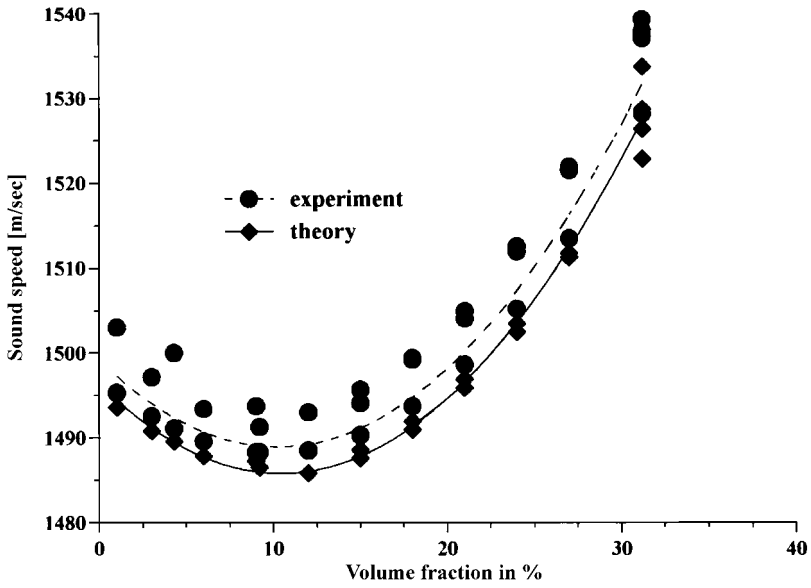

Fig. 9 Sound speed measured for silica Ludox at different weight fractions. Equilibrium dilution.

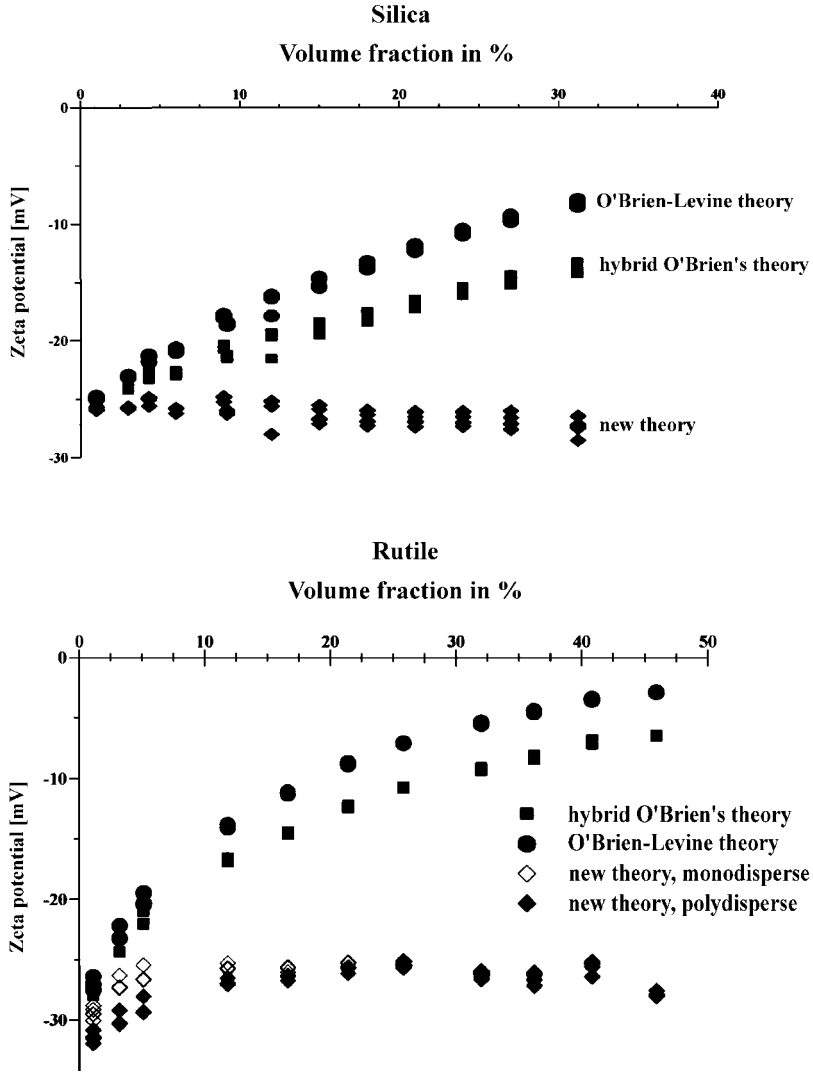

Fig. 10 ζ-Potential calculated for silica Ludox and rutile R-746 at different volume fraction prepared with equilibrium dilution.

F11 Attenuation spectra in Fig. 11 illustrate acoustic sensor precision. These attenuation spectra were measured using alumina Sumitomo AA-2 and silica Ludox. Alumina sample was measured 10 times in a row, and silica sample was measured 11 times in a row. We measured attenuation with precision 0.01 dB/cm/MHz.

This precision of measurement determines precision and resolution of the calculated particle size. Corresponding median particle size is given in Table 3. T3

It is seen that absolute variation of the median particle size is 0.9% for alumina and 1.5% for silica. These numbers illustrate precision of the acoustic sensor for characterizing particle size.

F12 Fig. 12 illustrates precision of the electroacoustic sensor. These shows results of 50 continuous CVI measurements for silica Ludox. It is seen that precision of the absolute value of the ζ-potential measurement is a fraction of mV.

Accuracy characterizes the correlation between real and measured values. Accuracy of PSD measurement is a measure of adequacy of the measured particle size distribution. In order to determine accuracy of PSD, one needs a standard system with a known particle size distribution. We used BCR Silica quartz with the median size of about 3 microns. It is a PSD standard in Europe.

Fig. 13 shows standard particle size distribution and F13 PSD measured with DT-1200. Difference of the median particle size between standard and DT-1200 is less than 1%. At the same time, there is some difference in the amount of small particles. It means that acoustic sensor

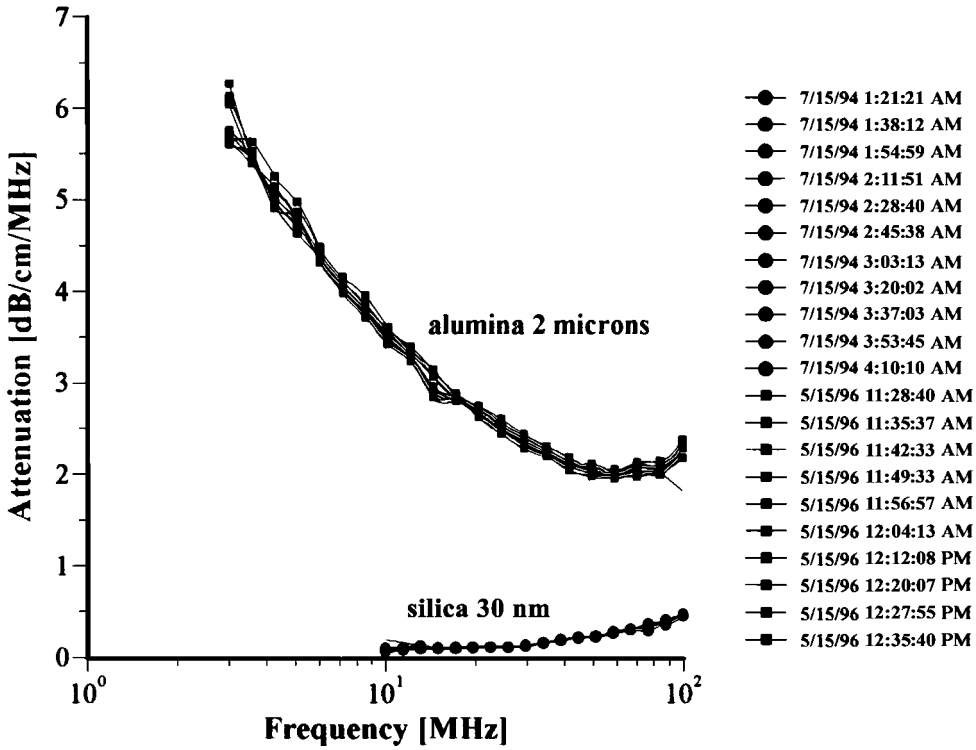

Fig. 11 Precision test. Multiple measurements of the attenuation spectra of alumina AA-2 (5%vl) and silica Ludox (10%wt).

determines median size with an accuracy of 1% and standard deviation with an accuracy of about 5%.

Test of the ζ-potential measurement accuracy is much more complicated because there is no ζ-potential standard for concentrated systems. Our experience is that CVI makes it possible to measure ζ with almost the same accuracy as microelectrophoresis?

Resolution

Resolution reflects the ability of the technique to detect particular details of the parameter of interest. It is especially important for acoustic particle size characterization. In principle, acoustic spectra contain information that is sufficient for calculating particle size distributions described with, at most four adjustable parameters. It allows us to apply this technique for characterizing bimodal particle size distributions.

There are two aspects of resolution for particle sizing. The first one is concern with the ratio of particle sizes, which can be resolved under the condition that these two fractions are presented in equal amounts. The second one gives the fewest number of large particles, which can be resolved on the background of the small particles.

In order to figure out the first resolution parameter, we prepared stable dispersions of two Sumitomo aluminas: AKP-30 and AA-2. They were prepared at 10%vl each. These two alumina have different particle sizes: 0.3 microns for AKP-30 and about 2 microns for AA-2. Attenuation of individual slurries and corresponding particle size distributions are shown in Fig. 14. F14

This figure also shows attenuation, which is measured for 50:50 mixture of these slurries. It is seen that attenuation of this artificially prepared bimodal mixture is a superposition of the attenuation of the initial slurries. Bimodal particle size distribution calculated from this at-

Table 3 Median particle size in microns

Alumina	2.015	2.076	2.057	2.092	2.065	2.047	2.035	2.075	2.039	2.085	
Silica	0.03	0.029	0.029	0.029	0.029	0.03	0.03	0.029	0.03	0.03	0.03

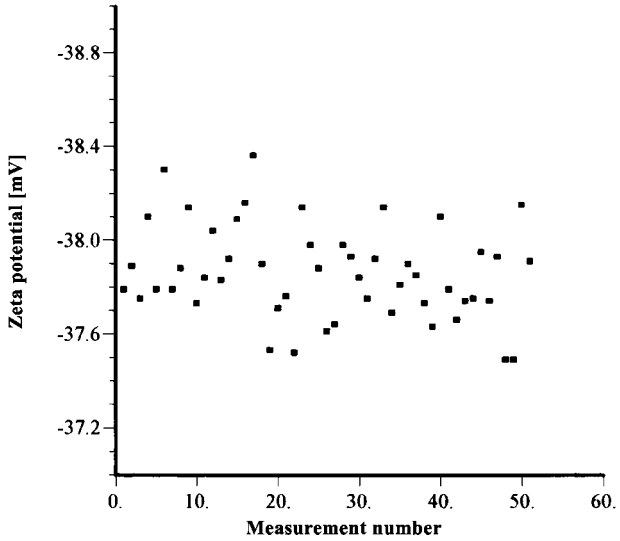

Fig. 12 Precision test: 50 measurements of ζ-potential of silica Ludox at 10%wt.

tenuation consists of the two modes, which coincides with the PSD of the initial slurries.

In this particular test, we had ratio of sizes 1:7. According to our experience, acoustics is able to resolve sizes as close as 1:2.

The second resolution test was performed with chemical-mechanical polishing slurry SS25 made by Cabot. The median particle size of this slurry is about 100 nm. We used this slurry as background and added a small amount of silica Geltech larger particles with a size of about 0.5 microns. Corresponding attenuation spectra and calculated bimodal PSD are shown in Fig. 15. It is seen that addition F15 of 2% larger particles relative to the total silica weight causes measurable variation of the attenuation spectra. This determines the resolution of the acoustics in terms of larger particles. On the number basis, it is equivalent to the single 1 micron particle per 100,000 particles with 100 nm size.

HARDWARE

There are several ultrasound-based commercially available instruments. Here describe sensors that have been developed by Dispersion Technology Inc. Both sensors described below use the same pulse signal processor, which is described in detail in the patents (5354).

Acoustic Sensor

Acoustic sensors have two piezo crystal transducers. The gap between transmitter and receiver is variable in steps. In default, it changes from 0.15 mm up to 20 mm in 21 steps. A variable gap provides several advantages. First of all, it eliminates the necessity to calibrate the instrument with known colloid. The calibration can be done based on the first principles because, instead of absolute power, we measure the variation of power, with gap.

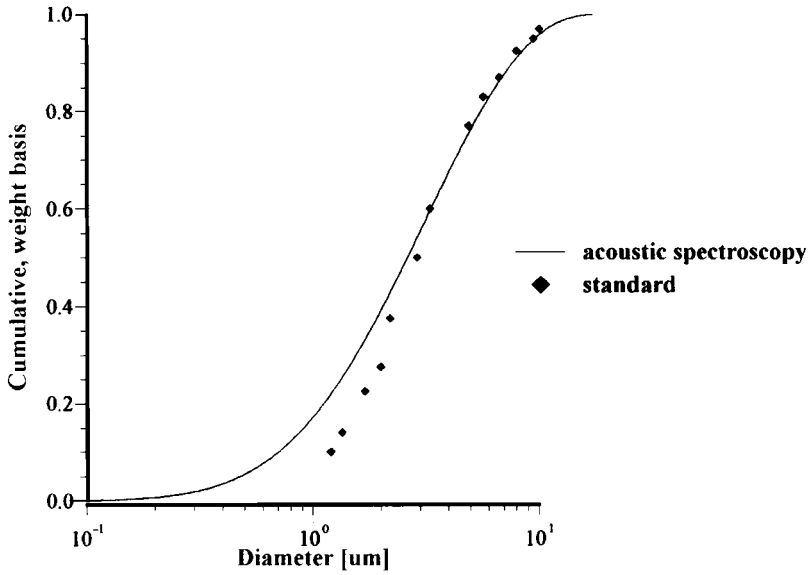

Fig. 13 Accuracy test. Standard and measured acoustically particle size distribution of silica BCR at 12%wt in ethanol.

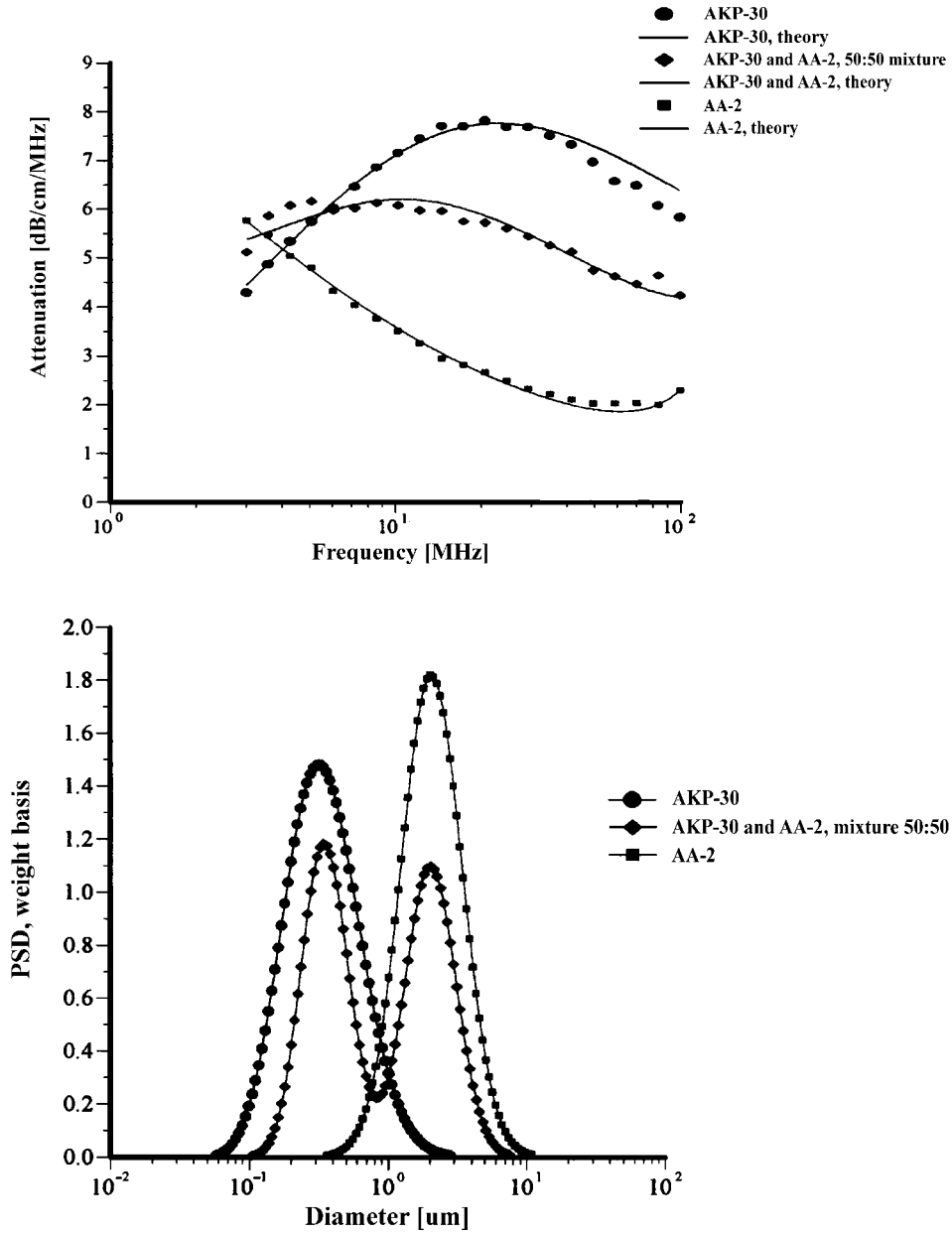

Fig. 14 Attenuation and PSD of two alumina samples (5%vl) and their 50:50 mixture.

The second significant advantage of using variable gap is related to the wide dynamic range of attenuations. The small gaps allow us to measure highly attenuating dispersions, whereas large gaps are suitable for measurements of sound transparent dispersions and pure liquids.

Transmitters generate acoustic pulses of the certain frequency and length. The basic frequency of pulse changes in steps as well. In default, it changes from 3 to 100 MHz in 18 steps. The number of pulses collected for the each gap and each frequency are automatically adjustable in order to reach the target signal-to-noise ratio.

Acoustic sensors measure energy losses. There are several sources of these losses. Part of the pulse energy is lost in electronics. Another part of the energy is lost due to the limited efficiency of the piezoelectric transducer to convert electric pulse to the sound pulse and vice versa. The most important part of the energy losses occurs while

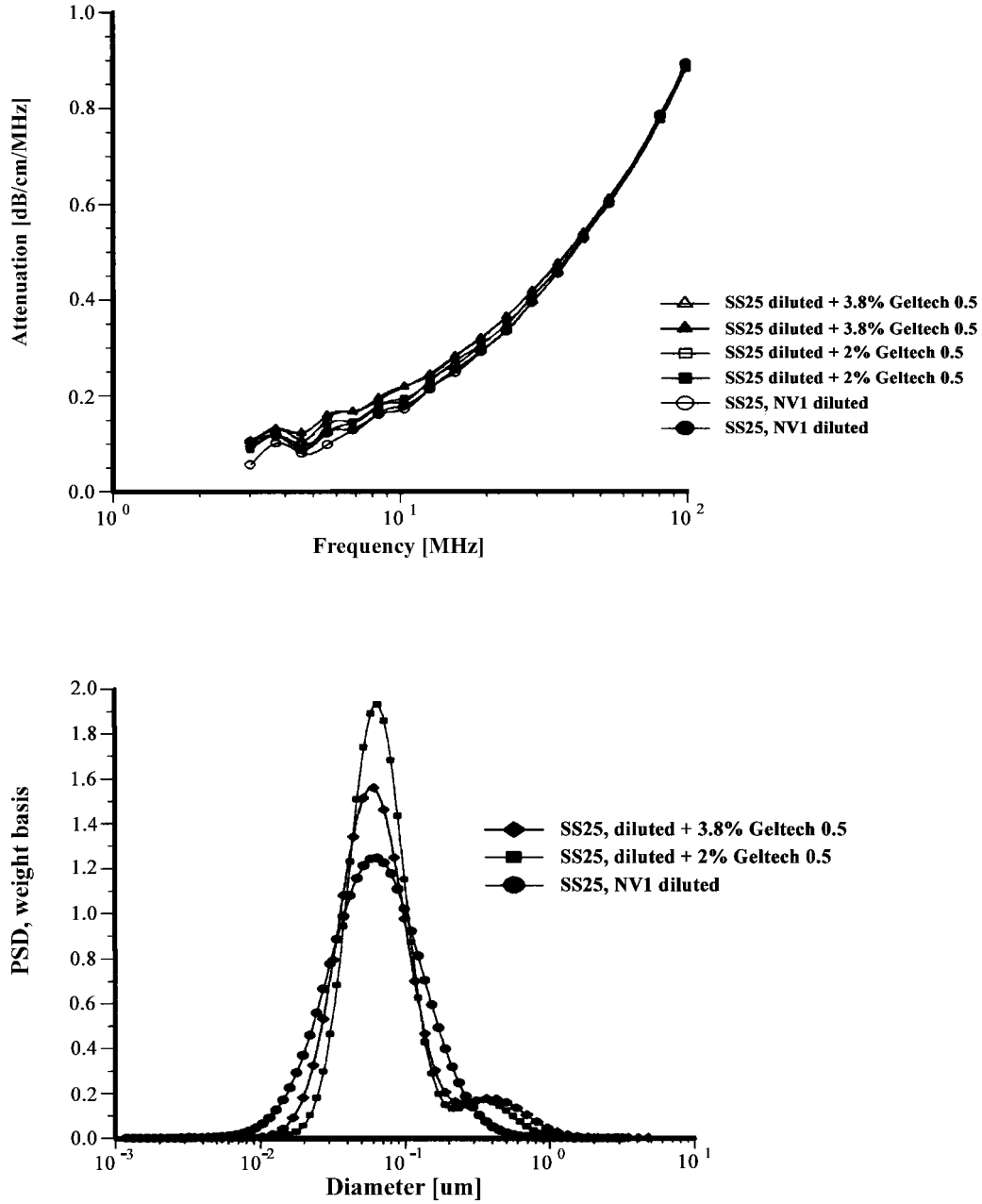

Fig. 15 Attenuation and PSD of Cabot CMP slurry with small additions of silica Geltech with the particle size 0.5 micron.

ultrasound pulse propagates through the sample and interacts with dispersion. These last energy losses (colloid losses) are the target, but actually acoustic sensor measures total energy losses including all possible sources. In order to extract colloid losses from the total losses, we should independently measure losses in electronics and losses in transducers. It is done automatically at the beginning of every measurement.

Acoustic sensor measures also sound speed at the one chosen frequency. This is done by using a time of the pulse arrival to the receiver. The instrument automatically adjusts pulse sampling depending on the value of the sound speed. It is necessary for eliminating possible artifact, like excess attenuation at the low frequencies.

Experimental output of the acoustic sensor is attenuation frequency spectra in dB/cm/MHz. These experimen-

tal data are independent of any assumptions about sample, which makes it very valuable.

In order to calculate particle size from the attenuation spectra, one has to apply theory and corresponding theoretical assumptions.

Electroacoustic ζ-Potential Probe

The electroacoustic sensor probe contains a piezoelectric transducer with a critical frequency 3 MHz and a sensing electrode, which is placed on the surface of the transducer. This electrode is separated from the external reference electrode with a nonconducting rigid ceramic insert. Internal electric impedance between these electrodes can be selected depending on the conductivity range of the samples by means of an internal transformer. The transformer is selected such that the input impedance is significantly less than the external impedance of the sample such that the resultant signal is proportional to the short circuit current. This transformer is located just behind the central electrode in order to minimize the stray capacitance.

There is a special plastic rod between transmitting transducer and the sensing electrode with a low acoustic impedance. This rod adjusts acoustic impedance of the probe and dispersion, eliminating a high reflection on this surface. This additional rod opens a way to calibrate an absolute power using reflection on the transducer-rod surface.

The signal processor generates the transmit gate, which defines the 1-watt pulse generated in the interface module as well as the necessary signals to set the frequency. Electroacoustic measurement can be performed either for one frequency or for the chosen set of frequencies from 1 to 100 MHz. Transducer converts these pulses to the sound pulses with some certain efficiency. Sound pulse propagates through the quartz delay rod, acoustic impedance rod, and eventually through the sample. Acoustic pulse propagating through the sample excites particles and disturbs their double layers. Particles gain dipole moments because of this excitation. These dipole moments generate electric field. This electric field changes the electric potential of the central sensing electrode. Difference of the electric potentials between central electrode and external reference electrode causes electric current. This current is registered as colloid vibration current. The value of this current is very low. It takes averaging at least 800 pulses in order to achieve the high signal-to-noise ratio. The number of pulses depends on the properties of colloid. Measurement of CVI in low conducting oil-based systems requires averaging of millions of pulses. In principle, this method makes it possible to measure any low energy signals.

The general expression for the local CVI (Eq. 47) contains one unknown parameter: P pressure. Piezocrystal converts initial 1-W electric signal to the sound with low efficiency, about 40 dB loss. The efficiency of this conversion is frequency dependent, which makes additional problems for frequency CVI spectra measurement. Sound intensity after piezocrystal is rather low and not very well defined. Each piezocrystal has unique efficiency. Then, pulse propagates through the delay rod and acoustic impedance rod and partially reflects from the sensor-liquid surface. This changes amplitude of pressure again. As a result, we do not know exact pressure at the point of the measurement.

Colloid vibration current can be presented in the simplified form:

$$\mathrm{CVI} = C\zeta\nabla PG(\varphi, a)Z_{\mathrm{dis}}/(Z_{\mathrm{dis}} + Z_{\mathrm{rod}}) \tag{48}$$

where C is a geometry calibration constant that characterizes complex distribution of the electric and sound fields near the electrodes surfaces, the multiplier with acoustic impedances of the dispersion $\boldsymbol{Z}$ and impedance rod Z characterizes reflection on the probe surface, function G is defined with Eq. 47.

Neither C nor P are known. In order to exclude them, we use the calibration procedure described below.

In order to eliminate unknown constants C and P, we use calibration with Ludox at 10%wt diluted with KCl 10^{-2} mol/L. These silica particles have ζ-potential−38 mV at pH 9.3. CVI value for this colloidal silica can be expressed as follows:

$$\mathrm{CVI}_{\mathrm{sil}} = C\zeta_{\mathrm{sil}}\nabla PG(\varphi_{\mathrm{sil}}, a_{\mathrm{sil}})Z_{\mathrm{dis.sil}}/(Z_{\mathrm{dis.sil}} + Z_{\mathrm{rod}}) \tag{49}$$

From this equation, we can calculate unknown C and P and use them for calculating CVI for other samples:

$$\mathrm{CVI} = \mathrm{CVI}_{\mathrm{sil}}\zeta/\zeta_{\mathrm{sil}}G(\varphi, a)/G(\varphi_{\mathrm{sil}}, a_{\mathrm{sil}})Z_{\mathrm{dis}} \times (Z_{\mathrm{dis.sil}} + Z_{\mathrm{rod}})/(Z_{\mathrm{dis}} + Z_{\mathrm{rod}})Z_{\mathrm{dis.sil}} \tag{50}$$

Eq. 50 can be used for calculating either ζ-potential only from the magnitude of the CVI.

In addition, DT,-300 measures a phase of the CVI signal. This phase yields particle size information. In the case of a single frequency, this measurement provides only a mean particle size. In the case of the multiple frequencies, more detailed information about particle size distribution is available. However, according to our experience, acoustic spectroscopy is much more suitable for characterizing the particle size distribution (55).

Titration Protocol

Electroacoustic ζ-potential probe offers a very simple and fast way to perform electrochemical characterization of

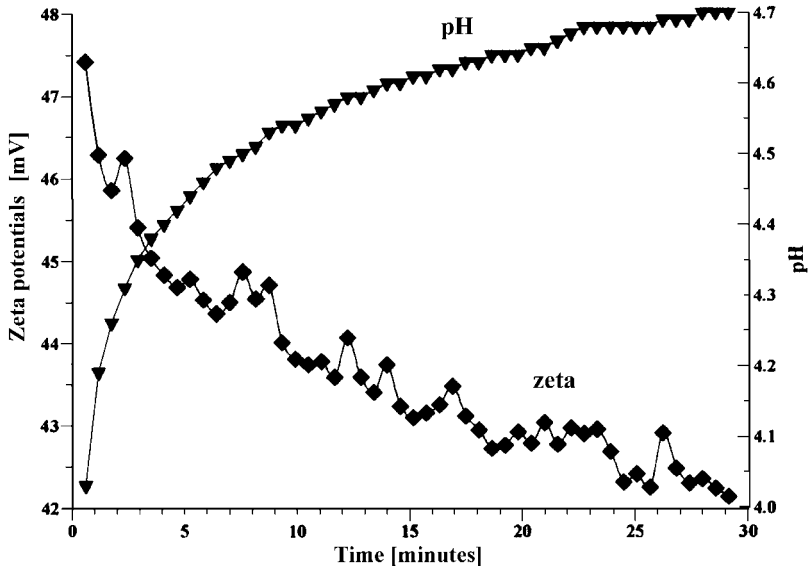

Fig. 16 Equilibration of zirconia slurry (3%vl).

the surface. Software of DT-300 has several optional titration protocols for running two burettes. These burettes are able to inject chemicals with increments as low as 0.2 microliter.

The most common is pH titration. The user should specify maximum and minimum pH, number of points, number of sweeps and direction. This software assumes 1 N acid and base. In addition, users can change equilibration time, tolerance, sample volume, etc.

Equilibration time is a very important parameter. Titration makes sense only if it follows the equilibrium root. Some systems exhibit a very long equilibration time. A good example is a concentrated zirconia dispersion. Fig. 16 shows evolution of the ζ-potential and pH of the 3%vl zirconia dispersion in time. It is seen that equilibration time is about 30 minutes. For comparison, silica Ludox reaches equilibrium in a fraction of a minute. A typical equilibrium titration of the silica Ludox at 10%wt is shown in Fig. 17. It is clear that it is almost impossible to make a similar equilibrium titration for zirconia because it takes a lot of time.

There is another type of titration when a user adds a certain amount of reagent with a certain increment. It is called ''ml protocol'' in the DT software. The user specifies a total amount of the injected substance and number of points. Burette automatically injects this substance and

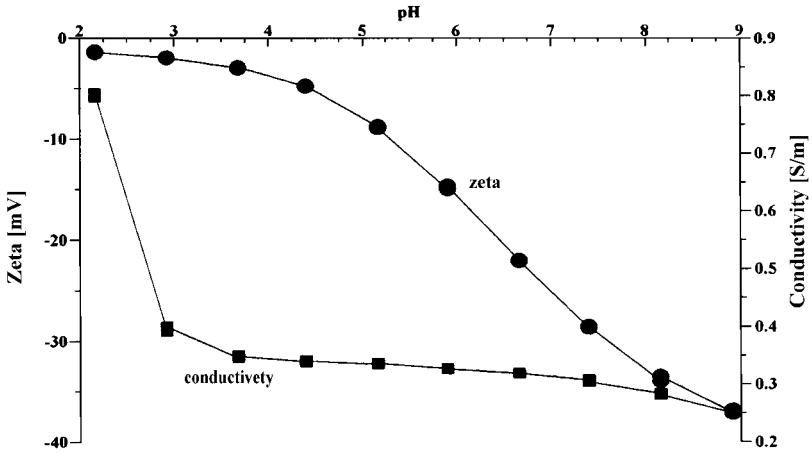

Fig. 17 Typical pH titration. Sample is silica Ludox at 10%wt.

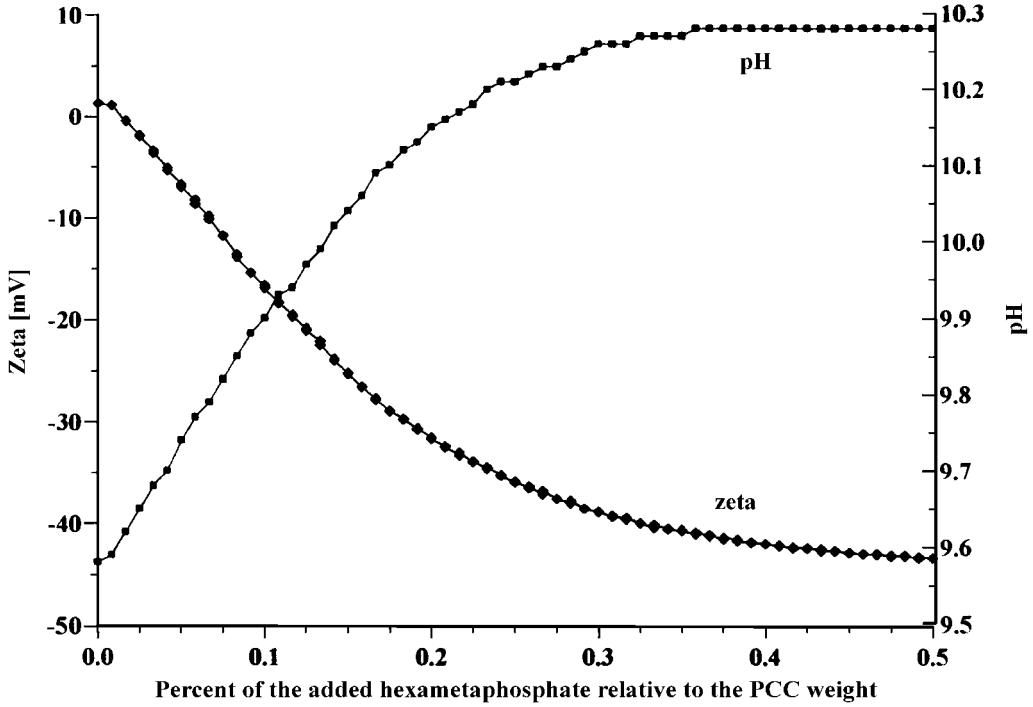

Fig. 18 Titration of precipitated calcium carbonate with hexametaphosphate.

waits the specified equilibration time, and then the CVI sensor measures ζ-potential. In addition, DT-300 monitors pH and temperature continuously. A typical titration of this F18 kind is shown in Fig. 18. It has been made using hexametaphosphate with precipitated calcium carbonate at 3%vl.

The most complicated problem for titrating concentrated dispersions is mixing. Mixing is absolutely necessary for the successful titration. However, it becomes hard to mix, especially in the ranges of instability.

We know only one solution to this problem: pumping sample through the measuring chamber. Traditional propeller mixers do not work with the pastelike samples. Pumping makes it possible to involve a complete sample whereas propellers perform mixing only in their own vicinity. Pumping functions properly only when the measuring chamber does not have hydrodynamically stagnated spaces. Otherwise, deposit built up in these spaces can interrupt the flow.

APPLICATIONS

Emulsions, Microemulsions, and Latex

There are many instances of successful characterization of the particle size distribution and zeta (ζ) potential of emulsion droplets. There are two quite representative reviews of these experiments published by McClements (4) (acoustics) and Hunter (12) (electroacoustics).

We present here results of some recent investigations of the various factors that affected stability, size, and ζ-potential of the emulsion droplets. One of the most important parameters that affects emulsions is the surfactant concentration. Fig. 19 illustrates this for 6% by weight F19 reverse water-in-oil emulsion The oil phase was simply commercially available oil diluted twice with paint thinner in order to reduce the viscosity of the final sample. This figure shows the attenuation spectra for the three samples. The pure oil phase sample exhibited the lowest attenuation. It is important to measure the attenuation of the pure dispersion medium when a new liquid is evaluated. In this particular case, the intrinsic attenuation of the oil phase was almost 150 dB/cm at 100 MHz, which is more than seven times higher than for water. This intrinsic attenuation is a very important contribution to the attenuation of ultrasound in emulsions. It is the background for characterizing the emulsion system.

The emulsion without any added surfactant was measured twice with two different sample loads. As the water content was increased, the attenuation became greater in magnitude. For this system, the attenuation was found to be quite stable with time. Addition of 1% by weight AOT (sodium bis 2-ethylhexyl sulfosuccinate) changed the atte-

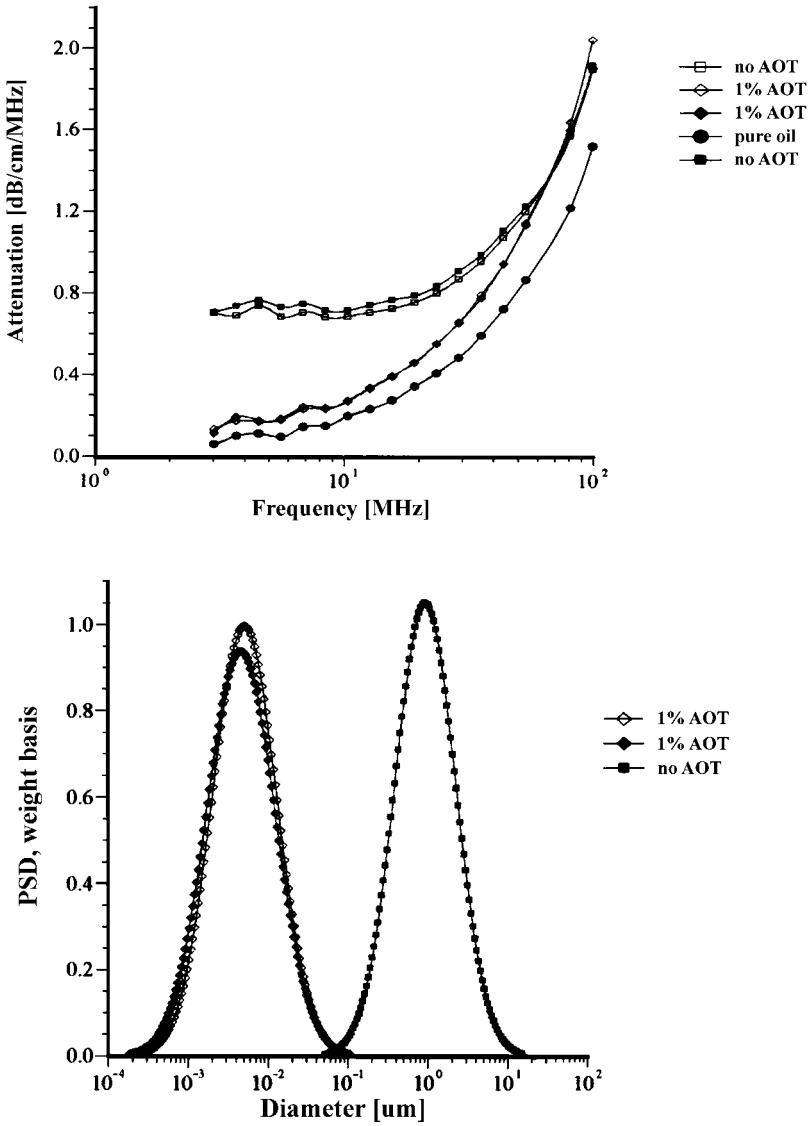

Fig. 19 Attenuation and droplet size distribution of 6% water in car oil emulsion with and without AOT.

nuation spectrum dramatically. This new emulsion with modified surface chemistry was measured twice in order to check reproducibility. The corresponding particle size distribution is shown in Fig. 19 and indicates that the AOT converted the regular emulsion into a microemulsion as one could expect.

These experiments proved that the acoustic technique is capable of characterizing the particle size distribution of relatively stable emulsions. In many instances, emulsions are found not to be stable at the dispersed volume concentration required to obtain sufficient attenuation signals (usually above 0.5 vl%). Hazy water in fuel emulsions (diesel, jet fuel, gasoline) may exist at low water concentrations of only a few 100 ppmv (0.01 vl%) of dispersed water. Attempts at characterizing these systems without added surfactant resulted in unstable attenuation spectra. Water droplets were discovered to separate from the bulk emulsion and settle out on the chamber walls. This problem is less important for thermodynamically stable microemulsions, which are discussed below (64).

The mixture of heptane with water and AOT is a classic three-component system that has been widely studied due to a number of interesting features it exhibits. This system forms stable reverse microemulsions (water in oil) without the complication introduced by the addition of co-surfactant, such as alcohol, required by many other reverse mic-

roemulsion systems. This simplification makes the alkane/water/AOT system a model for studying reverse microemulsions.

There have been many attempts to measure the droplet size of this microemulsion. Several different techniques were used: PCS (69–74), classic light scattering (71, 73, 74), the neutron scattering SANS (76–78) and SAXS (70, 79, 80), ultracentrifugation (72, 75, 81), and viscosity (70, 72, 75). It was observed that the heptane/water/AOT microemulsions have water pools with diameters ranging from 2 nanometers up to 30 nanometers. The water drops are encapsulated by the AOT surfactant so that virtually all of the AOT is located at the interface shell. The size of the water droplets can be conveniently altered by adjusting the molar ratios of water to surfactant designated as R ($[H_2O]$/[AOT]). At low R values ($R \leq 10$), the water is strongly bound to the AOT surfactant polar head groups and exhibits unique characteristics different from bulk water. At higher water ratios ($R > 20$), free water is predominant in the swollen reverse micellular solutions, and at approximately $R = 60$, the system undergoes a transition from a transparent microemulsion into an unstable turbid macroemulsion. This macroemulsion separates on standing into a clear upper phase and a turbid lower phase.

Despite all these efforts, there still remain questions regarding the polydispersity of the water droplets, and few studies are available above the R value of 60 where a turbid macroemulsion state exists.

Acoustic spectroscopy offers a new opportunity for characterizing these complicated systems. Details of this experiment are presented elsewhere (64). In all cases, the reported R values are based on the added water and were not corrected for any residual water that may have been in the dried AOT or heptane solvent. Karl Fischer analysis of the AOT-heptane solutions before the addition of water resulted in an R value of 0.4. This amount was considered to be negligible.

Measurements were made starting with the pure water and heptane and then the AOT-heptane sample with no added water ($R = 0$). The sample fluid was removed from the instrument cell and placed in a glass bottle with a Teflon cap. Additional water was titrated, and the microemulsion was shaken for 30 seconds before being placed back into the instrument cell. The sample cell contained a cover to prevent evaporation of the solvents. The samples were visually inspected for clarity and rheological properties for each R value. These steps were repeated for increasing water weight fraction or R ratios up to $R = 100$. At $R \geq 60$, the microemulsions became turbid. At $R > 80$, the emulsions became distinctly more viscous.

The weight fractions of the dispersed phase were calulated for water only without including the AOT. Each trial run lasted approximately 5–10 minutes with the temperature varied from 25–27°C. A separate microemulsion sample for $R = 40$ was made up a few days prior to the first study. For the $R = 70$ sample, a second acoustic measurement was made with the same sample used for the first study. The complete set of experiments for water, heptane, and the reverse microemulsions from $R = 0$ to 100 was repeated to evaluate the reproducibility.

Attenuation spectra measured in the first run up to $R = 80$ are presented in Fig. 20. The results for $R = 90$ F20
and $R = 100$ are not reported because they were found to vary appreciably. As the water concentration is increased, the attenuation spectrum rises in intensity, and there is a distinct jump in the attenuation spectrum from $R = 50$ to $R = 60$ in the low frequency range. This discontinuity is also reflected in the visual appearance as at $R = 60$, the system becomes turbid. The smooth shape of the attenuation curve also changes at $R > 60$. The stability and reproducibility of the system was questioned due to the irregular nature of the curve, so the experiment at $R = 70$ was repeated and gave almost identical results. An additional experiment was run at $R = 40$ for a separate microemulsion prepared a few days earlier. This showed excellent agreement with the results for freshly titrated microemulsion. For R values > 70, an increase in the viscosity and a decrease in the reproducibility of the attenuation measurement were observed. This could be due to the failure of the model for this system as a collection of separate droplets at high R values.

The two lowest attenuation curves in Fig. 20 correspond to that of the two pure liquids: water and heptane. This attenuation is associated with oscillation of liquid molecules in the sound field. If these two liquids are soluble in each other, the total attenuation of the mixture would lie between these two lowest attenuation curves. But it can be seen that the attenuation of the mixture is much higher than that of the pure liquids. The increase in attenuation, therefore, is due to this heterogeneity of the water in the heptane system. The extra attenuation is caused by motion of droplets, not separate molecules. The scale factor (size of droplets) corresponding to this attenuation is much higher than that for pure liquids (size of molecules).

The current system contains a third component—AOT. A question arises on the contribution of AOT to the measured attenuation. In order to answer this question, measurements were done on a mixture of 6.1%wt. AOT in heptane ($R = 0$). It is the third smallest attenuation curve in Fig. 20. It is seen that attenuation increases somewhat due to AOT. However, this increase is less than the extra attenuation produced by water droplets. The small increase in attenuation is attributed to AOT micelles that are

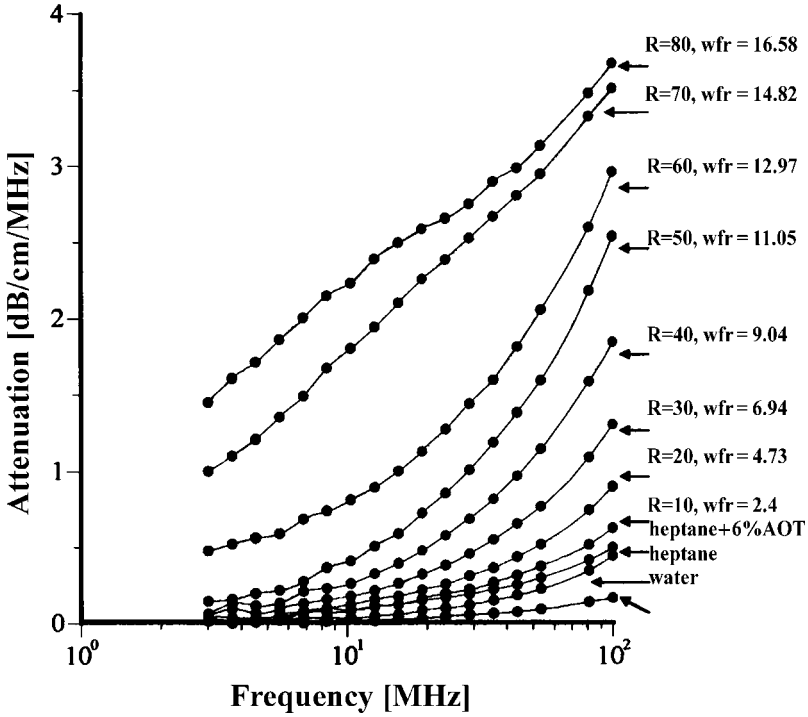

Fig. 20 Attenuation spectra of water in heptane microemulsion with 6% AOT.

known to form without the addition of water. Unfortunately, thermal properties of the AOT as a liquid phase are not known, and the size of these micelles could not be calculated.

The particle size distributions corresponding to the measured attenuation spectra are presented in Fig. 21. It can be seen that the distribution becomes bimodal for $R \geq 60$, which coincides with the onset of turbidity. It is to be noted that such a conclusion could not easily be arrived at with other techniques. There is a feature of this system, however, that can be compared with independent data from literature: mean particle size increases with R almost in a linear fashion. This dependence becomes apparent when mean size is plotted as a function of R as in Fig. 22.

It is seen that mean particle size measured using acoustic spectroscopy is in good agreement with those obtained independently using the neutron scattering (SANS) and x-ray scattering (SAXS) techniques (43, 48, 54) for R values ranging from 20 to 60. A simple theory based on equipartition of water and surfactant can reasonably explain the observed linear dependence.

At R = 10, the acoustic method gave a slightly larger diameter than expected. This could be due to the constrained state of the ''bound water'' in the swollen reverse micelles. The water under these conditions may exhibit different thermal properties than the bulk water used in the particle size calculations. Also at the low R values ($R \leq 10$ or $\leq 2.4\%$ water), the attenuation spectrum is not very large as compared to the background heptane signal. Contribution of droplets to attenuation spectrum then may become too low to be reliably distinguished from the background signal coming from heptane molecules and AOT micelles.

There have been many successful experiments characterizing latex systems using both acoustics and electroacoustics. For instance, Allegra and Hawley (28) measured polystyrene latex. There is another successful application, this time with neoprene latex, which is described elsewhere (33).

Successful examples of characterizing latex systems are possible only when thermal expansion coefficients are known. Unfortunately, this parameter is not known for many latex polymers. This problem becomes even more complicated for latex systems than for emulsions because the value of the thermal expansion depends strongly on the chemical composition of the polymer. Fig. 23 illustrates this fact for several ethylene copolymers with different ethylene contents. Variation of the ethylene content from 5% to 10% was found to cause significant changes in attenuation spectra. This change is associated with the thermal expansion coefficient, but not the particle size.

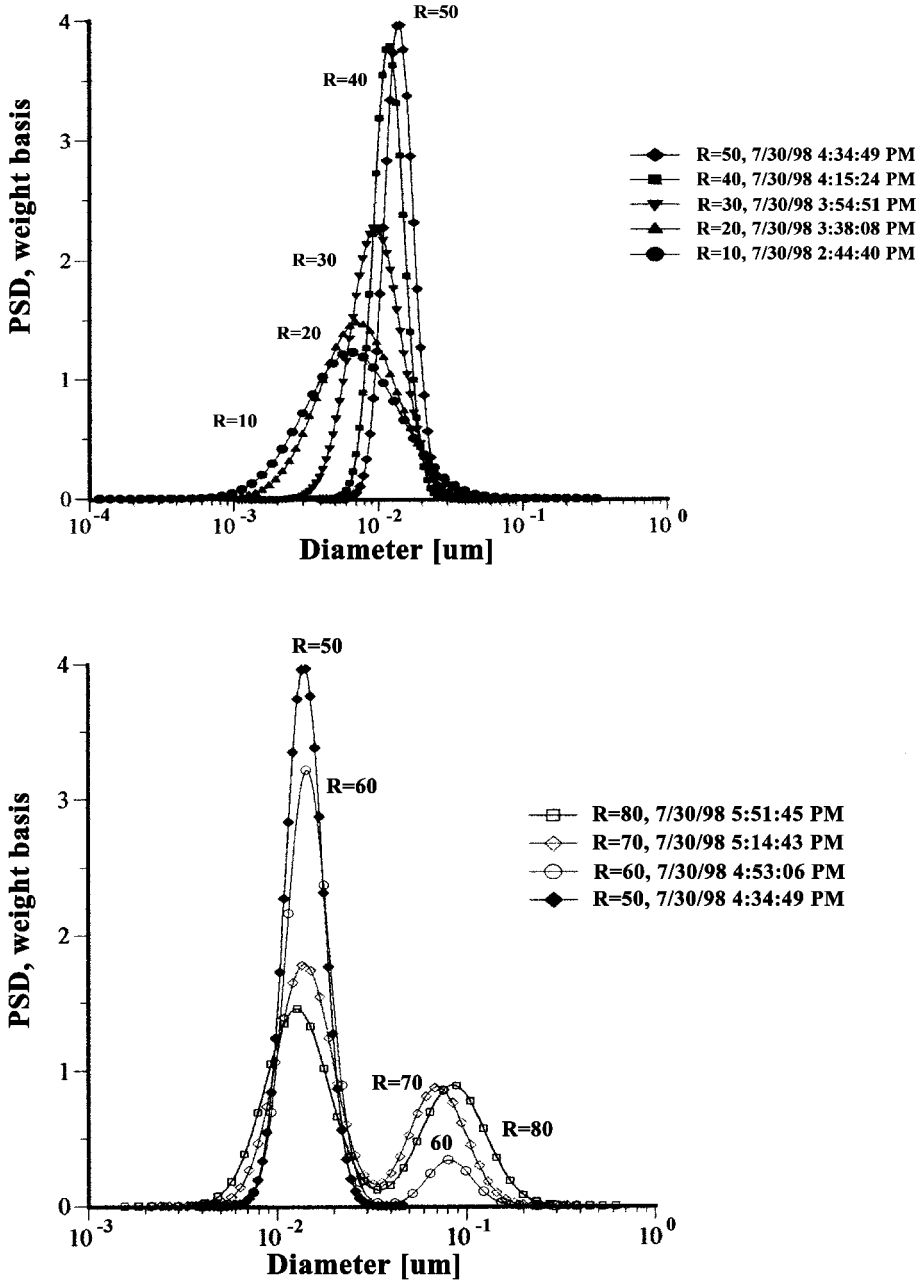

Fig. 21 Water droplets size distribution in heptane with 6% AOT at different water content.

The uncertainty related to the thermal expansion coefficient had been a major problem and kept latex systems the most complicated system for acoustics. The situation changed dramatically 6 months ago. We have developed new software that treats the thermal expansion coefficient of particles as the adjustable parameter and calculates it from attenuation spectra. This approach turned out to be very productive. We tested it with several latex dispersions produced by Dow Chemicals. These latices were different in terms of rheological properties (soft-to-hard ratio) because of variations in synthesis. Thermal expansion coefficient calculated from attenuation spectra was in good correlation with the known soft-to-hard ratio (Fig. 24). This new approach made latex even easier for acoustic characterization than solid particles.

F24

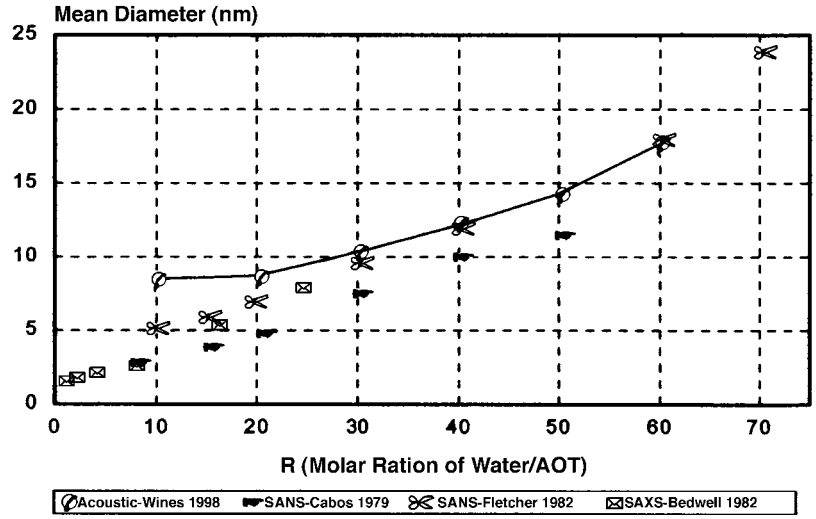

Fig. 22 Mean diameter of water droplets in heptane with 6% AOT measured with different techniques.

In addition to the particle size characterization, the new ζ-potential probe DT-300 is able to characterize ζ-potential of latices. For a long time, it has been impossible to do using electroacoustics because of the low density contrast. The new DT instruments have overcome this obstacle. It became possible because of the true pulse technique. Electroacoustic signal coming from latex is very weak but still measurable. It simply takes more

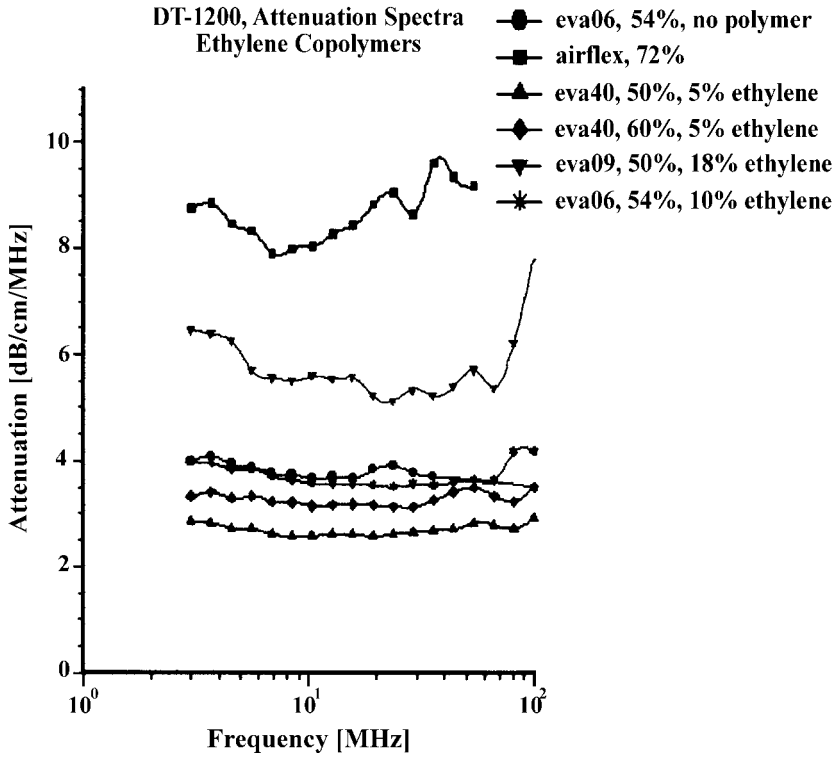

Fig. 23 Attenuation spectra of several latex dispersions with different ethylene contents.

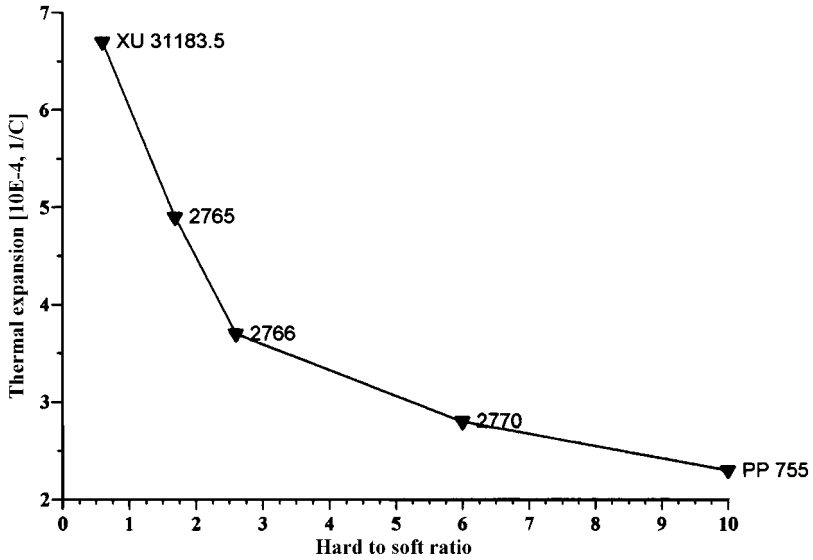

Fig. 24 Thermal expansion coefficient calculated from attenuation spectra for several latices with different rheological properties.

pulses to accumulate and reach the desirable signal-to-noise ratio. We already have many successful measurements of ζ-potential in concentrated latex dispersions with density contrast as low as 0.01.

Solid Particles: Alumina, Barium Titanate, Zinc Sulfate, Rutile

We use a notion of the ''solid particles'' for all dispersions that exhibit no ''thermo losses'' in attenuation spectra. Usually, it is rigid particles with substantial density contrast, like oxides, graphite, carbon black, etc. Even organic pigments with rather low density contrast attenuate sound through the ''viscous mode.'' Density of the particles is the key input parameter common for all these systems. Many examples of these systems were mentioned before. Here, we give several more applications.

The first example illustrates again accuracy of acoustics. This time, it is done with four different alumina slurries produced by Sumitomo. Fig. 25 shows attenuation spectra and corresponding particle size distributions. Table 4 gives median size obtained with acoustics, provided independently by manufacturer. It is seen that acoustics yields results that are very close to the independent manufacturer data.

Another example of the good reproducibility is shown in Fig. 26 for $BaTiO_3$ slurry. This slurry is rather complicated for characterization because the chemical composition of the surface depends on the liquid. As a result, dilution affects value of ζ-potential (Fig. 27). This slurry is a good example, illustrating importance of the ζ-potential measurement in concentrated dispersion. Complexity of the surface follows from the pH titration as well (Fig. 27). It is seen that the slope of the curve changes at the high pH. It looks like the total curve is a superposition of the two curves with two different iso-electric points. The total curve exhibits only one iso-electric point because the number of sites with the lower isoelectric point exceeds the number of sites with the iso-electric point at high pH.

We showed several times bimodal PSDs, which were calculated from the attenuation spectra for various dispersions. The question arises how could we decide that particular dispersion has bimodal PSD. We can prove that attenuation spectra contains enough information for determining not only median size, but the width of distribution and even bimodality. For instance, Fig. 28 shows attenuation spectra measured for ZnS slurry and theoretical attenuation calculated for the best lognormal and bimodal particle size distributions. These PSD are the best in terms of the minimum fitting error that can be achieved with PSD of the particular type. It means that there is no lognormal PSD that would provide the better fit to the measured data as the given one. Failure of lognormal PSD to fit experimental data allows us to add more adjustable parameters fitting bimodal PSD instead of lognormal. One can see in Fig. 29 that bimodal PSD yields theoretical attenuation that fits experiment much better. It leaves practically no room for improvement, which means that we cleared experimental information and have no right to increase the number of adjustable parameters.

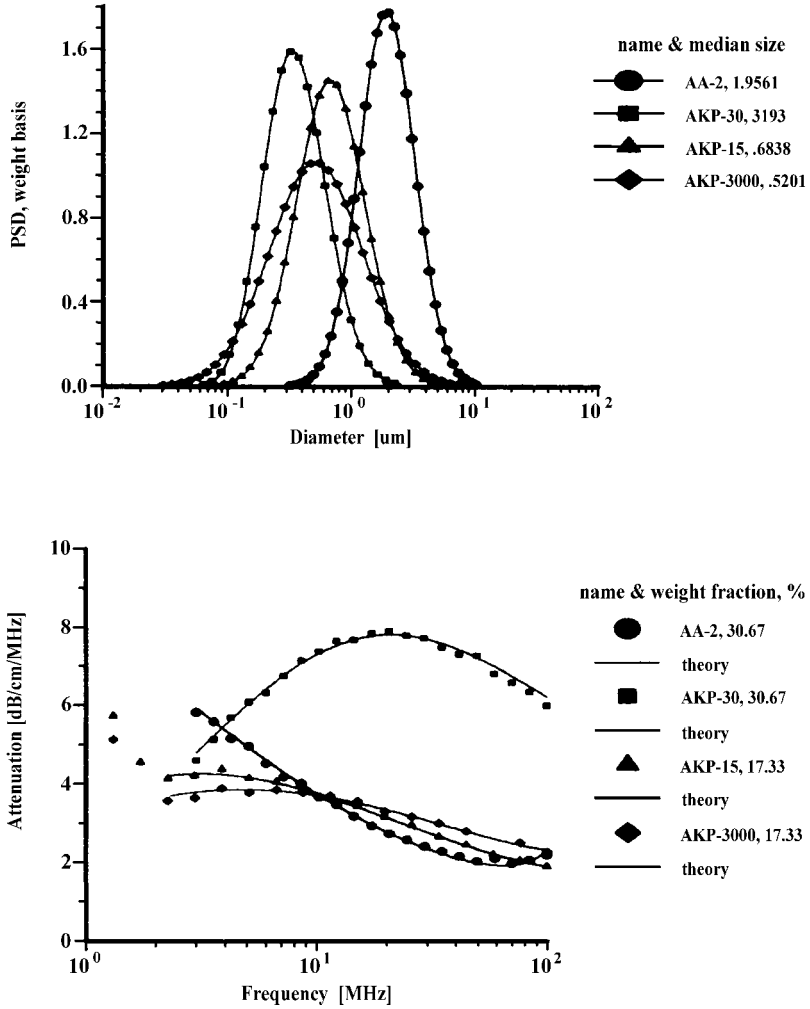

Fig. 25 Attenuation spectra and PSD for various alumina Sumitomo.

Attenuation spectra reflect variation of the particle size that occurs due to the aggregation. We show here dependence of the attenuation spectra on the pH for two different dispersions: ZnS (Fig. 29) and TiO_2 (Fig. 30). It is seen that attenuation spectra for ZnS remain the same for all pH even in the vicinity of the iso-electric point. For some reason these parcels remain stable even for low ζ-potential.

The situation with rutile is very different. Attenuation spectra near the iso-electric point are very different compared to the high pH stability range. This reflects aggregation of the rutile particles and transformation from lognormal to bimodal PSD (10).

Table 4 Median particle size in microns

	Acoustics	Manufacturer
AKP-15	0.684	0.7
AKP-30	0.319	0.3
AKP-3000	0.520	0.5
AA-2	1.956	2

Surfactant Titration: Kaolin, Calcium Carbonate

Electroacoustic titration using ζ-potential probe offers a fast and simple way to determine an optimal dose of the surfactant for stabilizing particular dispersion. One of the examples is shown in Fig. 18 for precipitated calcium carbonate. We show here more results obtained with several

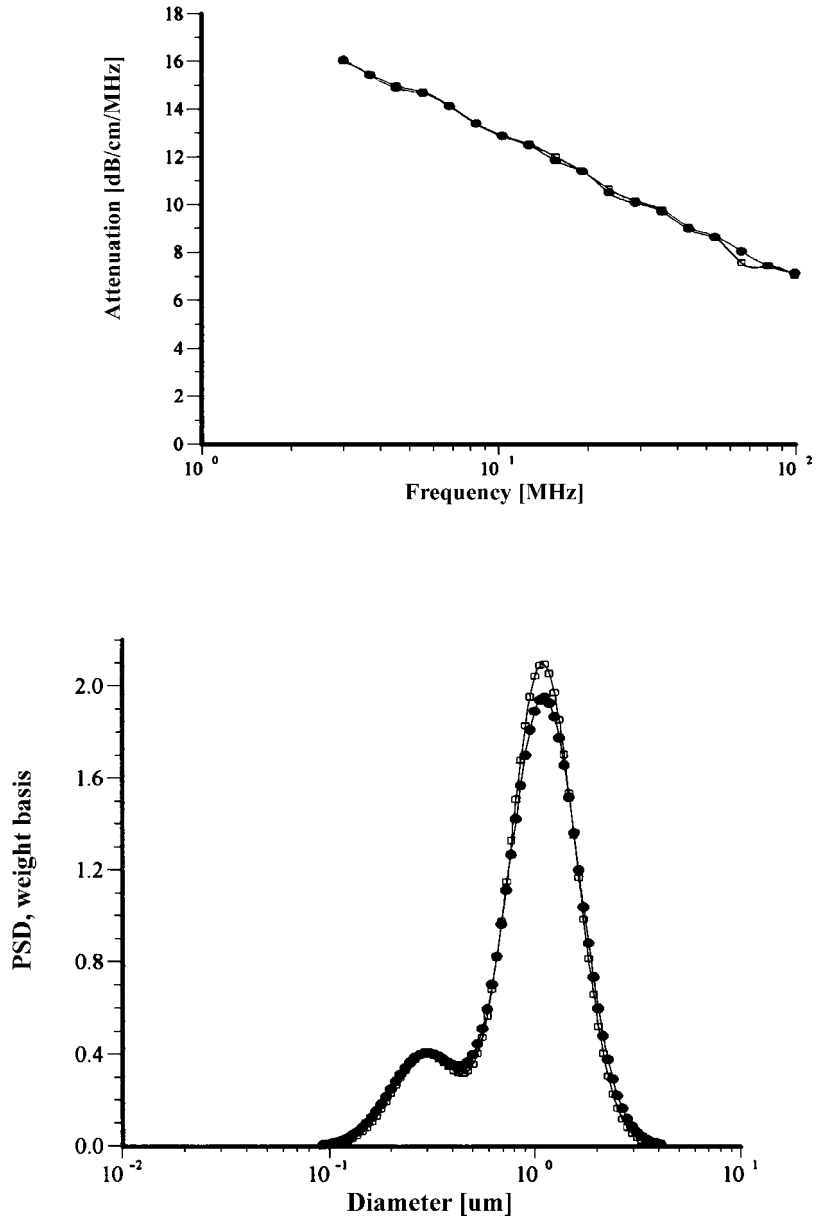

Fig. 26 Attenuation spectra and PSD of 50%wt $BaTiO_3$ slurry.

kaolin slurries. These data have been published elsewhere (56).

The kaolin used in this study was obtained from the Engelhard Corporation and was categorized as a fine-grade crude with high iron content. Kaolin, in general, is defined by platelet crystals in which one of the dominant faces is made up of octahedral alumina and the other consists of tetrahedral silica. Particle aggregation thereby occurs when the negative platelet faces (negative due to isomorphic substitutions) interact with positive charge sites on the crystal edges (due to pH sensitive aluminol and silanol sites). The two dispersants used to study this aggregation phenomenon were both common to the kaolin industry and consisted of 2.0 modulus silicate (Occidental Chemical Corporation) and sodium hexametaphosphate, SHMP (Albright and Wilson Americas Inc.). The 2.0 modulus was in reference to the average distribution of silicate species present (linear dimer, 3-D dimer, and trimer). The 2.0 modulus silicate was expected to interact with the positive edge sites of the kaolin platelet through

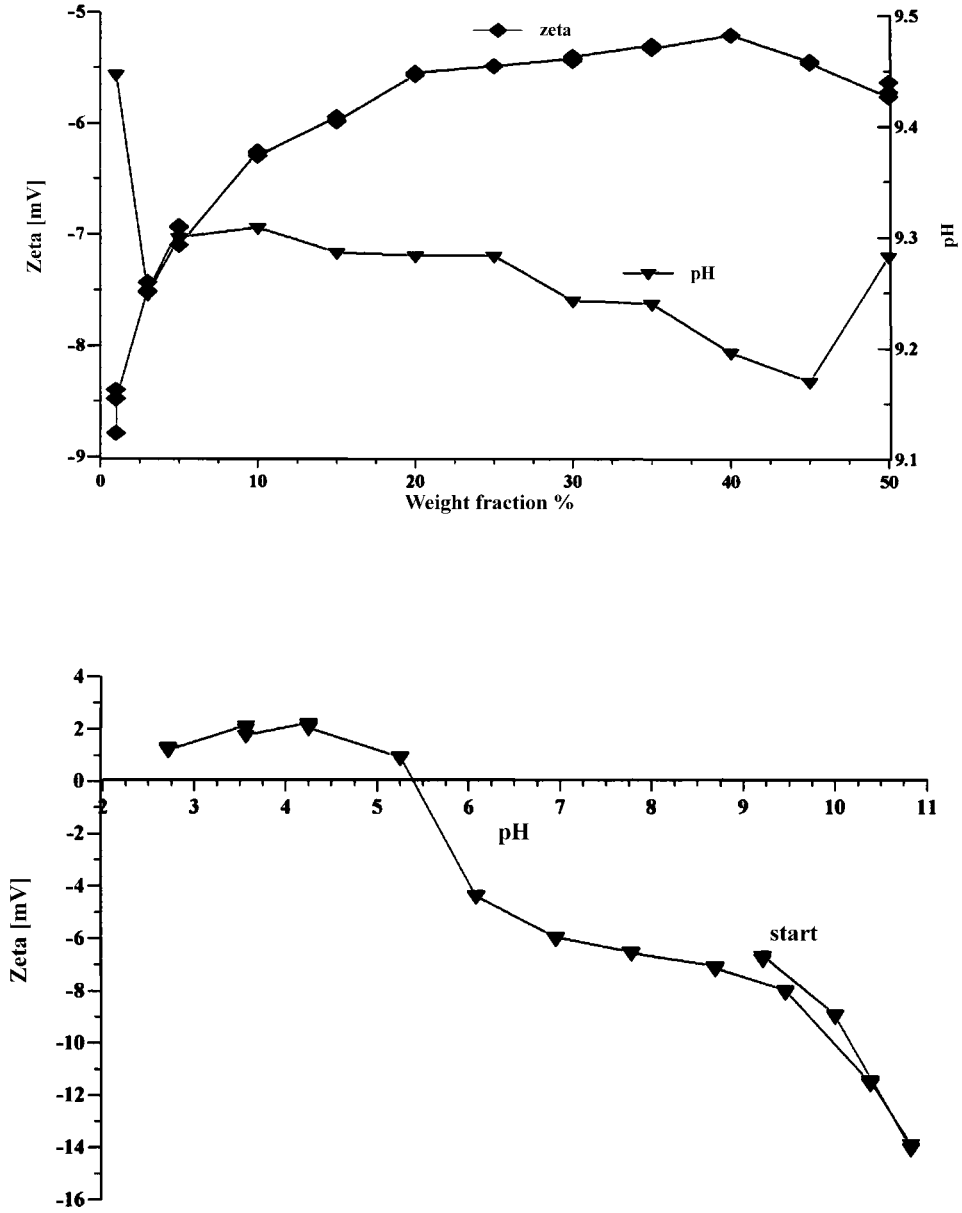

Fig. 27 ζ-Potential vs. weight fraction and ζ-potential vs. pH for $BaTiO_3$ slurry.

electrostatic interactions. The SHMP was a cyclic polyphosphate, which is expected to adsorb to the positive charges along the kaolin edges through both electrostatic and covalent bonding.

Titration of the kaolin EC1 slurry with hexametaphosphate revealed a strong pH dependence. Titration curve shifts depending on the initial pH value. It is illustrated in Fig. 31 for both ζ-potential and pH. It is not surprising because pH is a strong charge factor for kaolin. For instance, Fig. 32 presents pH titration of the 40%wt EC2 kaolin slurry. It is clear that ζ-potential goes up with pH.

Titration of EC1 kaolin slurry is a good example, showing importance of various factors, not only dispersant concentration. It is convenient to illustrate this complex titration using 3-D fingerprint. Fig. 33 shows this fingerprint for kaolin EC1 titration.

Titration of EC1 slurry illustrates existence of the optimum concentration of dispersant. One can see that increase of the hexametaphosphate concentration leads

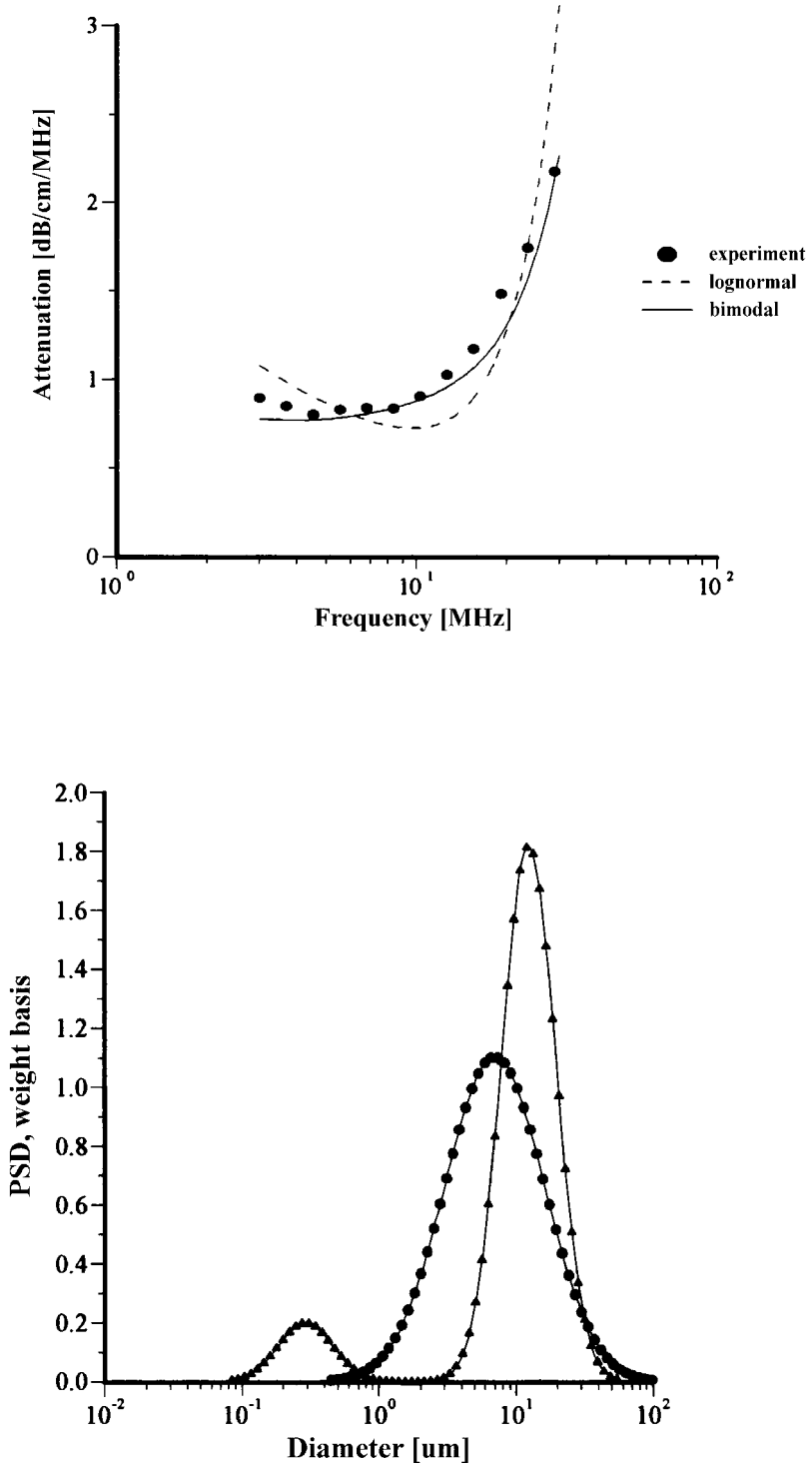

Fig. 28 Attenuation spectra and PSD of 17.4%wt ZnS slurry.

eventually to decreasing of ζ-potential. In this particular case, it is related to the increasing ionic strength and collapsing double layer.

Dependence of ζ-potential on pH is an additional factor that might be exploited for reaching higher ζ-potential values. From this viewpoint, hexametaphosphate has a

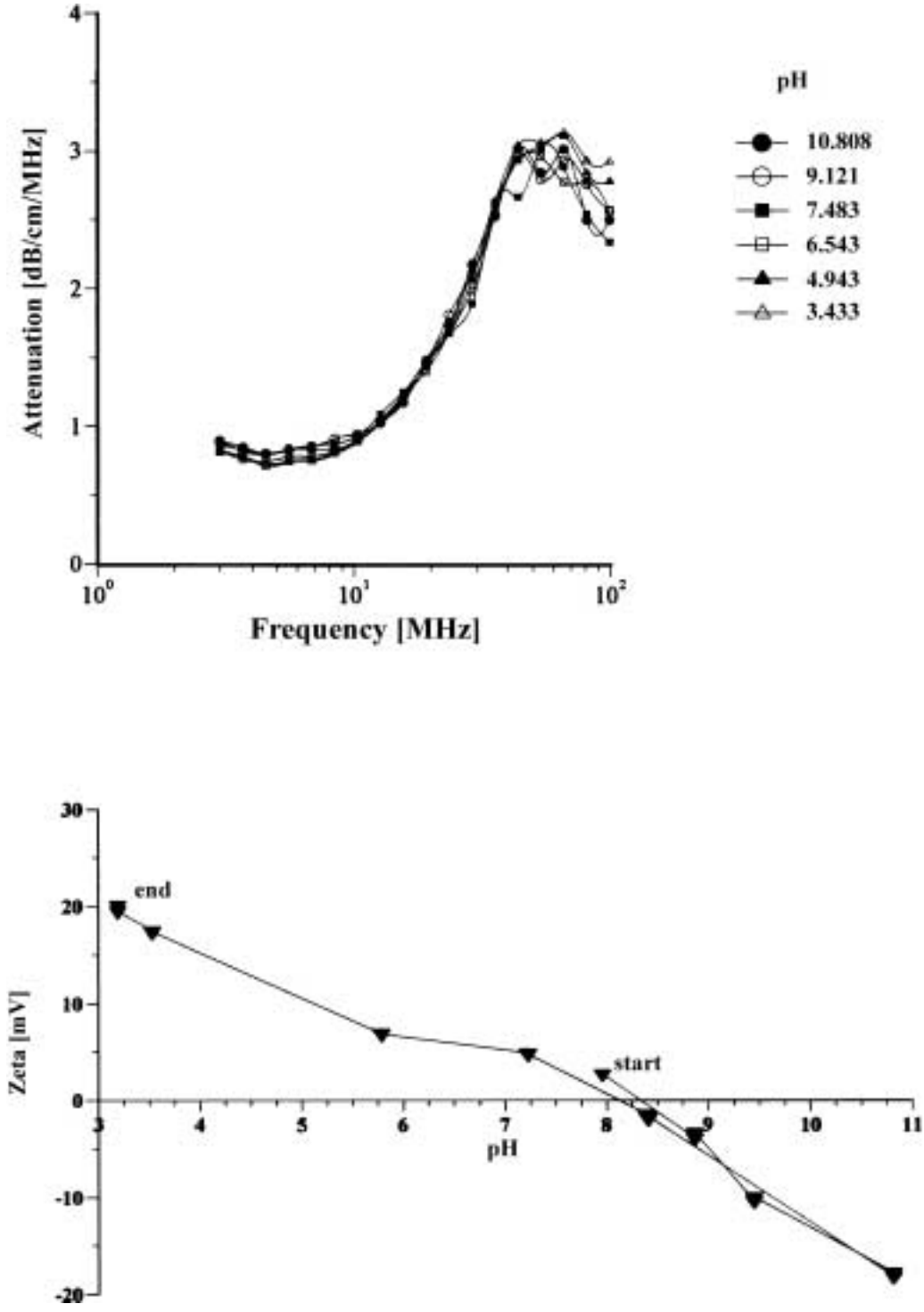

Fig. 29 Attenuation spectra and ζ-potential of 17.4%wt ZnS slurry for different pH.

disadvantage because it reduces pH. Another dispersant, silicate, is more advantageous from the pH viewpoint because its addition to the slurry increases pH, as it is shown in Fig. 34. However, even combined silicate-pH effect is not sufficient to gain ζ-potential values created with hexametaphosphate. Maximum value for silicate ti- F34

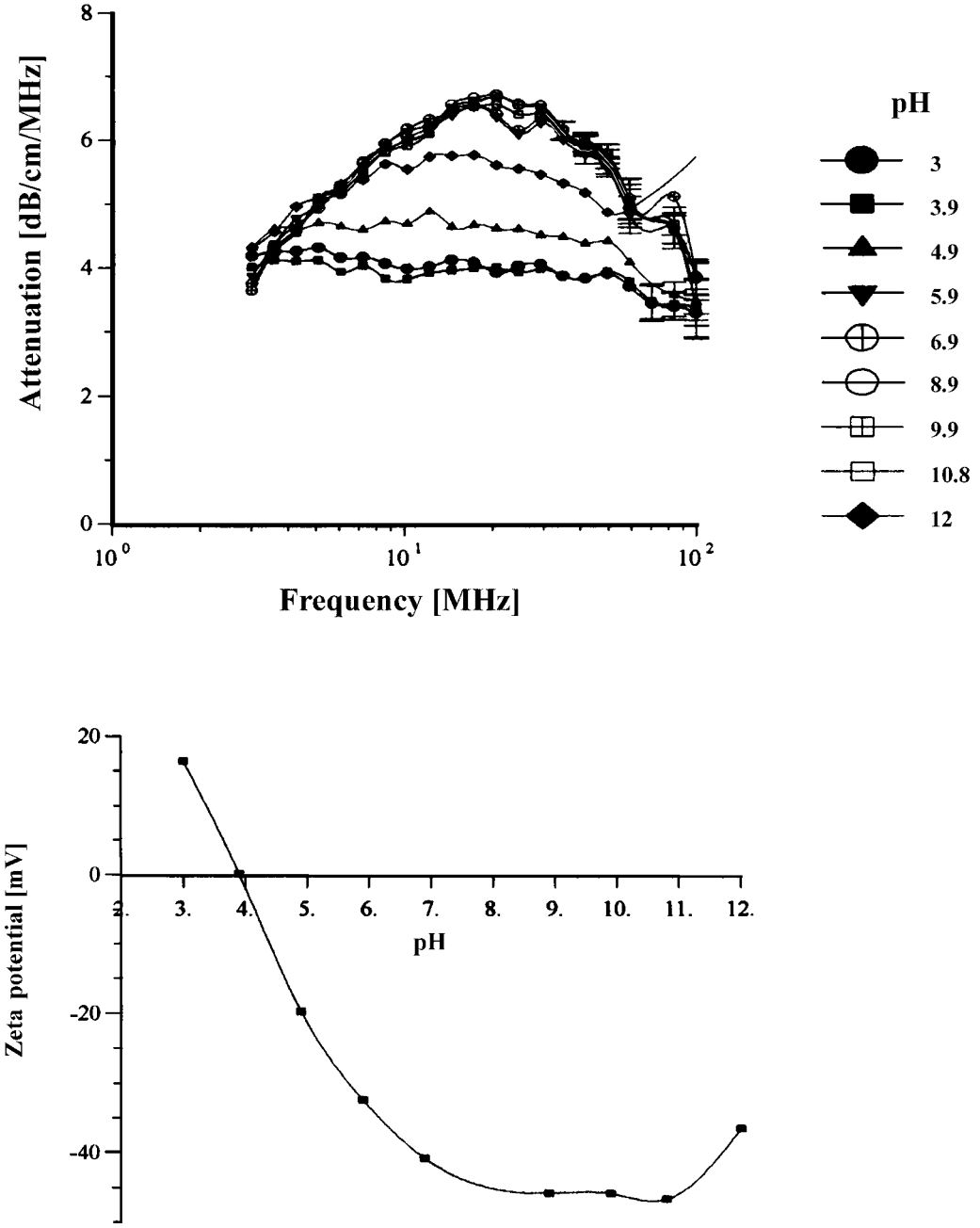

Fig. 30 Attenuation spectra and ζ-potential of 7%vl rutile slurry for different pH.

tration is − 28 mV, whereas hexametaphosphate yields −34 mV at maximum.

Hexametaphosphate is more efficient in terms of optimum amount as well. The maximum value of ζ-potential can be reached adding half as much hexametaphosphate (0.6% by kaolin weight) as silicate (1.3% by kaolin weight).

There is one more factor that affects stability of the kaolin dispersions: it is sonication. Apparently, none of the tested chemical factors (pH, hexametaphosphate, silicate) destroys initial aggregates. These chemical factors create an environment that is potentially beneficial for gaining a full stability, but in order to take advantage of this environment, one should apply a strong agitation that

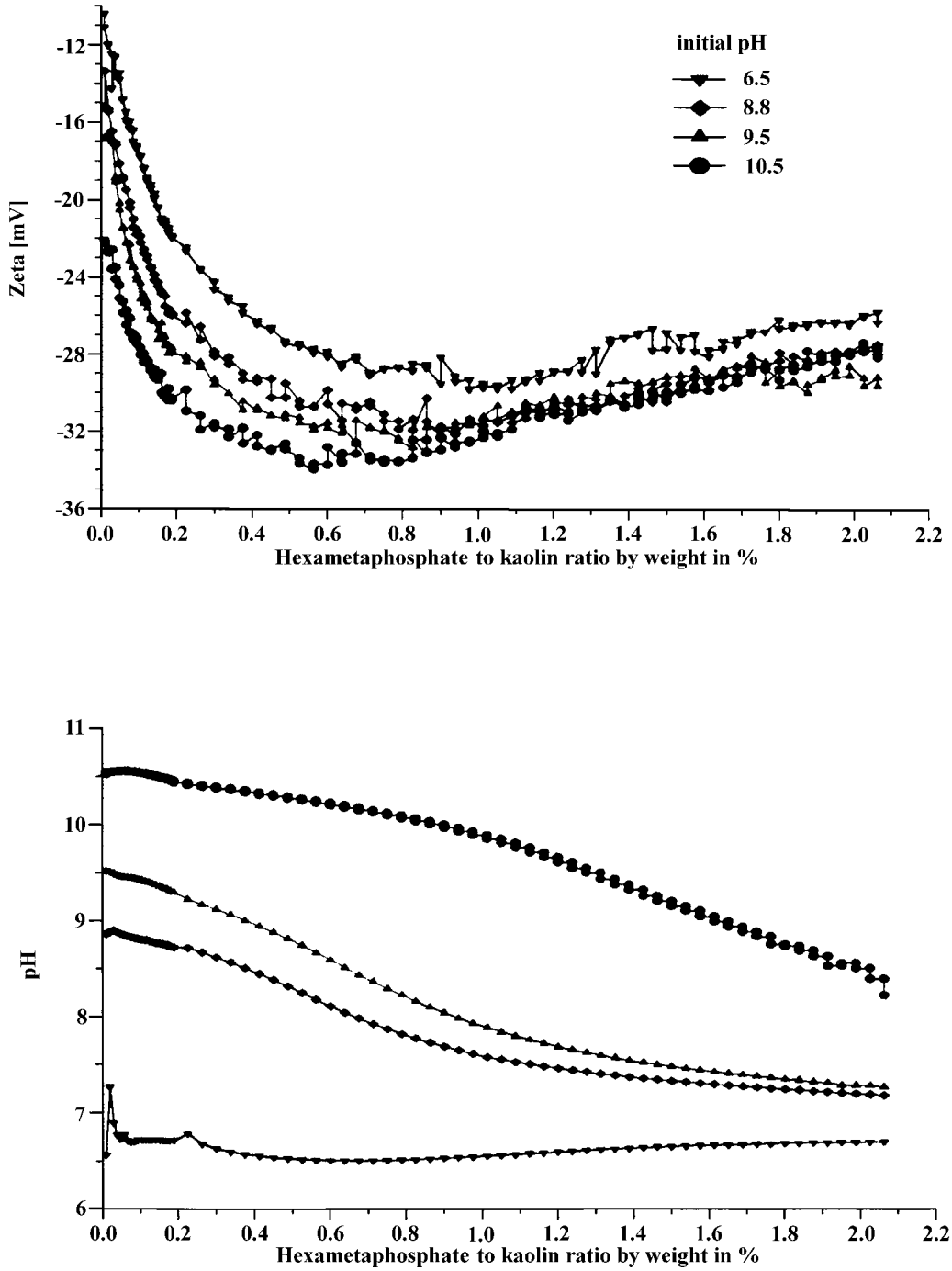

Fig. 31 Titration of the 40%wt kaolin EC1 slurry using hexametaphospate.

would destroy aggregates. It turned out that just mixing does not help. Only powerful sonication is able to break aggregates. This effect is illustrated in Fig. 35. It is seen that sonication causes a large 5 mV jump in ζ-potential value. Actually, it is somewhat misleading. Sonication does not affect surface charge. It creates a new surface and reduces particle size. Appearance of the new surface with the same ζ-potential leads to the larger CVI signal. This larger CVI signal can be interpreted as larger ζ-potential if we keep the same particle size.

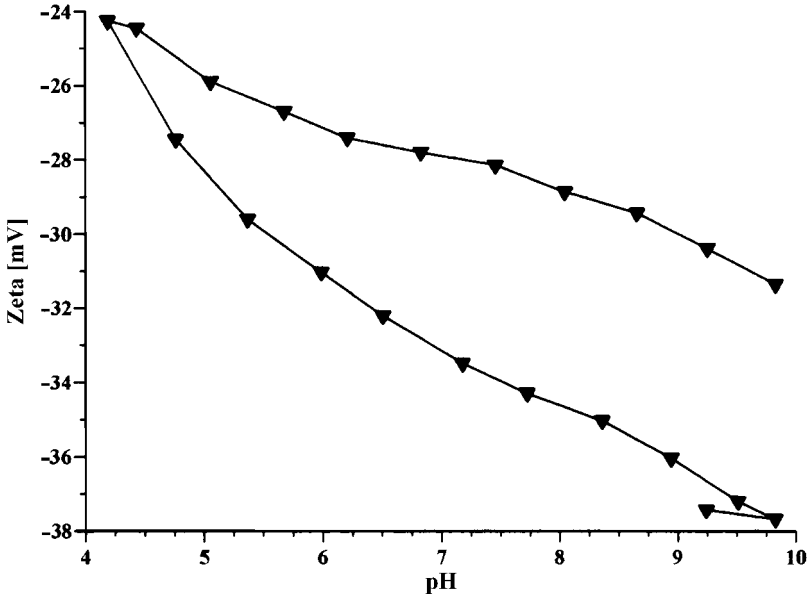

Fig. 32 pH titration of the 40%wt EC2 kaolin slurry.

Mixed Dispersions

There are many important natural and man-made dispersed systems containing a high concentration of more than one dispersed phase. For instance, whole blood contains many different types of cells, paint usually consists of latex with added pigment to provide color, and sunscreen preparations include both an emulsion as well as sun-

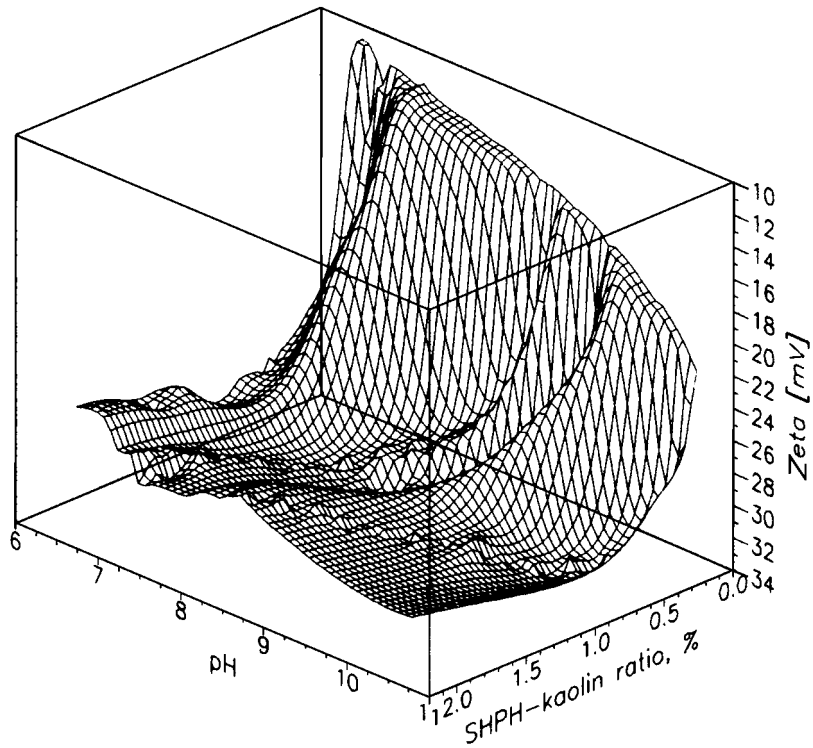

Fig. 33 Titration ζ-pH-hexametaphosphate fingerprint of the 40%wt kaolin EC1 slurry.

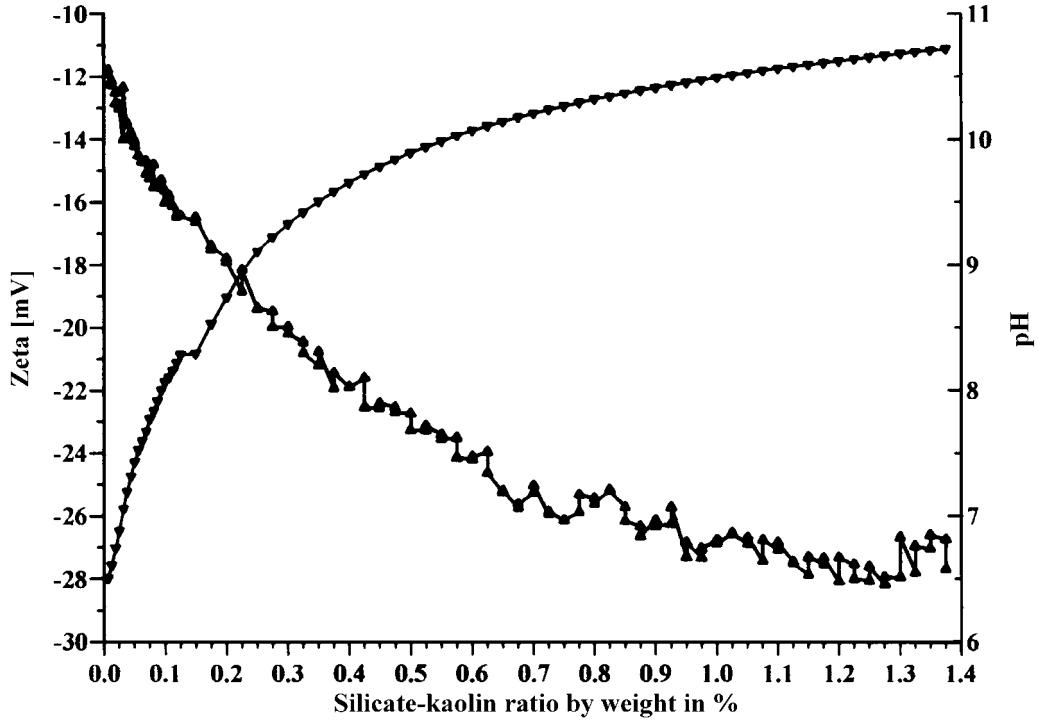

Fig. 34 Titration of 40%wt EC1 kaolin slurry using silicate.

absorbing particles. In many such systems, there is a practical need to determine the PSD of one or more ingredients. In general, light-based techniques are not well suited to provide this information because most optical methods require the sample to be diluted prior to measurement, thereby distorting or destroying altogether the particle size information being sought. Furthermore, most light-based systems cannot handle multiple disperse phases, even in the most dilute case. In contrast, acoustic attenuation spectroscopy (4, 55, 60–64) opens an opportunity to eliminate this undesirable dilution step.

There are at least three quite different philosophical approaches for interpreting these acoustic spectra.

In the simplest "empirical" approach, we forego any size analysis per se and simply observe the measured acoustic attenuation spectra to learn whether, for example, the sample changes with time or if ''good'' or ''bad'' samples differ in some significant respect. Importantly, this empirical approach provides useful engineering solutions even in cases where we know nothing about the physical properties of the sample or whether indeed the sample is adequately described by our theoretical model.

In a more subtle "validation" approach, we assume in advance that we know the correct particle size distribution and furthermore assume the real dispersion conforms to some model. We then use some predictive theory based on this model, as well as the assumed size distribution, to test whether this predicted attenuation matches that actually measured. If the validation fails, it is a very strong indication that the model is inadequate to describe the system at hand.

As an example of this validation approach, consider the case where we construct a mixed system by simply blending two single-component slurries. The PSD of each single-component slurry can be measured prior to blending the mixed system. Because we have control of the blending operation, we know precisely how much of each component is added. If we claim that the combined PSD is simply a weighted average of the individual PSD for each component, we are in effect assuming that there is no interaction between these components. In this case, the prediction theory allows us to compute the theoretical attenuation for this mixed system. If the experimental attenuation spectrum matches the predicted spectrum, then the assumption that the particles did not interact is confirmed. However, if the match is poor, it is then likely that the mixing of the two components caused some changes in the aggregative behavior of the system. Perhaps new composite particles were formed by some interaction of the two species. Or perhaps some chemical component in one sample interacted with the surface of another. Many interaction possibilities exist. Nevertheless, it seems ap-

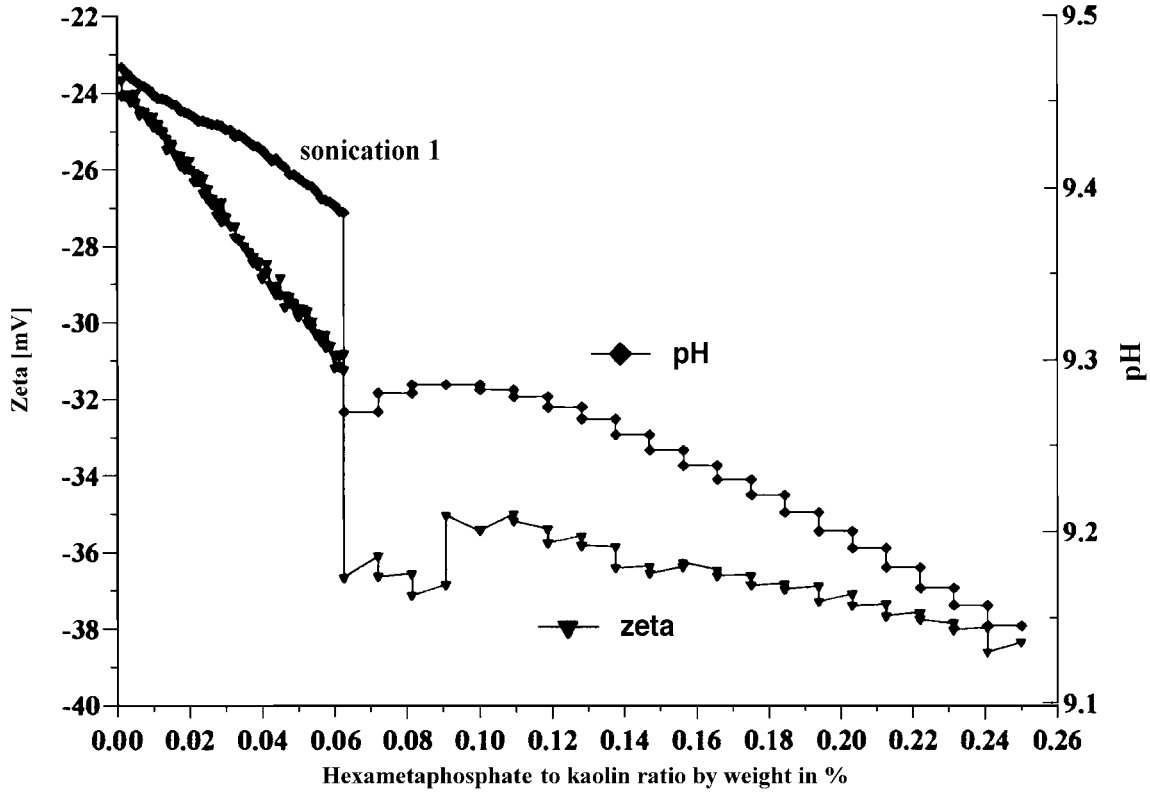

Fig. 35 Effect of sonication on the EC1 40%wt kaolin titration with hexametaphosphate.

propriate to conclude that a necessary condition to rule out aggregation on mixing is that the experimental and predicted attenuation curves match. In addition, we can probably also conclude that an error between theory and experiment is sufficient to say that some form of aggregation or disaggregation on mixing has occurred. We will show that such prediction arguments are indeed able to monitor such aggregation phenomena.

Finally, we can take the ultimate leap and use an "analysis" algorithm to search for that particle size distribution that in accordance with the model and the predictive theory, best matches the experimental data.

Importantly, both the "validation" and "analysis" approach assume that we can accurately model the real world, while at the same time making some simplifying assumptions. For example, it is common to assume that the particles can be treated as spheres, even though we know that this may not be exactly the case. Here, we follow a paper (57) that suggests two models that can be particularly helpful for describing mixed dispersions.

The first ''multi-phase'' model assumes that we can represent the PSD of a real-world dispersion as a sum of separate lognormal distributions, one for each component in the mixed system. For this article, we assume that there are only two components, which reduces the overall PSD to a simple bimodal distribution. When we calculate the attenuation of such a multi-phase system, we take into account the individual density and other particle properties for each component in the mixture. For a bimodal case, the multi-phase approach would typically require the analysis algorithm to fit five adjustable parameters: the median size and standard deviation of both modes and the relative mass fraction of each mode. In this work, we will assume that the weight fraction of each mode is known in advance. Furthermore, in an effort to avoid the well-known problem of multiple solutions, we will further assume that both modes have the same standard deviation. Altogether, these simplifications reduce the number of adjustable parameters to just three: the median size of each mode and the standard deviation. The implications of these simplifications will be discussed later.

The second ''effective medium'' model further assumes that one needs to determine the PSD of just one component in an otherwise complex mixed system. All other disperse phases are lumped together into an effective homogeneous medium characterized by some composite density, viscosity, and acoustic parameters. By adopting this viewpoint, we significantly reduce a complex real-

world mixture to a simpler dispersion of a single pre-selected dispersed phase in a newly defined ''effective medium.'' We need not even define the exact nature and composition of this new medium because we can simply measure, or perhaps calculate, the required composite density, viscosity, attenuation, and sound speed. If we assume that the key disperse phase can be described by a lognormal distribution, then we have reduced the degree of freedom to just two adjustable parameters, a median size and standard deviation.

In the article, we have evaluated the effectiveness of both the multi-phase and the effective medium model using the same set of experimental data. As a result, we gain a better understanding of the restrictions and benefits of each method.

We used three pigments from Sumitomo Corporation: AKP-30 alumina (nominal size 0.3 microns), AA-2 alumina (2 microns), and TZ-3YS zirconia (0.3 microns). In addition, we used precipitated calcium carbonate (PCC) supplied by Specialty Minerals Corp. (0.7 microns) and Geltech silica (1 micron).

Slurries of the AA-2 alumina and the zirconia were prepared in such a manner as to have quite good aggregative stability. Each slurry was prepared at 3% volume by adding the powder to a 10^{-2} mol/L KCl solution, adjusted initially to pH 4 in order to provide a significant ζ-potential. Both slurries were judged to be quite stable under these conditions as indicated by the absence of any noticeable settling.

Preparation of a 3% volume PCC slurry was more problematic because the ζ-potential right after dispergating was very low (1.3 mV). Control of pH alone was insufficient, and we therefore used sodium hexametaphosphate in order to increase the surface charge and to improve the aggregative stability of this slurry. The ζ-potential reaches saturation at a hexametaphosphate concentration of about 0.5% by weight relative to the weight of the PCC solid phase.

The Geltech silica and the AKP-30 alumina were used only as dry powders, being added to the PCC slurry as needed.

The goals of the experiment were met in the following steps.

Step 1. Three single-component slurries of alumina AA-2, zirconia, and PCC respectively were prepared as described above.

Step 2. The attenuation spectra of these single-component slurries were measured, and the particle size distribution for each was calculated.

Step 3. Three mixed alumina/zirconia slurries were prepared by blending the above slurries in different proportions, and the attenuation spectrum for each mixture was measured.

Step 4. Geltech silica powder was added to the initial PCC slurry, and the attenuation spectrum was measured for this mixed system.

Step 5. AKP-30 alumina powder was added to the initial PCC slurry, and the attenuation spectrum for this mixed system was measured.

Step 6. The particle size distribution was calculated for all of the mixed systems using the ''multi-phase model.''

Step 7. The properties of the ''effective medium'' were calculated for all mixtures.

Step 8. The particle size distribution for each of these mixed systems was calculated using the ''effective medium model.''

Step 9. The results of the particle size calculation using two different approaches were compared.

Step 10. The validation approach was used to test for possible particle interactions in the mixed systems.

The experimental attenuation spectra for the three single-component slurries and five mixtures are shown in Fig. 36. In order to demonstrate reproducibility, each F36
sample was measured at least three times. Mixture 1, in fact, was measured yet a fourth time after a fresh sample was loaded just to show that sample handling was not a factor. It is clear that the reproducibility is sufficient for resolving the relatively large differences in attenuation between different samples.

The attenuation spectrum for the single-component slurries of the AA-2 alumina, the zirconia and the PCC allows us to calculate the particle size distribution for each of these materials. The calculated sizes are given in Tables 5 and 6, and it is seen that these acoustically de- T5/T6
fined sizes agree quite well with the nominal sizes given by the producers of these materials.

As shown in Fig. 36, the attenuation spectra of the mixtures differ significantly from the attenuation spectra of the single-component slurries. This difference in the attenuation spectra reflects the differences in both the particle size distributions and the density of the constituent components in the mixtures.

We want to compare the effectiveness of the ''multi-phase'' and the ''effective medium'' approach in calculating the PSD of these five different mixed systems.

First, let us consider the more or less straightforward ''multi-phase'' model. To use this approach, we need only know the weight fraction and density of both disperse materials. The present software implementation assumes that the total particle size distribution is bimodal and that each mode corresponds to one disperse phase material. For

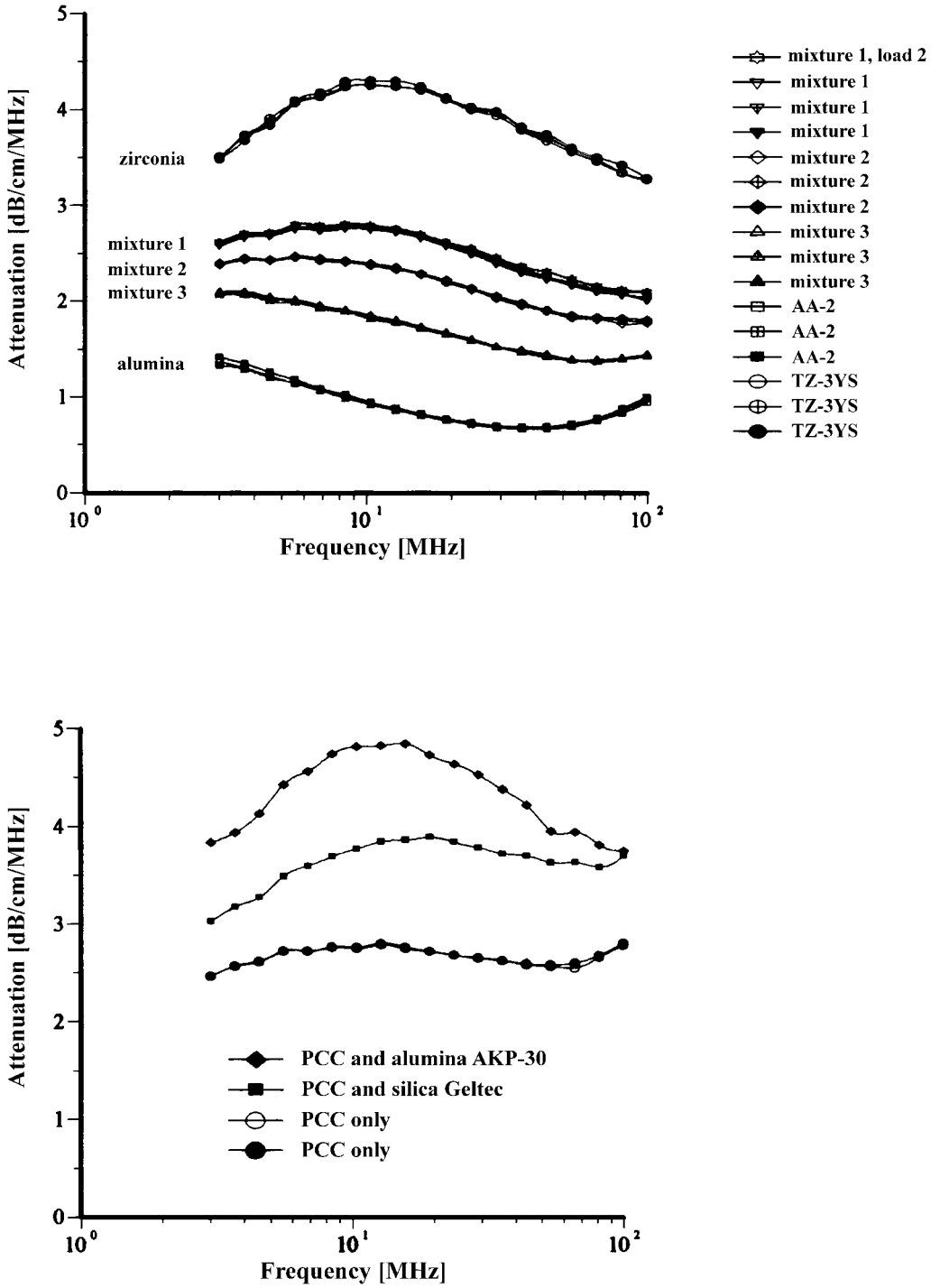

Fig. 36 Experimental attenuation spectra for initial alumina AA-2 and zirconia TZ-3YS from Sumitomo and their mixtures with weight fractions given in Table 4. Experimental attenuation spectra for initial PCC slurry and its mixture with the added silica and alumina powders. Weight fractions are given in Table 5.

instance, in the alumina/zirconia mixture, the smaller mode corresponds to the zirconia, and the larger mode corresponds to the alumina. The software takes into account the difference in densities between materials of the

first and the second modes. The PSD of each mode is itself assumed to be lognormal. In order to reduce the number of adjustable parameters, and in an effort to reduce the likelihood of multiple solutions, the present software implementation assumes that both modes have the same standard deviation. The software searches for some com-

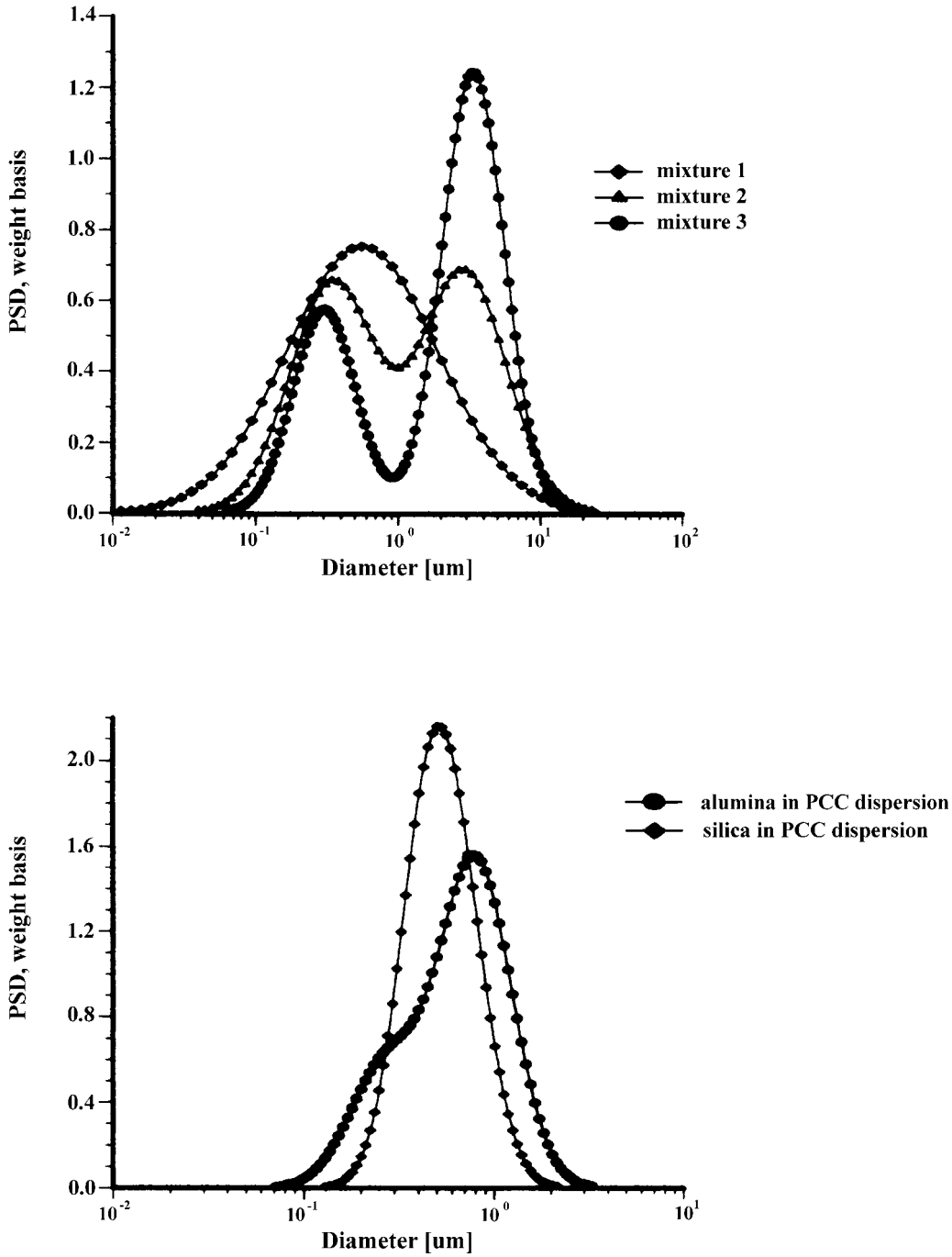

Fig. 37 Particle size distributions calculated for alumina-zirconia mixtures using ''multi-phase model.'' The smaller size mode corresponds to zirconia; the larger size mode is alumina AA-2. Weight fraction and PSD parameters are given in Table 4. Particle size distributions calculated for PCC-alumina and PCC-silica mixtures using ''multi-phase model.'' Weight fraction and PSD parameters are given in Table 5.

bination of three adjustable parameters (two median sizes and their common standard deviation) that provide the best fit to the experimental attenuation spectra. It assumes the relative content of the modes to be known.

The corresponding PSDs for these five mixed systems are shown in Fig. 37. The parameters of these PSDs are given in Tables 5 and 6. It is seen that in some cases this ''multi-phase'' approach yields approximately the correct size. For instance, the two zirconia/alumina mixtures with a lower zirconia content (mixtures 2 and 3) have almost the correct size combination. The size of the alumina particles is somewhat higher than expected (2.15 microns) but is still rather acceptable. We can say the same about the PCC/alumina mixture from Table 6. The difference of the sizes relative to the nominal values does not exceed 10%.

However, the multi-phase model appears to be a complete failure for the alumina/zirconia mixture 1 as well as the PCC/silica mixture. It is not clear yet why this ''multi-phase model'' works for some systems and not for others. We think it probably is related to the fact that the present software assumes that both particle size modes have the same width. It is seen that the single-component zirconia slurry has a PSD that is much broader (st. dev = 0.43) than the PSD of the AA-2 alumina (st. dev = 0.26). The bimodal searching routine finds the correct intermediate value for the standard deviation (0.3) only for mixture 2. It is interesting that this PSD solution is the closest match to the superposition of the initial PSD. The standard deviations for the other two mixtures are out of range completely, and the corresponding PSD also deviate from the expected superposition.

This observation allows us to conclude that our restriction that the standard deviation be the same for both modes might itself create an artificially wrong solution. It is easy to eliminate this restriction but, as one adds additional degrees of freedom, it is not uncommon to be faced with the problem of multiple solutions.

This multiple solution problem appears when the error function (difference between experimental and theoretical attenuations) has several local minimums with different combinations of the adjustable parameters. In general, the problem of multiple solutions increases as the number of adjustable parameters increases. It seems clear that the maximum number of adjustable parameters to avoid multiple solutions is not a fixed number but rather depends on a combination of factors: the accuracy and amount of experimental data points, the degree to which the real world sample is described by the model, and how accurately the key parameters of the colloid, such as weight fraction, density, etc. are known. Our experience is that bimodal PSD with even four adjustable parameters some-

Table 5 Characteristics of alumina AA-2 and zirconia TZ-3YS slurries and their mixtures

	Initial		Mixture 1		Mixture 2		Mixture 3	
	Alumina	Zirconia	Alumina	Zirconia	Alumina	Zirconia	Alumina	Zirconia
Volume fraction, %	3	3	1.55	1.45	1.85	1.15	2.28	0.72
Weight fraction, %	10.96	15.91	5.5	7.9	6.6	6.3	8.2	4
Eff. viscosity [cp]			0.92		0.93		0.94	
Eff. density [g/cm^3]			1.04		1.05		1.06	
Att M0	1.593		1.21		0.982		0.823	
Att M1	0.0845		0.0642		0.0521		0.0437	
Att M2	− 1.251		− 0.95		− 0.771		− 0.646	
Att M3	0.528		0.401		0.326		0.273	
Parameters of the particle size distributions, effective medium approach								
Median lognormal [micron]	2.15 ± 0.02	0.33 ± 0.006		0.293 ± 0.006		0.303 ± 0.005		0.317 ± 0.003
St. deviation	0.26	0.43		0.38		0.378		0.372
Fitting error, %	6.6	1.9		1.4		1.2		0.95
Parameters of the particle size distributions, two dispersed phases approach								
Median size [micron]			0.565 ± 0.002	0.558 ± 0.001	2.922 ± 0.088	0.352 ± 0.005	3.582 ± 0.182	0.303 ± 0.003
St. deviation			0.53		0.3		0.21	
Fitting error, %			5		7.6		4.4	

Table 6 Characteristics of PCC slurry and its mixtures with alumina AKP-30 and silica Geltech

	Initial PCC	Initial silica	PCC and silica		PCC and alumina	
		powder	PCC	silica	PCC	alumina
Volume fraction, %	10.55		9.19	6.29	10.27	2.52
Weight fraction, %	23.53		19.6	11.3	21.6	8.1
Eff. viscosity [cp]	1.125		1.094		1.118	
Eff. density [g/cm^3]	1.17		1.13		1.15	
Att M0	1.053					
Att M1	4.431					
Att M2	− 3.648					
Att M3	0.9296					
Parameters of the particle size distributions, effective medium approach						
Median lognormal [micron]	0.684	1.26		0.454		0.325
St. deviation	0.31	0.35		0.015		0.015
Fitting error, %	1.1	1.3		7.5		2.4
Parameters of the particle size distributions, two dispersed phases approach						
Median size [micron]			0.449	0.681	0.798	0.2715
St. deviation			0.16		0.19	
Fitting error, %			8		1.9	

times exhibits multiple solutions. We have found ways to resolve these multiple solutions in the case of single-component dispersions; however, the situation is more complicated for mixed dispersions with two or more chemically different components. For this reason, we restricted the number of the adjustable parameters to only three for this work.

These results indicate that the ''multi-phase'' model might sometimes lead to wrong solutions, and it is unclear at this point how to completely eliminate the problem.

In contrast, the ''effective medium'' approach circumvents this problem by addressing only the question of determining a simple lognormal distribution that describes only one disperse phase in an otherwise complex mixture. Because we are then dealing only with two adjustable parameters (median size and standard deviation), the possibility for multiple solutions is most likely diminished. On the downside, when using the ''effective medium'' approach, we need to perform an additional experiment to measure the properties of this ''effective medium,'' and this may not always be possible or without other difficulties.

In the case of the PCC mixtures with the added alumina or silica, the original PCC slurry itself serves as the ''effective medium.'' We need just three parameters to characterize this ''effective medium'' namely density, viscosity, and attenuation. Importantly, all three parameters can be directly measured if we have access to this medium. The attenuation is the most important of these three required parameters. It is also the most challenging to characterize because we need the attenuation of this medium as a function of frequency from 3 to 100 MHz. The current version of the DT 1200 software allows us to define the attenuation of the effective medium the same way we would normally define the ''intrinsic attenuation'' of even a pure liquid medium. This intrinsic attenuation as measured in dB/cm/MHz can be described in terms of a polynomial function:

$$\mathrm{att}(f) = \mathrm{att\,M0} + f\,\mathrm{att\,M1} + f^2\mathrm{att\,M2} + f^3\mathrm{att\,M3}$$

where i is frequency in MHz and M0, M1, M2, and M3 are the polynomial coefficients.

For example, in the simplest case, we can say that our effective medium is just water. Water has an attenuation that, for practical purposes, can be said to simply increase as a linear function of frequency if attenuation is expressed in dB/cm/MHz. Thus, M0, M2, and M3 are zero, and M2 represents this linear dependence.

To use the effective medium approach for mixed systems, we simply need to define new coefficients to describe the intrinsic attenuation of this new medium. In the case of the alumina/zirconia mixtures, we use the alumina slurry as the ''effective medium.'' The coefficients for the alumina slurry can be calculated by doing a polynomial fit to the attenuation data as shown in Fig. 38. These F38
coefficients are also given in Table 5. Similarly, the coefficients for the PCC ''effective medium'' can be calcu-

lated from a polynomial fit of the attenuation data for that material as shown in Fig. 38. Likewise, these coefficients are given in Table 6.

We should keep in mind that the initial alumina slurry is diluted when we mix it with increasing amounts of the zirconia slurry. As a result, we need to recalculate the attenuation coefficients for each mixture, taking into account the reduced volume fraction of the alumina in each mixture. The suitably modified values for the attenuation coefficients of the effective medium for all three alumina-zirconia slurries are also given in the Table 5. We avoided the need for making these additional calculations in the case of the PCC mixtures by simply adding dry silica or alumina powder to the PCC effective medium, and therefore the coefficients for the PCC effective medium are the same for both mixtures.

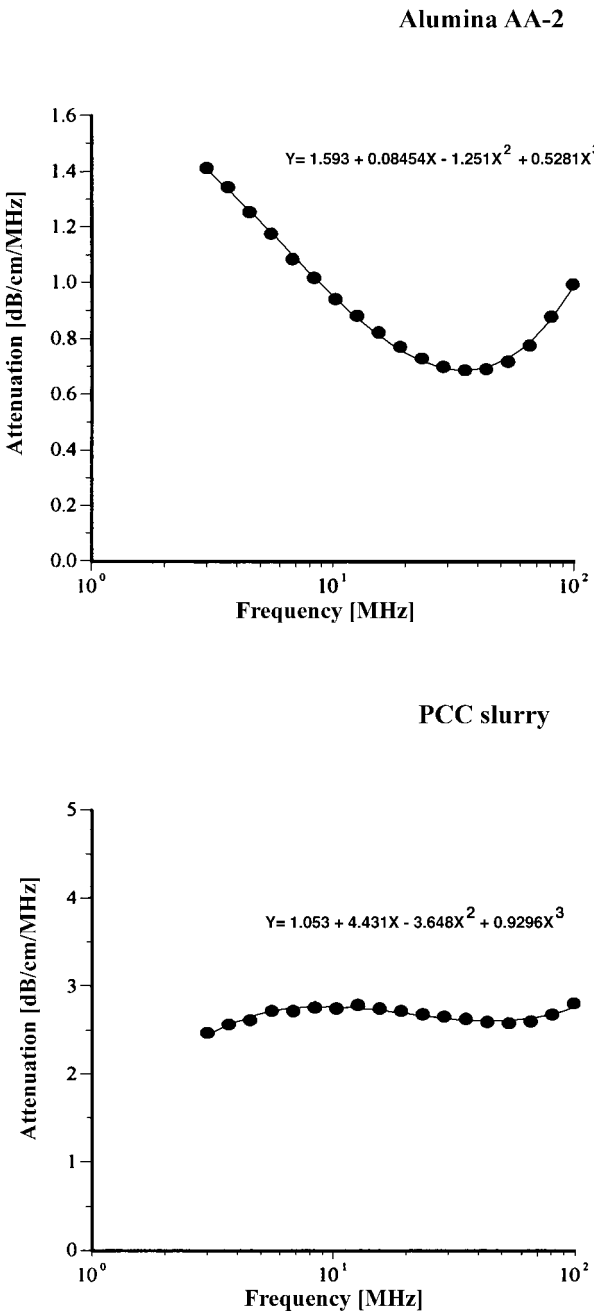

Fig. 38 Experimental attenuation spectra measured for individual alumina AA-2 slurry and PCC slurry with polynomial fit.

For an aqueous medium, the software automatically calculates the intrinsic attenuation of water and subtracts this from the measured attenuation to deduce the attenuation caused solely by the presence of the disperse particles. When using the ''effective medium'' model, the software actually works in the same way, except that the intrinsic attenuation of water is replaced by the attenuation of this new effective medium. For instance, in the case of the PCC-alumina mixture, the software calculates the attenuation due to the PCC contribution and subtracts it from the total attenuation of the mixture. The residual part corresponds to the attenuation due to the alumina particles and is the source of the particle size information for the alumina component. The software assumes a lognormal PSD and fits this residual attenuation using the median size and standard deviation as adjustable parameters.

This effective medium approach allows us to calculate the particle size distribution of the zirconia in the alumina-zirconia mixtures and of the silica or the alumina in the case of PCC mixtures. The corresponding values are shown in Tables 5 and 6. Fig. 39 illustrates the corresponding PSD for each case. F39

In the case of zirconia, we have almost the same PSD for all three mixtures. This PSD agrees well with the initial slurry. The fitting error is much smaller than in the ''multi-phase model,'' which is an additional indication of the consistency.

In the case of PCC mixtures, the situation is more complicated. We have a very good correlation with the nominal size for the AKP-30 alumina for PCC-alumina mixture with a good fitting error.

The other PCC-based mixture gives a particle size that is half the size expected. You can see from Table 6 that the calculated size of the silica Geltech is only 0.454 microns whereas the nominal size is at least 1 micron. We measured acoustically for this silica of even larger size, of 1.26 microns. It might happen because of the dispersing problems. We have found that this silica is difficult to disperse properly even at high pH and high zeta potential. For instance, we measured ζ-potential of -66 mV for this silica at pH 11 but even this was apparently not sufficient to disperse it completely.

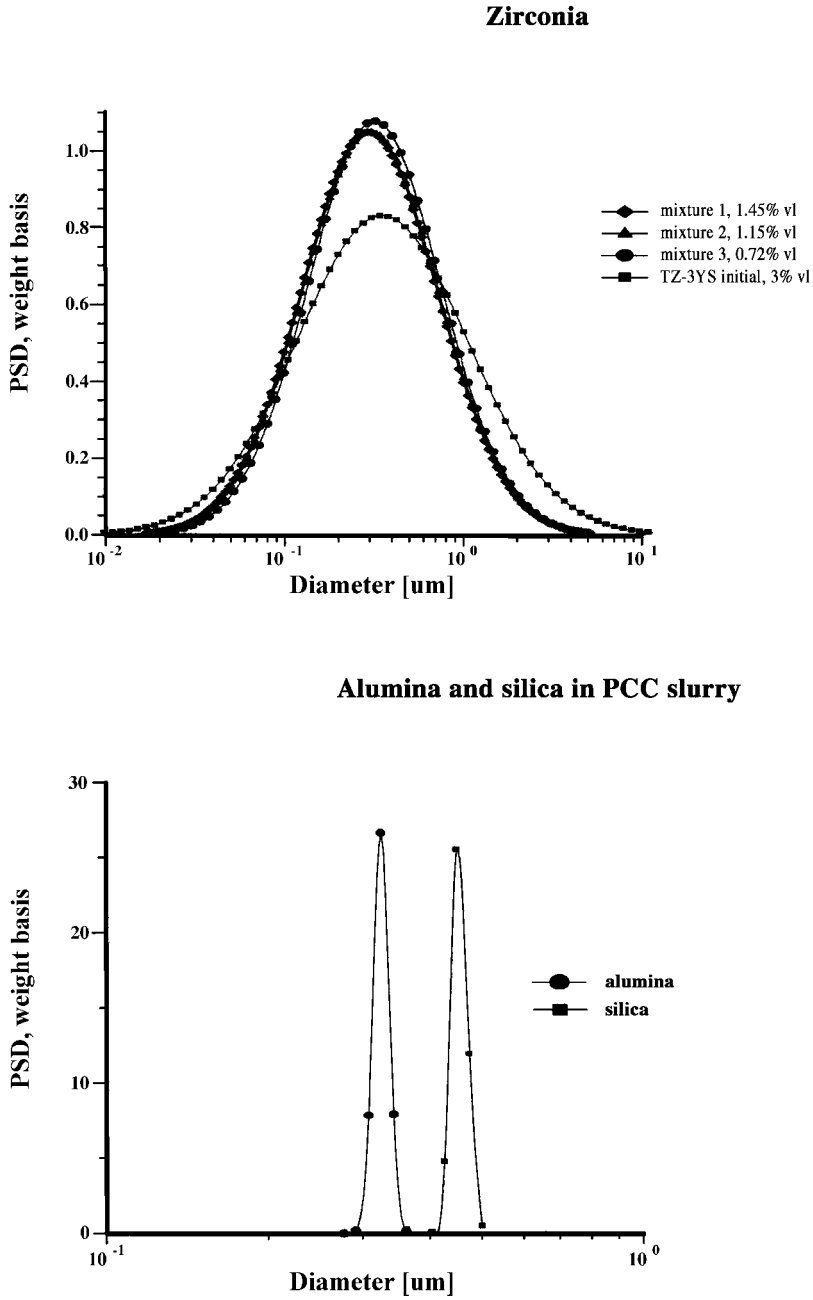

Fig. 39 Particle size distribution calculated using ''effective medium model.'' The case of zirconia in the alumina AA-2 dispersion as the effective medium. Attenuation of the alumina is reduced according to volume fractions from Table 4. Density and viscosity are adjusted as effective medium. Particle size distribution calculated using ''effective medium model.'' The case of alumina AKP-30 and silica in the PCC dispersion as effective medium.

Summarizing the analysis results for these five mixtures, we conclude that in the case of the three mixed dispersions (alumina-zirconia mixtures 2 and 3, and the PCC-alumina mixture), the ''multi-phase model'' and the ''effective medium model'' gave similar results and reasonable PSD. For the other two mixtures, the results are more confusing. We suspect that the failure of the ''multi-phase model'' for the alumina-zirconia mixture 1 is related to the restriction on the PSD width, but particle aggregation is still a candidate as well. In the case of the

PCC-silica mixture, a double failure of both modes certainly points toward particle aggregation.

We can evaluate these ideas about aggregation of the two troubled mixtures using the "validation" approach. To do this, we must first compute the total PSD using the known PSD of the individual single component dispersions. Next, we calculate the predicted attenuation for this combined PSD. This predicted attenuation should agree with the experimental spectrum for the mixed system if there is no particle interaction between the species.

Fig. 40 illustrates the predicted and experimental attenuation spectrum for the zirconia-alumina mixture 1 and the PCC-silica Geltech mixture. For both mixtures, we have also added the predicted attenuation corresponding to the best PSD calculated using the ''multi-phase model'' analysis. F40

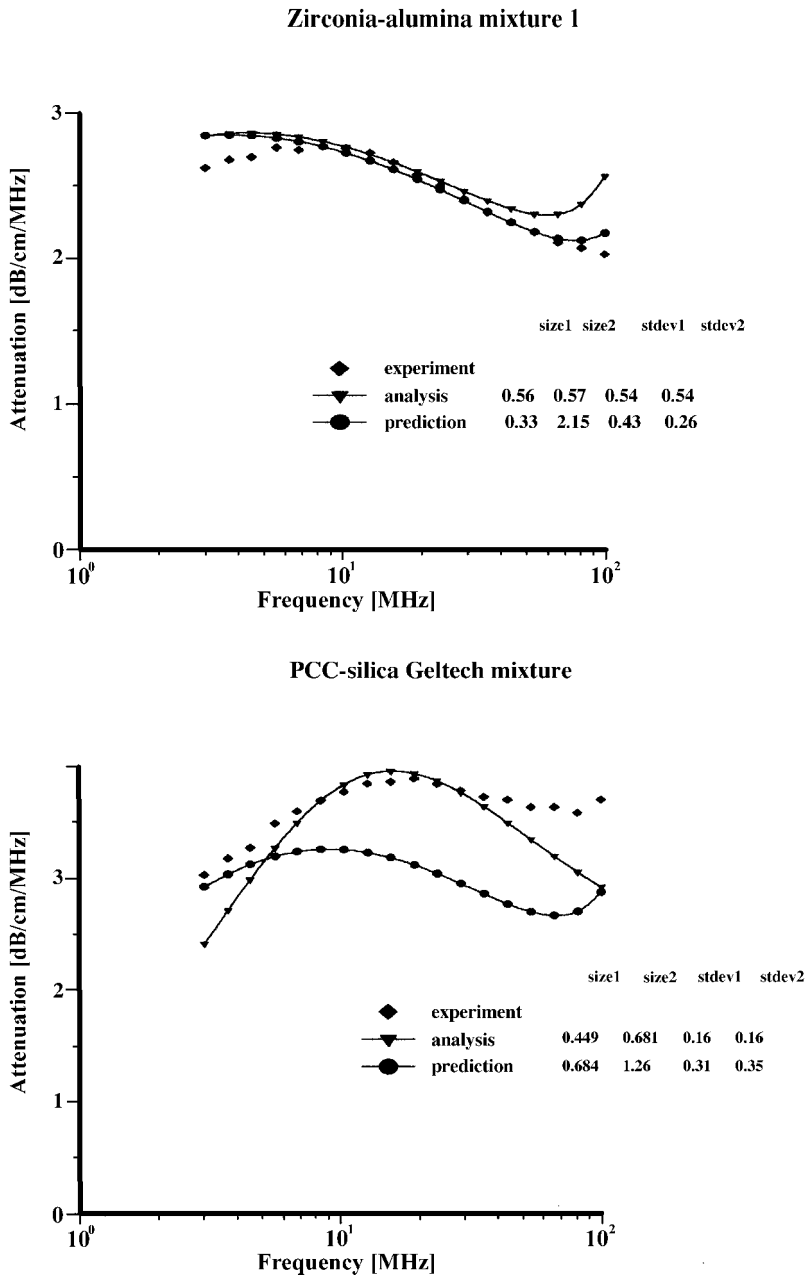

Fig. 40 Experimental and theoretical attenuation for zirconia-alumina mixture 1 and PCC-silica mixture. Theoretical attenuations are calculated for the best analysis result and for combined PSD build from the individual distributions assuming no particle aggregation.

Table 7 Particle size of the two alumina samples

	Median particle [micron]	
	ALM-41-01	AL-160SG-4
Size, Horiba	1.47	0.56
Size, Sympatec	1.98	0.71
Size, PenKem, vfr < 20%	1.79	0.52
Size, Acoustics, vfr = 40% **with structural losses**	1.63 (fit error 6.1%)	0.77 (fit error 2.3%)
Size, Acoustics, vfr = 40% **no structural losses**	1.07 (fit error 19.2%)	0.8 (fit error 18.4%)

It is seen that, in the case of the zirconia-alumina mixture, a superposition PSD generates an attenuation spectrum that fits experimental spectra much better than the best ''multi-phase model'' analysis PSD. The fitting error has improved from 5% to 2.3% and becomes comparable with the best fitting errors of the ''effective medium" model. This correlation between prediction and experiment proves that our concern about using a common standard deviation for both modes was well founded. The prediction program allows us to apply independent standard deviation for each mode of the PSD, and, as a result, we achieve much better fitting than in the case of the analysis ''multi-phase" model that uses the same standard deviation for both modes.

In addition, we conclude that there is no aggregation between the alumina and zirconia particles in this mixed dispersion. Otherwise, the theoretical attenuation based on the superposition assumption would not fit experimental data.

The situation with the second mixture (PCC-silica) is very different. In this case, the predicted attenuation provides a much worse fit than the best ''multi-phase" model analysis. The fitting error degrades from 8% to 17.2%. This means that superposition assumption is not valid. In this case, there is apparently some aggregation between the PCC and silica particles.

Structured Dispersions

In many really concentrated dispersions, particles build a structural network. They are not independent in these systems, and oscillation of this network causes the additional mechanism of the sound attenuation: ''structural losses.'' This complicates characterization of the particle size distribution. Fortunately, in many cases, structural losses are negligible even at very high volume fractions. For instance, experimental dilution test with concentrated rutile and silica (13) dispersions yields correct particle size taking into account only viscous losses.

However, there are some instances when theory of viscous losses only fails to fit the experimental data. One such example is given in the paper of several Japanese scientists (65) from the National Institute for Resources and Environment, Tsukuba, Japan. We have used this paper in order to show that the additional mechanism of structural losses provides required theoretical framework for characterizing particle size distribution in the highly concentrated (up to 40%vl) and not completely stable dispersions.

The two alumina powders were used: Showa Denko AL-160SG-4 and Sumitomo Chemical Industry ALM-41-01. The median size of the each powder was measured by laser diffraction using a Sympatec Helos and by photo-

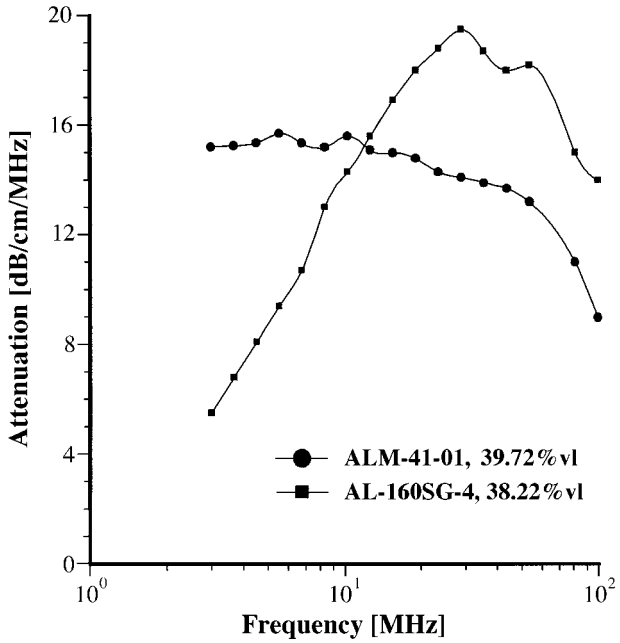

Fig. 41 Experimental attenuation spectra of the two alumina slurries characterized in Ref. 65.

centrifugation using a Horiba CAPA-700. These data are T7 summarized in Table 7.

Both samples were stabilized with sodium polycalboxyl acid as a surfactant and ball milled for 3 days. The volume fractions of the slurries varied from 1% to 40%.

They used PenKem Acoustophor 8000 for measuring the acoustic attenuation spectra of these slurries. The particle size calculated from these attenuation spectra agreed with independent measurements at volume fractions below 20%. These size data is summarized in Table 7.

The attenuation at the highest volume fraction is shown F41 in Fig. 41. We have reproduced these curves from the published graphs because the numerical data were not available in their paper. As a result, one may assume some small deviations from the original data.

We use attenuation spectra at the highest volume fraction in the further analysis.

Fig. 42 shows the experimental and theoretical attenua- F42 tion spectra at the highest volume fractions, about 40% vl for both alumina samples. It is seen that the theory does not fit the experimental data very well because the experimental attenuation exceeds the theory by a substantial degree. Based on this excess, the authors concluded that there is an unknown factor that becomes significant at high volume fraction.

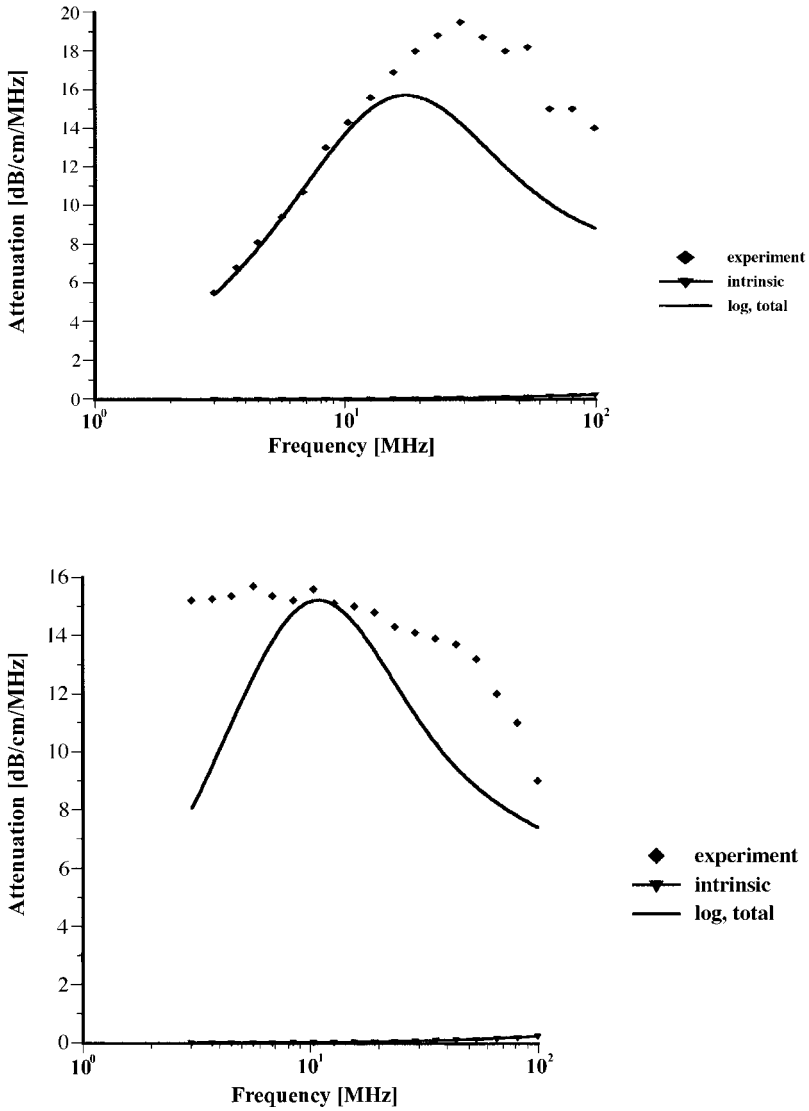

Fig. 42 Theoretical fit to the experimental data presented in Ref. 65 assuming no structural losses.

We suggest ''structural losses'' as this hypothetical factor. We used Eq. 11 for calculating the theoretical attenuation spectra. We assumed that the first virial coefficient β is zero. The second virial coefficient is then used as an adjustable parameter in addition to median size and standard deviation of the lognormal particle size distribution. This searching routine looks for the particle size distribution that generates a theoretical attenuation spectra that fits the experimental spectra with the least error.

The addition of this new adjustable parameter, δ, allowed us to achieve much better theoretical fit as illustrated in Fig. 43. Table 6 gives the results of the calculated particle sizes and fitting errors. It is seen that the addition of these structural losses leads to dramatic improvements in the fitting error, which strongly suggests that this mechanism can indeed explain the observed excess attenuation.

The particle size data (Fig. 44) confirms this conclusion as well. It is seen that particle sizes calculated including these structural losses are much closer to independent measurement performed with diluted system using light-based instruments.

It is interesting that the value of the second virial coefficient turns out to be the same for both samples, 0.8. It is independent of the particle size, as it is supposed to be. This parameter characterizes flexibility of rheology of the polymer chains linking particles together into the structure at high-volume fractions.

We would like to finish with the warning that addition of the structural losses is justified only when traditional

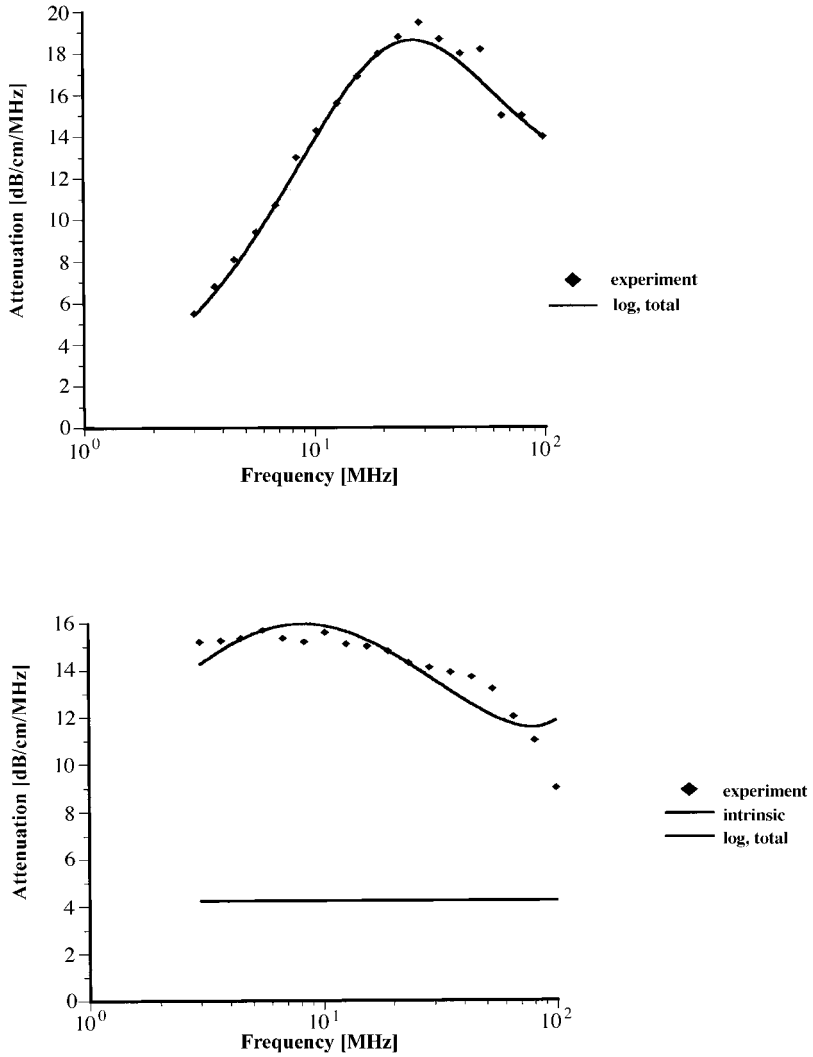

Fig. 43 Theoretical fit to the experimental data presented in Ref. 65 with structural losses.

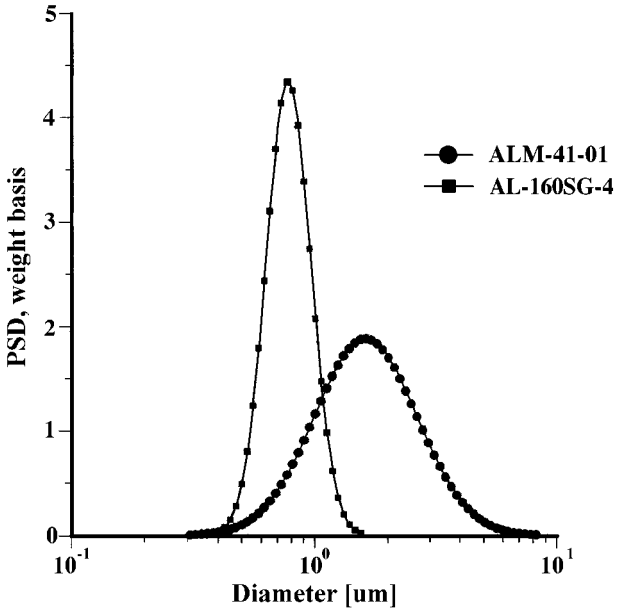

Fig. 44 Particle size distribution calculated for the two alumina samples described in Ref. 65.

theory fails and experiment shows an excess attenuation. This excess attenuation is a source of experimental information for calculating microrheological properties.

CONCLUSIONS

In the past few years, the fields of acoustics and electroacoustics have made significant advancements in theoretical modeling, instrumentation, and experimental applications. The measurement of particle size by acoustic attenuation has been improved by new theoretical models that account for specific particle-particle interactions in concentrated structured systems and mixed dispersions. Refinements in the analysis of the different acoustic loss mechanisms have been presented in detail.

The combination of acoustic and electroacoustic spectroscopy provides more reliable and complete characterization of the disperse system than either one of those spectroscopes separately. Electroacoustic phenomena are more complicated when compared to acoustics because an additional electric field is involved. This problem becomes even more pronounced for concentrated systems, and the best approach is to use acoustic attenuation to determine particle size and electroacoustics separately to measure electric surface properties.

New applications of the acoustic attenuation method and the colloid vibration current include ceramics, bimodal systems, chemical polishing materials, emulsions, microemulsions, latex, structured dispersions, mixed dispersions, clays, minerals, paints, inks, etc. Further applications of these techniques are underway, especially in the field of nonaqueous systems that cannot be easily studied by other methods. While theoretical models have made great advancements, more work is needed to extend electroacoustic theory to nonaqueous systems and for explaining the role of the thermal effects in the electroacoustics.

APPENDIX: SPECIAL FUNCTIONS

There are several special functions used in the abovementioned theory. They are specified below.

$$
\begin{aligned}
H(\alpha) &= \frac{ih(\alpha)}{2\alpha} - \frac{idh(x)}{2dx_{x=\alpha}} \\
h(x) &= h_1(x)h_2(\beta) - h_1(\beta)h_2(x) \\
I &= I(\beta) - I(\alpha) \\
I(x) &= -h_1(\beta)e^{x(1+j)} \\
&\quad \times \left[\frac{3(1-x)}{2\beta^3} + j\left(\frac{x^2}{\beta^3} - \frac{3x}{2\beta^3} - \frac{1}{x}\right)\right] \\
&\quad + h_2(\beta)e^{-x(1+j)} \qquad\qquad I_{13} \\
&\quad \times \left[\frac{3(1+x)}{2\beta^3} + j\left(\frac{x^2}{\beta^3} + \frac{3x}{2\beta^3} - \frac{1}{x}\right)\right] \\
I_I &= -j\frac{e^{-x(1+j)x=b}}{x_{x=a}} \\
I_2 &= -j\frac{e^{x(1+j)x=b}}{x_{x=a}} \\
&= -\frac{e^{-x(1+j)}}{b^3}[1.5(x+1) + j(x^2+1.5x)]_{x=a}^{x=b} I_{23} \\
&= \frac{e^{x(1+j)}}{b^3}[1.5(x-1) + j(-x^2+1.5x)]_{x=a}^{x=b} h_1(x) \\
&= \frac{\exp(-x)}{x}\left[\frac{x+1}{x}\sin x - \cos x \right. \\
&\quad \left. + j\left(\frac{x+1}{x}\cos x + \sin x\right)\right]_{h_2(x)} \\
&= \frac{\exp(x)}{x}\left[\frac{x-1}{x}\sin x + \cos x \right. \\
&\quad \left. + j\left(\frac{1-x}{x}\cos x + \sin x\right)\right]
\end{aligned}
$$

NOMENCLATURE

List of Abbreviations

a = particle radius
b = cell radius
C_p = heat capacity at constant pressure
c = sound speed
Du = Dukhin number
d = particle diameter
E = external electric field
$<E>$ = macroscopic electric field strength
F_f = hydrodynamic friction force
K = conductivity attributed with index
I_r = local current in the cell
$<I>$ = macroscopic current
I = intensity of the sound
j = complex unit
h = special function (see Special Functions)
H = special function (see Special Functions)
l = complex wave number
l_i = cell layer thickness
L = gap in the electroacoustic chamber
M^* = stress modulus
N = number of the volume fractions
P = pressure
r = spherical radial coordinate
t = time
S_{exp} = measured electroacoustic signal
u = speed of the motion attributed according to the index
Z = acoustic impedance
α = attenuation specified with index
β = thermal expansion attributed with index
δ_v = viscous depth
δ_t = thermal depth
ε = dielectric permittivity of the media
ε_0 = dielectric permittivity of the vacuum
ϕ = electric potential
γ = hydrodynamic friction coefficient
η = dynamic viscosity
φ = volume fraction
κ = reciprocal Debye length
κ^σ = surface conductivity
λ = wave length
μ_d = dynamic electrophoretic mobility
ν = kinematic viscosity
θ = spherical angular coordinate
ρ = density attributed according to the index
τ = heat conductance attributed according to the index
ω = frequency
ζ = electrokinetic potential
Ω = drag coefficient

Indexes

i = index of the particle fraction
p = particles
m = medium
s = dispersion
r = radial component
θ = tangential component
vis = viscous
th = thermal
sc = scattering
int = intrinsic
in = acoustic input
out = acoustic output
rod = delay rod properties

REFERENCES

1. Pellam, J.R.; Galt, J.K. Ultrasonic propagation in liquids: application of pulse technique to velocity and absorption measurement at 15 magacycles. J. Chem. Phys. **1946**, *14* (10), 608–613.
2. Sewell, C.T.J. The extinction of sound in a viscous atmosphere by small obstacles of cylindrical and spherical form. PhilTrans. R. Soc. London **1910**, *210*, 239–270.
3. Epstein, P.S.; Carhart, R.R. The absorption of sound in suspensions and emulsions. J. Acoust. Soc. Am. **1953**, *25* (3), 553–565.
4. McClements, D.J. Ultrasonic characterization of emulsions and suspensions. Adv. Colloid Interface Sci. **1991**, *37*, 33–72.
5. *Ultrasonic and Dielectric Characterization Techniques for Suspended Particulates*; Hackley, V.A., Texter, J., Eds.; The American Chemical Society: Ohio, 1998. AQ5
6. Lyklema, J. *Fundamentals of Interface and Colloid Science*; Academic Press: 1993; Vol. 1.
7. Hunter, R.J. *Foundations of Collid Science*; Oxford University Press: Oxford, 1989.
8. Dhadwal, H.; Ansari, R.; Mayer, W. Rev. Sci. Instrum. **1991**, *62* (12), 2963. AQ6
9. Dukhin, A.S.; Goetz, P.J. Acoustic spectroscopy for concentrated polydisperse colloids with high density contrast. Langmuir **1996**, *12* (21), 4987–4997.
10. Dukhin, A.S.; Goetz, P.J. Characterization of aggregation phenomena by means of acoustic and electroacoustic spectroscopy. Colloids Surf. **1998**, *144*, 49–58.
11. Debye, P.J. J. Chem. Phys. **1933**, *1*, 13. AQ7
12. Hunter, R.J. Review. Recent developments in the electroacoustic characterization of colloidal suspensions and emulsions. Colloids Surf. **1998**, *141*, 37–65.

13. Dukhin, A.S.; Shilov, V.N; Ohshima, H.; Goetz, P.J Electroacoustics phenomena in concentrated dispersions. New theory and CVI experiment. Langmuir **1999**, *15* (20), 6692 6706.
14. Dukhin, A.S.; Goetz, P.J. Acoustic and electroacoustic spectroscopy. Langmuir **1996**, *12* (19), 4336–4344.
15. Strout, T.A. Attenuation of Sound in High-Concentration Suspensions: Development and Application of an Oscillatory Cell Model. A Thesis, The University of Maine, 1991.
16. Riebel, U The fundamentals of particle size analysis by means of ultrasonic spectrometry. Part. Part. Syst. Charact. **1989**, *6*, 135–143.
17. Harker, A.H.; Temple, J.A.G. Velocity and attenuation of ultrasound in suspensions of particles in fluids. J. Phys. D: Appl. Phys. **1988**, *21*, 1576–1588.
18. Gibson, R.L.; Toksoz, M.N. Viscous attenuation of acoustic waves in suspensions. J. Acoust. Soc. Am. **1989**, *85*, 1925–1934.
19. Happel, J.; Brenner, H. *Low Reynolds Number Hydrodynamics*; Martinus Nijhoff Publishers: Dordrecht, The Netherlands, 1973.
20. Dukhin, A.S.; Shilov, V.N.; Borkovskaya, Y. Dynamic electrophoretic mobility in concentrated dispersed systems. Cell model. Langmuir **1999**, *15* (10), 3452–3457.
21. Pendse, H.P.; Bliss, T.C.; Han, W. Particle Shape Effects and Active Ultrasound Spectroscopy. In *Ultrasonic and Dielectric Characterization Techniques for Suspended Particulates*; Hackley, V.A., Texter, J., Eds.; American Ceramic Society: Westerville, OH, 1998.
22. Dispersion Technology Web Site: http://www.dispersion.com.
23. Happel, J. Viscous flow in multiparticle systems: slow motion of fluids relative to beds of spherical particles. AIChe J. **1958**, *4*, 197–201.
24. Kuwabara, S. The forces experienced by randomly distributed parallel circular cylinders or spheres in a viscous flow at small reynolds numbers. J. Phys. Soc. Jpn. **1959**, *14*, 527–532.
25. Shilov, V.N.; Zharkih, N.I.; Borkovskaya, Y.B. Theory of nonequilibrium electrosurface phenomena in concentrated disperse system 1. Application of nonequilibrium thermodynamics to cell model. Colloid J. **1981**, *43* (3), 434–438.
26. Kozak, M.W.; Davis, J.E. Electrokinetic phenomena in fibrous porous media. JCIS **1986**, *112* (2), 403–411.
27. Levine, S.; Neale, G.H. The prediction of electrokinetic phenomena within multiparticle systems. 1. Electrophoresis and electroosmosis. J. Colloid Interface Sci. **1974**, *47*, 520–532.
28. Allegra, J.R.; Hawley, S.A. Attenuation of sound in suspensions and emulsions: theory and experiments. J. Acoust. Soc. Am. **1972**, *51*, 1545–1564.
29. McClements, J.D. Ultrasonic determination of depletion flocculation in oil–in–water emulsions containing a nonionic surfactant. Colloids Surf. **1994**, *90*, 25–35.
30. McClements, D.J. Comparison of multiple scattering theories with experimental measurements in emulsions. J. Acoust. Soc. Am. **1992**, *91* (2), 849–854, February.
31. Holmes, A.K.; Challis, R.E.; Wedlock, D.J. A wide-bandwidth study of ultrasound velocity and attenuation in suspensions: comparison of theory with experimental measurements. J. Colloid Interface Sci. **1993**, *156*, 261–269.
32. Holmes, A.K.; Challis, R.E.; Wedlock, D.J. A wide-bandwidth ultrasonic study of suspensions: the variation of velocity and attenuation with particle size. J.Colloid Interface Sci. **1994**, *168*, 339–348.
33. Dukhin, A.S.; Goetz., P.J.; Hamlet, C.W. Acoustic spectroscopy for concentrated polydisperse colloids with low density contrast. Langmuir **1996**, *12* (21), 4998–5004.
34. Dukhin, A.S.; Goetz, J.P.; Wines, T.H.; Somasundaran, P. AQ8 acoustic and electroacoustic spectroscopy. Colloids Surf. A **2000**.
35. Anson, L.W.; Chivers, R.C. Thermal effects in the attenuation of ultrasound in dilute suspensions for low values of acoustic radius. Ultrasonic **1990**, *28*, 16–25.
36. Isakovich, M.A.Zh. Eksp. Theor. Phys. **1948**, *18*, 907. AQ9
37. Waterman, P.S.; Truell, R.J. Math. Phys. **1961**, *2*, 512. AQ10
38. Chanamai, R.; Coupland, J.N.; McClements, D.J. Effect of temperature on the ultrasonic properties of oil–in–water emulsions. Colloids Surf. **1998**, *139*, 241–250.
39. Temkin, S. Sound speed in suspensions in thermodynamic equilibrium. Phys. Fluids **1992**, *4* (11), 2399–2409, November.
40. Temkin, S. Sound propagation in dilute suspensions of rigid particles. J. Acoust. Soc. Am. **1998**, *103* (2), 838–849, February.
41. Booth, F.; Enderby, J. On electrical effects due to sound waves in colloidal suspensions. Proc. Am. Phys. Soc. **1952**, *208A*, 32.
42. Enderby, J.A. On electrical effects due to sound waves in colloidal suspensions. Proc. R. Soc., London, **1951**, *A207*, 329–342.
43. Marlow, B.J.; Fairhurst, D.; Pendse, H.P. Colloid vibration potential and the electrokinetic characterization of concentrated colloids. Langmuir **1983**, *4* (3), 611–626.
44. Dukhin, S.S.; Derjaguin, B.V. Electrokinetic Phenomena. In *Surface and Colloid Science*; Matijevic, E., Ed.; John Wiley and Sons: New York, 1974; Vol. 7.
45. O'Brien, R.W. Electro–acoustic effects in a dilute suspension of spherical particles. J. Fluid Mech. **1988**, *190*, 71–86.
46. O'Brien, R.W Determination of Particle Size and Electric Charge. US Patent 5,059,909, Oct. 22, 1991.
47. Ohshima, H. Dynamic electrophoretic mobility of spherical colloidal particles in concentrated suspensions. J. Colloid Interface Sci. **1997**, *195*, 137–148.
48. Dukhin, A.S.; Ohshima, H.; Shilov, V.N.; Goetz, P.J. Electroacoustics for concentrated dispersions. Langmuir **1999**, *15* (10), 3445–3451.
49. Ohshima, H.; Dukhin, A.S. Colloid vibration potential in a concentrated suspension of spherical colloidal particles. J. Coll. Interface Sci. **1999**, *212*, 449–452.

50. Dukhin, A.S.; Shilov, V.N.; Ohshima, H.; Goetz, P.J. Electroacoustics phenomena in concentrated dispersions. Effect of the surface conductivity. Langmuir, submitted.
51. Dukhin, S.S.; Shilov, V.N. *Dielectric Phenomena and the Double Layer in Disperse Systems and Polyelectrolytes*; John Wiley and Sons: New York, 1974.
52. Dukhin, A.S.; Goetz, P.J. Particle size distribution in structured concentrated slurries. Langmuir, submitted.
53. Dukhin, A.S.; Goetz, P.J. Method and device for characterizing particle size distribution and zeta potential in concentrated system by means of Acoustic and Electroacoustic Spectroscopy, patent USA, pending.
54. Dukhin, A.S.; Goetz, P.J. Method and device for Determining Particle Size Distribution and Zeta Potential in Concentrated Dispersions, patent USA, pending.
55. Dukhin, A.S.; Goetz, P.J. Acoustic and electroacoustic spectroscopy for characterizing concentrated dispersions and emulsions. Adv. Colloid Interface Sci. **2000**.
56. Dukhin, A.S.; Goetz, P.J.; Truesdail, S. Titration of concentrated dispersions using electroacoustic ζ-potential probe. Langmuir, submitted.
57. Dukhin, A.S.; Goetz, P.J. Characterization of concentrated dispersions with several dispersed phases by means of acoustic spectroscopy. Langmuir, accepted.
58. Babchin, A.J.; Chow, R.S.; Sawatzky, R.P. Electrokinetic measurements by electroacoustic methods. Adv. Colloid Interface Sci. **1989**, *30*, 111.
59. Sawatzky, R.P.; Babchin, A.J. Hydrodynamics of electrophoretic motion in an alternating electric field. J. Fluid. Mech. **1993**, *246*, 321–334.
60. Takeda, S.; Goetz, P.J. Dispersion/flocculated size characterization of alumina particles in highly concentrated slurries by ultrasound attenuation spectroscopy. Colloids Surf. **1998**, *143*, 35–39.
61. Takeda, S.; Chen, T.; Somasundaran, P. Evaluation of particle size distribution for nanosized particles in highly concentrated suspensions by ultrasound attenuation spectroscopy. Colloids Surf. **1999**.
62. Takeda, S. Characterization of Ceramic Slurries by Ultrasonic Attenuation Spectroscopy. In *Ultrasonic and Dielectric Characterization Techniques for Suspended Particulates*; Hackley, V.A., Texter, J., Eds.; American Ceramic Society: Westerville, OH.
63. Dukhin, A.S.; Goetz, P.J Characterization of chemical polishing materials (monomodal and bimodal) by means of acoustic spectroscopy. Colloids Surf., accepted.
64. Wines, T.H.; Dukhin, A.S.; Somasundaran, P. Acoustic spectroscopy for characterizing heptane/water/AOT reverse microemulsion. JCIS **1999**, *216*, 303–308.
65. Hayashi, T.; Ohya, H.; Suzuki, S.; Endoh, S. Errors in size distribution measurement of concentrated alumina slurry by ultrasonic attenuation spectroscopy. J. Soc. Powder Technol., Jpn. **2000**, 498–504.
66. Ennis, J.P.; Shugai, A.A.; Carnie, S.L. Dynamic mobility of two spherical particles with thick double layers. J. Colloid Interface Sci. **2000**, *223*, 21–36.
67. Ennis, J.P.; Shugai, A.A.; Carnie, S.L. Dynamic mobility of particles with thick double layers in a non-dilute suspension. J. Colloid Interface Sci. **2000**, *223*, 37–53.
68. Dukhin, A.S.; Goetz, P.J. Method for Determining Particle Size Distribution and Mechanical Properties of Soft Particles in Liquids, US patent, pending.
69. Crupi, V.; Maisano, G.; Majolino, D.; Ponterio, R.; Villari, V.; Caponetti, E. J. Mol. Struct. **1996**, *383*, 171.
70. Bedwell, B.; Gulari, E. *Solution Behavior of Surfactants*; Mittal, K.L., Ed.; Plenum Press: New York, 1982; Vol. 2.
71. Gulari, E.; Bedwell, B.; Alkhafaji, S. J. Colloid Interface Sci. **1980**, *77* (1), 202.
72. Zulauf, M.; Eicke, H.-F.J. Phys. Chem. **1979**, *83* (4), 480.
73. Eicke, H.-F. *Microemulsions*; Rob, I.D., Ed.; Plenum Press: New York, 1982; 10.
74. Nicholson, J.D.; Doherty, J.V.; Clarke, J.H.R. *Microemulsions*; Rob, I.D., Ed.; Plenum Press: New York, 1982; 33.
75. Eicke, H.-F.; Rehak, J. Helv. Chim. Acta **1976**, *59* (8), 2883.
76. Fletcher, P.D.I.; Robinson, B.H.; Bermejo-Barrera, F.; Oakenfull, D.G.; Dore, J.C.; Steytler, D.C. *Microemulsions*; Rob, I. D., Ed.; Plenum Press: New York, 1982; 221.
77. Cabos, P.C.; Delord, P. J. App. Cryst. **1979**, *12*, 502.
78. Radiman, S.; Fountain, L.E.; Toprakcioglu, C.; de Vallera, A.; Chieux, P. Prog. Colloid Polym. Sci. **1990**, *81*, 54.
79. Huruguen, J.P.; Zemb, T.; Pileni, M.P. Prog. Colloid Polym. Sci. **1992**, *89*, 39.
80. Pileni, M.P.; Zemb, T.; Petit, C. Chem. Phys. Lett. **1985**, *118* (4), 414.
81. Kabanov, A.V. Makromol. Chem., Macromol. Symp. **1991**, *44*, 253.